ORGANIC DYES REMOVAL BY HETEROGENEOUS FENTON AND FENTON-LIKE PROCESSES USING IRON OXIDE MAGNETIC CATALYST

CH'NG SU YEN

A project report submitted in partial fulfilment of the requirements for the award of Bachelor of Engineering (Hons.) Chemical Engineering

Lee Kong Chian Faculty of Engineering and Science
Universiti Tunku Abdul Rahman

May 2016

DECLARATION

I hereby declare that this project report is based on my original work except for citations and quotations which have been duly acknowledged. I also declare that it has not been previously and concurrently submitted for any other degree or award at UTAR or other institutions.

Signature   : _____

Name   : Ch'ng Su Yen

ID No.   : 11UEB02864

Date   : _____

APPROVAL FOR SUBMISSION

I certify that this project report entitled **"ORGANIC DYES REMOVAL BY HETEROGENEOUS FENTON AND FENTON-LIKE PROCESSES USING IRON OXIDE MEGNETIC CATALYST"** was prepared by **CH'NG SU YEN** has met the required standard for submission in partial fulfilment of the requirements for the award of Bachelor of Engineering (Hons.) Chemical Engineering at Universiti Tunku Abdul Rahman.

Approved by,

Signature   : _____

Supervisor : Dr. Pang Yean Ling

Date   : _____

The copyright of this report belongs to the author under the terms of the copyright Act 1987 as qualified by Intellectual Property Policy of Universiti Tunku Abdul Rahman. Due acknowledgement shall always be made of the use of any material contained in, or derived from, this report.

Specially dedicated to

my beloved parents

ACKNOWLEDGEMENTS

I would like to thank everyone who had contributed to the successful completion of this project. I would like to express my gratitude to my research supervisor, Dr. Pang Yean Ling for her invaluable advice, guidance and her enormous patience throughout the development of the research.

In addition, I would also like to express my gratitude to my loving parent and friends who had helped and given me encouragement to complete this project. I would not resolve the problems which I faced during my research without their cooperation.

ORGANICS DYES REMOVAL BY HETEROGENEOUS FENTON AND FENTON-LIKE PROCESSES USING IRON OXIDE MEGNETIC CATALYST

ABSTRACT

Heat-treated iron (II, III) oxides (Fe_3O_4) were developed and characterized by using XRD and SEM-EDX. Heat treated Fe_3O_4 at various temperatures ranging from 200 to 800 ℃ for 2 h could induce phase change to maghemite (γ-Fe_2O_3) and further changed to hematite (α-Fe_2O_3) at higher temperature. Majority Fe_3O_4 particles were spherical shape and composed of iron (Fe) and oxygen (O) atoms only. Mean particle sizes of Fe_3O_4 were increased with increment of temperature as excessive heat treatment caused the agglomeration of particles. The effect of heat treatment of Fe_3O_4 for Fenton and Fenton-like processes was identified. Original Fe_3O_4 showed the highest catalytic activity as it comprised Fe^{2+} and Fe^{3+} ions to undergo Fenton and Fenton-like processes simultaneously. Several parameters were also investigated including types of organic dyes used, Fe_3O_4 dosage, hydrogen peroxide (H_2O_2) dosage, dye concentration, temperature and solution pH in order to determine the optimum condition for the Fenton and Fenton-like processes. Degradation of organic dyes was influenced by their chemical structures. Malachite green exhibited the highest degradation rate as its chemical structure was the most vulnerable to chemical oxidation. The highest degradation efficiency of malachite green (96 %) was achieved in 1 h at the optimum conditions with dye concentration of 20 mg/L, Fe_3O_4 dosage of 2.5 g/L, H_2O_2 dosage of 0.20 M, solution pH of 9 and reaction temperature at 30 ℃. Reusability of Fe_3O_4 and kinetic study were studied. Reused Fe_3O_4 still maintained high catalytic activity. Moreover, Fe_3O_4 had high stability as leaching of Fe was low. The degradation kinetics of malachite green at different temperatures were fitted well to pseudo first-order model. The activation energy for degradation of malachite green was 36.40 kJ/mol.

TABLE OF CONTENTS

LIST OF TABLES

LIST OF FIGURES

LIST OF SYMBOLS / ABBREVIATIONS

Ag	silver
Al	aluminium
A_0	activation energy, kJ/mol
C	carbon atom
Cl	chlorine atom
C_{MG}	concentration of malachite green, mg/L
$C_{\cdot OH}$	concentration of $\cdot OH$
C_0	concentration of dye at time 0, mg/L
C_t	dye concentration at time t, mg/L
D	crystalline size, nm
d	d-spacing
Fe	iron atom
Fe^{2+}	ferrous ion
Fe^{2+}/H_2O_2	Fenton process
Fe^{3+}/H_2O_2	Fenton-like process
FeCl$_3$	iron (III) chloride hexahydrate
Fe$_3$O$_4$	magnetite
HCl	hydrogen chloride
H^+	hydrogen ion
H$_2$O$_2$	hydrogen peroxide
$H_3O_2^+$	hydroperoxonium ion
K	shape factor
$K_2Cr_2O_7$	potassium dichromate
k_{app}	apparent rate constant
k_0	apparent pseudo-zero order rate constant, mg/(L·min)
k_1	apparent pseudo-first order rate constant, /min

k_2	apparent pseudo-second order rate constant, L/(mg·min)
m	reaction order with respect to malachite green
n	integer
n	reaction order with respect to $\cdot OH$
NaOH	sodium hydroxide
O	oxygen atom
O_2	oxygen molecules
OH^-	hydroxyl ion
$\cdot OH$	hydroxyl radical
R	ideal gas constant, 8.314 J/(mol·K)
T	absolute temperature, K
t	reaction time, min
V	volume, ml
ρ	density, g/ml
θ	half scattering angle, ˚
β	full width at half maximum (FWHM), °
λ	wavelength of X-rays, 1.540562 Å
λ_{max}	wavelength with highest absorbance
γ-Fe$_2$O$_3$	maghemite
α-Fe$_2$O$_3$	hematite
AOPs	advanced oxidation processes
BC	before crist
BET	Brunauer-Emmett-Teller
BOD	biochemical oxygen demand
CCP	cubic closed packed
COD	chemical oxygen demand
HCP	hexagonal closed packed
ICP-OES	inductively coupled plasma-optical emission spectroscopy
MNPs	ferromagnetic nanoparticles
SEM-EDX	scanning electron microscopy coupled with energy dispersive X-ray
TDS	total dissolved solid

TOC	total organic carbon
UV-vis	ultraviolet-visible-infrared
XRD	X-ray diffraction

LIST OF APPENDICES

CHAPTER 1

INTRODUCTION

1.1   Water Pollution in Malaysia

Around 71 % of the Earth's surface is covered by water whilst 29 % comprises continents and islands (Williams, 2014). Therefore, it can be seen that water is a very essential resource for people and environment. The increasing of population growth, industry processes, agricultural and domestic activities contribute to the water pollution. The main sources of water pollution are point source and non-point source (DOE, 2012). For instance, point sources are industrial and municipal wastewater originating from a specific point such as sewage treatment plants. Non-point sources cannot be simply tracked back to specific location and come from land use activities such as agricultural activities. The water quality degrades as the addition of chemical, physical or biological substances in certain concentrations (Tchobanoglous, Burton and Stensel, 2003).

In 21st century, water pollution has turned into a severe problem around the world including Malaysia. Malaysia is one of the countries which face the issues on the sustainability of water resource. Moreover, plants, living organisms, people's health and economy are also strongly affected by water pollution. Water pollution is a critical issue in Malaysia with reports representing a decreasing trend annually (Afroz, et al., 2014). Since Malaysia is rapidly turning into an industrial nation, many wastes have been discharged into rivers. Consequently, many rivers have become contaminated. The water and lives revolve around the rivers have been harmed as those rivers have been used as an exit for chemicals to flow out. Total water availability has

reduced as the expense to treat the polluted water is too costly and some polluted water is not suitable to consume although has been treated. Therefore, sufficient water supply to all users cannot be ensured although Malaysia has a substantial amount of water available in catchment (Ling, 2010).

According to environmental quality report 2012, out of 473 rivers, there were 278 (59 %) clean rivers, 161 (34 %) slightly polluted rivers and 34 (7 %) polluted rivers (DOE, 2012). Figure 1.1 demonstrates that throughout 2007 to 2012, the number of clean rivers was continue decreasing except there was a slightly increase in year 2012. On the other hand, the number of polluted river was increased from year 2007 to 2010 and after that slightly decreased in year 2012. Although the number of clean river was increased and polluted river was decreased from year 2011 to 2012, the number of slightly polluted river was increased. This indicates that the rivers in Malaysia are continuously being polluted.
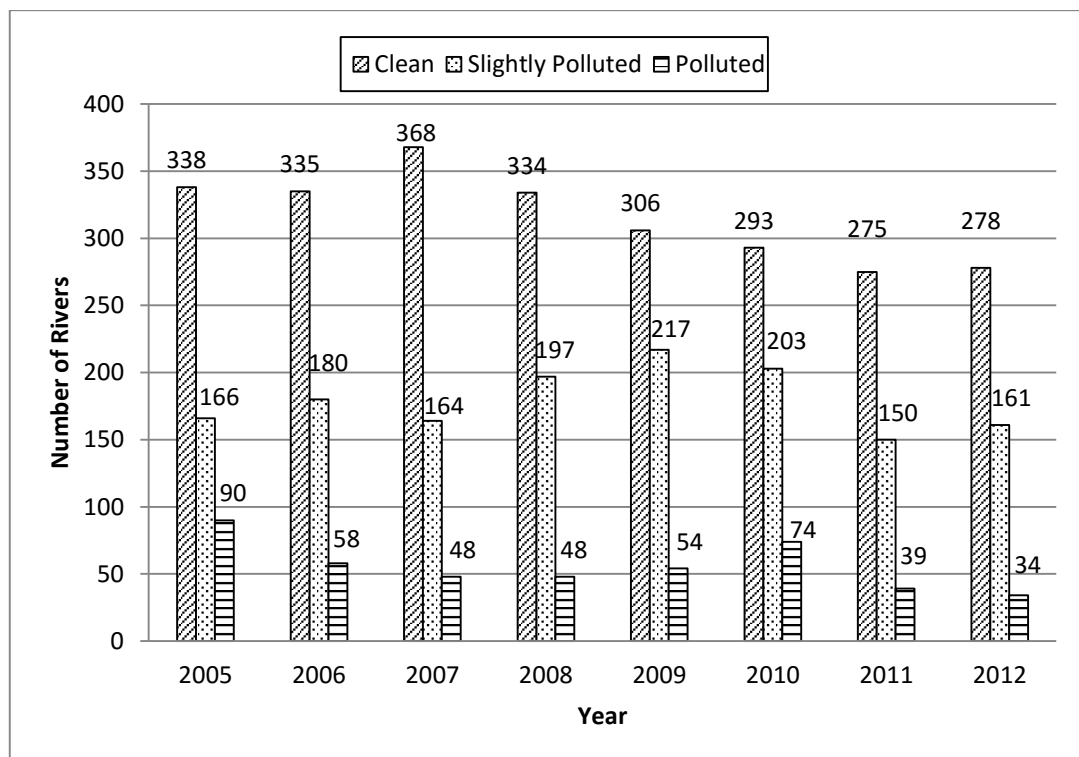
Figure 1.1: Malaysia River Water Quality Trend from 2005 to 2012 (DOE, 2012)

1.2   Dye Production and Environmental Impacts

More than 100 000 commercially available dyes have been reported in the literature. Furthermore, over 7×10^5 tonnes of dyestuffs are produced annually and 40 000 to 50 000 tonnes of dyes are released to surface water yearly (Rangabhashiyam, Anu and Selvaraju, 2013). China is the largest consumer of synthetic dyes as it has the largest consumption of dyes which is around 40 to 50 % in 2013 as shown in Figure 1.2.
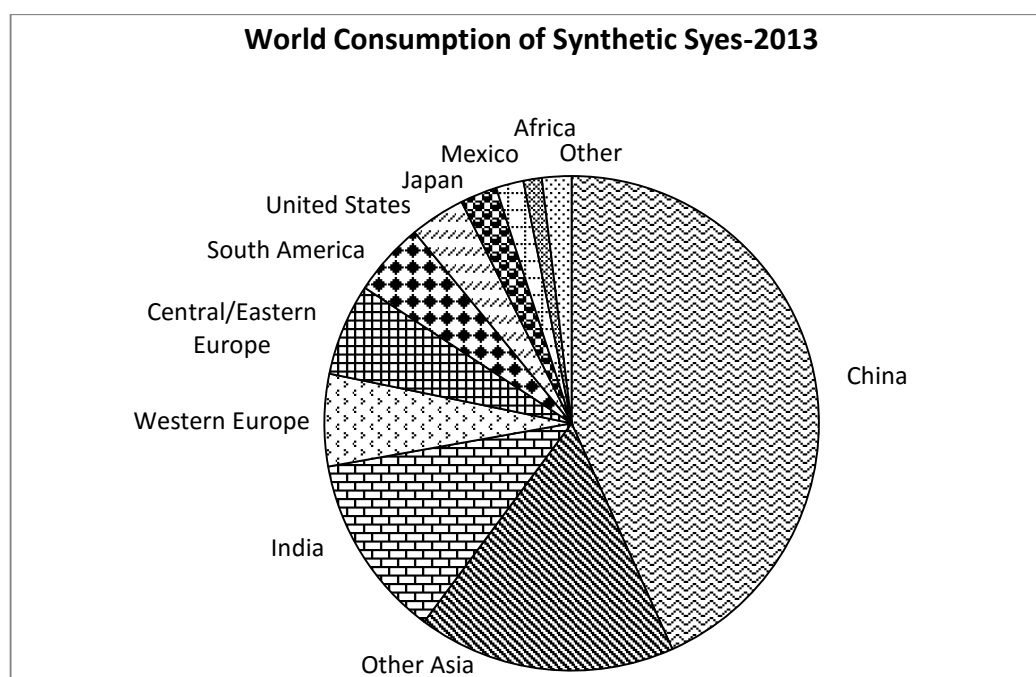
Figure 1.2: World Consumption of Synthetic Dyes−2013 (IHS, 2014)

The industries like textile, dyestuffs, paper and plastics utilize dyes for dyeing their products. Around 67 % of the total dyestuff market is used by textile industries. Textile industry ranks the first among all industries in application of dyes for colouration of fibre (Rangabhashiyam, Anu and Selvaraju, 2013). World Bank estimated that approximately 20 % of global industrial water pollution originated from treatment and dyeing of textiles (Kant, 2012).

Pang and Abdullah (2013) stated that there is no complete degree of fixation of dyes to fibre. Improper dye uptake and degree of fixation on substrate lead to the

release of dyes which subsequently bring impact to the environment. According to Table 1.1, reactive dyes have the poorest degree of fixation on fibre. However, the percentage of loss of effluent for metal-complex is slight higher than reactive dyes although degree of fixation for metal-complex dye is very high which is from 90 to 98 %.

Table 1.1: Estimated Degree of Fixation for Different Dye/ Fibre Combinations (Joshi, Bansal and Purwar, 2004)

Dye Class	Fibre	Loss of effluent (%)	Degree of fixation (%)
Acid	Polyamide	5−20	80−95
Basic	Acrylic	0−5	95−100
Direct	Cellulose	5 − 30	70−95
Disperse	Polyester	0−10	90−100
Metal-complex	Wool	2−10	90−98
Reactive	Cellulose	10−50	50−90
Sulphur	Cellulose	10−40	60−90
Vat	Cellulose	5−20	80−95

In Malaysia, when the country commenced import-export oriented industrialization and commercialization, textile industry grew rapidly in the early 1970s. Consequently, there was a high demand of dye production. In the East Coast Peninsular Malaysia and Sarawak, homemade textile industry is very popular (Ahmad, et al., 2002). In this industry, effluents comprise of grease, wax, heavy metals, surfactants, suspended solids and dyes are produced. In the process of producing Batik, substantial volume of water has been utilized and thus large volume of wastewater has been discharged.

Wastewater generated from textile industry is more polluted as compared to other industrial sectors by considering the composition of effluent and the volume produced. In the textile effluent, the main pollutants are recalcitrant organic, surfactant, coloured toxicant, salt and chlorinated compounds. Textile effluents are characterized

by great fluctuations in many parameters. For instance, the parameters are pH, salinity, colour, biochemical oxygen demand (BOD) and chemical oxygen demand (COD) (Chequer, et al., 2013). Table 1.2 and Table 1.3 show that large amount of water are consumed as processing water in textile industry. According to Table 1.2, substantial volume of organic load and wastewater are consumed in preparation, dyeing and printing process as compared to other processes.

Table 1.2: Organic Load and Water Consumption in Different Textile Finishing Procedures (Carmen and Daniela, 2012)

Operation/ Process	Organic load (% from total organic load of textile plant)		Water Consumption (% from total consumption of textile plant)	
	Minimum	**Maximum**	**Minimum**	**Maximum**
General facilities	0.1	8	6	33
Preparation	45	77	16	54
Dyeing	4	47	4	53
Printing	42	75	42	38
Wetting	0	0.1	0.3	0.6
Fabric washing	1	25	3	52
Finishing	0.1	7	0.3	4

Approximately 2 % of dye generated is estimated to be released in aqueous effluent. Afterwards, 10 % is lost in the colouration procedure. Therefore, approximately 20 % of colourants go into surroundings via effluents from wastewater treatment plants are reasonably to be assumed (Arora, 2014). Low degree of fixation of dye on fibre is an important factor that liable for the release of water-soluble and water-insoluble dyes. Moreover, colour greatly affects the public aesthesis of water quality. In wastewater, colour will be recognized easily even small amount of dyes present in water as it is extremely visible (Wu, et al., 2012). This seriously influences clarity of water bodies and brings harm to aquatic environment.

Table 1.3: Specific Water Consumption in Textile Finishing Processes (Carmen and Daniela, 2012)

Type of finishing process	Water Consumption, 10^{-3} m³/kg textile product		
	Minimum	Medium	Maximum
Cloth finishing			
• Simplified processing	8.3	135.9	392.8
• Complex process	20	83.4	377.8
• Panty processing	5.8	69.2	289.4
Carpet finishing	8.3	46.7	162.6
Fibre finishing	3.3	100.1	557.1
Fabric finishing			
• Short process	12.5	78.4	275.2
• Complex process	10.8	86.7	276.9
Non-fabrics finishing	2.5	40	82.6
Raw wool washing	4.2	11.7	77.6
Wool finishing	110.9	283.6	657.2
Yarn finishing	33.4	212.7	930.7

Furthermore, some dyes maybe toxic to some aquatic life because of the existence of metals and aromatics. The example of dye which is toxic is azo dye as it can form the toxic amines in effluent through the reactive cleavage of azo linkage (Joshi, Bansal and Purwar, 2004). Some dyes are also carcinogenic for example complex dye which is normally chromium based (Yagub, et al., 2014). Dyes also reduce the penetration of light into water subsequently affect photosynthetic activity of aquatic plants and therefore having adverse impact on their growth. Moreover, it causes oxygen deficiency and restricts the benefit uses of downstream for instance drinking water and recreation. The existence of dyes in effluent brings adverse effects to many forms of life as it will cause substantial environmental pollution and adversely affect health of living organisms. Wastewater from textile industry has high colour intensity and high composition variability. Thus, it is difficult to treat satisfactory.

1.3   Problem Statement

Dyes and pigments are extremely visible materials. Incomplete fixation of dyes onto textile fibre is the major source for the release of colour into environment. Colour may appear in water and may be toxic to the aquatic living although only slight amount of it releases into environment. Therefore, it is essential to decrease the quantity of residue dye in textile effluent (Christie, 2015).

Many colour removal techniques have been developed to remove organic dyes from textile wastewater. For instance, the removal techniques are coagulation, aerobic and anaerobic microbial degradation, membrane separation and filtration (Gonawala and Mehta, 2014). However, some conventional techniques for instance coagulation and adsorption are only capable to merely transfer the organic pollutants to another phase such as from wastewater to other media that produce sludge and lead to disposal problems (Inoue, et al., 2006). Conventional treatment process will also become ineffective in degrading and destroying organic pollutants because of the existence of benzene rings in dye structure (Wang, et al., 2007).

Therefore, advanced oxidation processes (AOPs) provide a stunning substitute to the conventional processes because of more efficient in the degradation of any kind of organic pollutants (Swaminathan, Muruganandham and Sillanpaa, 2012). Treatment of wastewater by using AOPs involves $\cdot OH$, a strong oxidant that completely degrade and mineralize the organic compound non-selectively into harmless products (Pang, Abdullah and Bhatia, 2010).

Fenton and Fenton-like processes are one of the AOPs. It can be conducted at atmospheric pressure and room temperature. Moreover, the Fenton's reagents needed for Fenton process are readily obtainable, liable to store and process. Nevertheless, there are two main shortcomings of homogeneous Fenton and Fenton-like processes. Firstly, it refers to the wastage of oxidant because of the radical scavenging effect of H_2O_2 and self-decomposition of it. The second drawback of it is that iron ions are lost continuously and solid sludge is formed (Babuponnusami and Muthukumar, 2014).

Therefore, in order to overcome these drawbacks, heterogeneous Fenton and Fenton-like processes which replace the dissolved iron with solid catalyst need to be further studied. Furthermore, the influence of operating parameters such as Fe_3O_4 dosage, H_2O_2 dosage, pH of solution, dye concentration, temperature and different types of organic dye should be identified so as to maximize and optimize the effectiveness of Fenton and Fenton-like processes.

Apart from that, conventional filtration and centrifugation can only separate the solid catalyst size at least about $3 \, \mu m$ (Xu, et al., 2010). However, magnetic separation is a new promising method to solve the separation of nanocatalyst. Thus, the separation and reusability of Fe_3O_4 magnetic nanocatalyst are required to be examined as it is expected to be recycled and reused in the process in order to save cost. Last but not least, a reliable reaction kinetic for the degradation of organic dyes by Fenton and Fenton-like processes is required to be determined.

1.4 Research Objectives

The main objective of this study was to investigate the heterogeneous Fenton and Fenton-like processes using iron oxide magnetic catalyst. In order to achieve the main objective of this study, the following sub-objectives were identified:

1. To prepare and characterize heat-treated Fe_3O_4 catalysts.
2. To identify the effect of various operating parameters such as various organic dyes, Fe_3O_4 dosage, H_2O_2 dosage, dye concentration, temperature, and pH of solution for Fenton and Fenton-like processes using Fe_3O_4 catalyst in order to determine the optimum conditions.
3. To study the reusability of Fe_3O_4 catalyst on the degradation of organic dyes.
4. To study the reaction kinetics of Fenton and Fenton-like reaction on degradation of organic dyes.

1.5   Scopes of Study

In order to achieve the objectives, the following scopes are studied. Fe_3O_4 are prepared by heat treating at different temperatures which are 200, 400, 600 and 800 ˚C. Effect on the characteristics of heat-treated Fe_3O_4 catalysts and catalytic activity are studied and compared. Characteristics of Fe_3O_4 are studied by using X-ray diffraction (XRD) and scanning electron microscopy coupled with energy dispersive X-ray (SEM-EDX).

Then, a series of experiments will be carried out to investigate the effect of process variables which are various types of organic dyes, Fe_3O_4 dosage, H_2O_2 dosage, dye concentration, temperature and pH of solution. Fe_3O_4 catalyst is then reused for the subsequence experiments to evaluate its reusability on the organic dye degradation rate. Furthermore, a suitable kinetics is proposed for a better understanding on the reaction order for Fenton and Fenton-like processes.

CHAPTER 2

LITERATURE REVIEW

2.1   Classification of Dye

Dyes are coloured organic compounds that can be fixed on a substance with more or less permanence in the form of a colour through the sensation of colour is evoked. It is normally used in solution. It also has affinity for one or more textile fibre in the existence of specific auxiliaries under precise circumstances of temperature (Choudhury, 2006). Three methods that have been used to classify dyes are classification based on source of materials, classification based on chemical structure and classification based on application.

According to the sources of origin, dyes can be assorted as natural and synthetic dyes. Natural dyes are extracted from nature via organic and inorganic materials such as roots, leaves, iron buffs, wood and cochineal. It can be categorized into three classes which are natural dyes obtained from plants, animals and minerals. Carmen and Daniela (2012) stated natural dyes were mostly used in textile processing until 1856, commencing in 2600 Before Crist (BC) in China. Tyrian purple yielded from certain kind of crushed sea snails in 15th century BC and indigo dye yielded from indigo plant since 3000 BC were utilized by Phoenicians. In South America, Egyptian mummies clothes and Incas fine textures were wrapped and coloured by utilizing the dyes made from madder plants.

In 1856, the synthetic dye, Mauveneine was first discovered accidentally by William Henry Perkin from United Kingdom who was attempting to produce anti-

malaria drug quinine. Afterward, in 1858, German scientist, O. Gries invented the reaction mechanism diazotization that can produce the azo dyes (Saranraj, 2013). Synthetic dyes rapidly displace natural dyes which are eco-friendly, biodegradable, less allergic and less toxic (Nisar, Ali and Hussian, 2007). This is because synthetic dyes are cheaper and offered an extensive range of new colours and imparted better properties to dyed materials. Nowadays, synthetic dyes have occupied dye market and being utilized by most of the dyeing operation.

Dyes can be classified by their chemical structures. There are two main functional groups that dye molecules have which are chromophores and auxochromes. Chromophores normally are electron withdrawing substituents that principally responsible for colour of dye. The common types of chromophores are azo group $(-N = N-)$, carbon nitrogen group $(-C - N-)$, carbonyl group$(-C = O-)$, nitroso group $(-N = O-)$ and nitro group$(-NO_2)$. Auxochromes normally are electron donating substituents which create or intensify the colour of chromophores. In other words, it does not create colour by itself but deepens the colour of chromogen. The general classes of auxochromes are carboxyl group$(-COOH)$, amine group $(-NH_3)$, sulfonate group $(-SO_3H)$ and hydroxyl group $(-OH)$ (Pang and Abdullah, 2013).

On the other hand, dyes can be classified based on the application. The general classes of dyes based on the application are acid dyes, reactive dyes, basic dyes, direct dyes, mordant dyes, disperse dyes, vat dyes and solvent dye. Different dyes will be used in different application areas. Dyes can also be classified in anionic, non-ionic and cationic dyes by considering only the general structure. Direct, acid and reactive dyes are the major anionic dyes. In addition, highly water soluble reactive and acid dyes are very troublesome because it cannot be get rid of by conventional treatment methods (Choudhury, 2006). Disperse dyes are the major non-ionic dyes that does not ionize in aqueous environment (Carmen and Daniela, 2012). Moreover, azo, basic, anthraquinone disperse and reactive dyes are the major cationic dyes. Classification of dyes and chemical types are shown in Table 2.1

Table 2.1: Classification of Dyes and Types of Chemicals (Beyene, 2014)

Class	Principle Substrate	Method of Application	Chemical Types
Acid	Nylon, wool, silk, paper and leather	Usually from neutral to acidic dyebaths	Azo (including premetallized), anthraquinone, triphenylmethane, azine, xanthene, nitro and nitroso
Basic	Paper, Polyacrylonitrile, modified nylon, polyester and inks	Applied from acidic dyebaths	Cyanine, hemicyanine, diazahemicynanine, diphenylmethane, trialrylmethane, azo, azine, xanthene, acridine, oxazine, and anthraquinone
Direct	Cotton, rayon, paper, leather and nylon	Applied from neutral or slightly alkaline baths containing additional electrolyte	Azo, anthraquinone, styryl, nitro and benzodifuranone
Disperse	Polyester, polyamide, acetate, acrylic and plastics	Fine aqueous dispersions often applied by high temperature/ pressure or lower temperature carried methods; dye may be padded on cloth and baked on thermo fixed	Azo, anthraquinone, styryl, nitro and benzodifuranone
Reactive	Cotton, wool, silk, and nylon	Reactive site on dye reacts with functional group on fiber to bind dye covalently under influence of heat and pH (alkaline)	Azo, antraquinone, phthalocyanine, formazan, oxazine and basic

Table 2.1: Continued.

Class	Principle Substrate	Method of Application	Chemical Types
Solvent	Plastics, gasoline, varnishes, lacquers, stains, inks, fats, oils and waxes	Dissolution in the substrate	Azo, triphenylmethane, antraquinone and phthacyanine
Sulfur	Cotton and rayon	Aromatic substrate vatted with sodium sulfide and reoxidized to insoluble sulphur containing products on fiber	Indeterminate structures
Vat	Cotton, rayon and wool	Water-insoluble dyes solubilized by reducing with sodium hydrogen sulfite, then exhausted on fiber and reoxidized	Antraquinone (including polycyclic quinones) and indigiods

2.2 Colour Removal Methods

Verma, Dash and Buhnia (2012) stated that textile wastewater displayed wide range of pH from 2 to 14, COD from 50 to 18 000 mg/L, total dissolved solid (TDS) from 50 to 6000 mg/L as well as variety of synthetic dyes. These indicate that treatment of textile effluent is rather difficult. Therefore, numerous technologies have been investigated to treat the wastewater effluent as existence of dyes in the effluent is extremely undesirable. There are various types of treatment methods such as physical, chemical and biological methods for the removal of synthetic dyes from wastewater to decrease their impact on environment.

There are various physical methods to treat the wastewater for example adsorption, membrane filtration and ion exchange. Adsorption is used to collect the

soluble substances in the solution on an appropriate interface (Soudani, et al., 2011). Activated carbons have been used as adsorbent as it is able to adsorb various dyes with great adsorption capacity. Nevertheless, activated carbon regeneration is required and it is costly (Cecen and Aktas, 2012). Low cost adsorbent materials have been paid attention in recent years such as wood chips and corn cobs (Pang and Abdullah, 2013). Widespread availability and low cost are their benefit. Although adsorption has been certified that it is efficient to remove multiple solutes, but it still has its limitation in the disposal problem as it will produce waste sludge.

Membrane filtration is applied after coagulation and flocculation or after biological wastewater treatment. This method is able to clarify, concentrate and segregate dye from effluent continuously (Mattioli, Malpei and Bortone, 2002). The common types of filtration are microfiltration, ultrafiltration, nanofiltration and reverse osmosis. This method is effective in removing all types of dyes and has special features for instance resistance to temperature. However, high capital cost is required and clogging is possible to be occurred. Lifetime of membrane is relatively short because of clogging on the pores and it is practically limited to smaller wastewater flow rate only (Pang and Abdullah, 2013).

Ion exchange is used to remove unwanted anions and cations from wastewater. Wastewater will pass through the ion exchange resin until the available exchange sites are saturated. There is no loss of adsorbent on regeneration, reclamation of solvent after use and the removal of soluble dyes are the merits of this method (Evans and Furlong, 2003). Although ion exchange has these merits, it still has the drawback that it only workable in removing the unwanted anions and cations from wastewater effectively but very poor in removing non-ionic dyes such as disperse dyes. Furthermore, it is quite expensive due to the involvement of expensive organic solvents and cannot accommodate several types of dye.

Generally, biological treatment involves the application of microorganisms to degrade organic dyes either aerobic or anaerobic condition by applying fixed or suspended growth system. Aerobic biological treatment is not an effective method in textile wastewater treatment because azo dyes cannot be removed significantly. Low biodegradability index ($BOD_5/COD < 0.1$) of azo dyes is the factor that it is resistant

to conventional biological treatment (Baban, et al., 2010). The other drawbacks of this method are large aerobic tank is required as long hydraulic retention time, production of unknown oxidation compounds that intensify the colour of wastewater as well as the formation of undesirable floc which decreases the efficiency of organic dyes biodegradation.

On the other hand, anaerobic biological treatment method has an advantage that methane gas is produced from process and can be used as a renewable energy. However, degradation of dye by microorganism may lead to the creation of aromatic amines through the azoreductase cleavage of azo bond. Aromatic amines are more toxic as compared to dye itself (You and Teng, 2009). Moreover, it is not adequate as a last step of treatment because process is simply a partial degradation process and it needs a long acclimatization time as the growth rate of microorganisms is slow and it is direct consequent of slow growth of methanogenic bacteria (Pang and Abdullah, 2013).

Chemical treatment involves coagulation/ flocculation and chemical oxidation processes. Coagulation and flocculation method is used in primary treatment of textile effluents for eliminating colloidal and other suspended particles from wastewater by adding coagulant. It is an efficient method that has been widely used in textile industry due to their short detention time and easy to operate. However, this method will generate large quantity of sludge which will lead to disposal problem and hardly get rid of highly water-soluble dyes (Verma, Dash and Bhunia, 2012). On top of that, it is an expensive treatment method as the coagulating or flocculating agent is costly. Capital cost for operation is also high because it is required to handle substantial volume of concentrated sludge. Moreover, Joshi, Bansal and Purwar (2004) stated that it can efficiently remove sulphur and disperse dye while it cannot remove acid, direct, mordant and reactive dye well due to the poor quality flocs which does not settle well. In addition, it cannot remove cationic dyes as coagulation does not happen at all.

Chemical oxidation processes have many types of process to treat textile wastewater such as ozonation, photocatalytic process and Fenton process. It is utilised to degrade organic dyes as it is simple and effective in destructing organic compounds with non-biodegradable property, toxic or inhibitory to microbial growth and even

inorganic compounds. For ozonation of textile wastewater, colour can be removed efficiently, biodegradability is enhanced, phenolic compounds are destructed and COD value is reduced (Kharea and Boseb, 2015). The advantages are the volume of wastewater and production of sludge do not increase because of the use of gaseous ozone. Soluble dyes can be decolourized rapidly by ozone whereas for non-soluble dyes need longer time to oxidise. In order to avoid over consumption of ozone by other organic pollutants, pre-treatment of raw textile wastewater is required before ozone process.

Photocatalytic process uses semiconductor metal oxide as catalyst in the presence of ultraviolent light to degrade organic pollutants in water. It is possible to mineralize organic dyes completely in fairly short time as compared to biological treatment but UV light has low penetration ability in water medium. Therefore, it is limited to low concentration or lightly coloured effluent or as a post-treatment process only. Fenton oxidation encompasses reactions of H_2O_2 with iron ions to generate active oxygen species that oxidize organic or inorganic compounds. Wide range of textile dyes can be completely degraded by Fenton and Fenton-like treatments in rather short reaction times. On top of that, it is able to be carried out at room temperature and atmospheric pressure. Reagents that are needed in this method are easily available and liable to store. They do not bring any damage to environment. Babuponnusami and Muthukumar (2014) states that the drawback of homogeneous Fenton process is the large sludge production via flocculation of reagent and dye molecules and wastage of oxidants because of the radical scavenging effect of H_2O_2 as well as self-decomposition of it. Thus, intensive investigation has been shift towards heterogeneous Fenton and Fenton-like processes to overcome the disadvantages encountered by homogeneous Fenton and Fenton-like processes.

2.3   Oxidation by Fenton and Fenton-like Processes

AOPs are alternative wastewater treatment processes which can be operated near ambient temperature and pressure. It is capable to degrade biorefractory organic compounds with the involvement of the production of highly reactive $\cdot OH$. $\cdot OH$ is the

strongest oxidants among others except fluorine depending on the substrate to be degraded and it can be shown in Table 2.2. Sufficient quantities of $\cdot OH$ can attack extensive variety of organic compounds due to its high oxidation potential (2.80 V). Fenton (Fe^{2+}/H_2O_2) and Fenton-like (Fe^{3+}/H_2O_2) processes are probably among the most adopted APOs for the treatment of industrial effluent (Lopez, et al., 2012).

Table 2.2: Standard Reduction Potential of Common Oxidants (Babuponnusami and Muthukumar, 2014)

Oxidant	Oxidation Potential (V)
Fluorine (F_2)	3.03
Hydroxyl radical ($\cdot OH$)	2.80
Atomic oxygen (O)	2.42
Ozone (O_3)	2.07
Hydrogen peroxide (H_2O_2)	1.77
Potassium permanganate ($KMnO_4$)	1.67
Chlorine dioxide (ClO_2)	1.50
Hypochlorous acid ($HClO$)	1.49
Chlorine (Cl_2)	1.36
Oxygen (O_2)	1.23
Bromine (Br_2)	1.09

Fenton process involves the production of highly reactive $\cdot OH$ under acidic conditions via the reaction between H₂O₂ and ferrous ions (Fe^{2+}) (Bagal and Gogate, 2014). In Fenton-like process, Fe^{2+} ions are replaced by ferric ions (Fe^{3+}). Jiang, et al. (2013) stated that there was an inherent relationship between Fenton and Fenton-like processes. Fe^{2+} ions catalyse Fenton reaction, whereas Fe^{3+} ions, which is the product of Fenton reaction, catalyze Fenton-like reaction. Shaobin (2008) reported that the degradation of dye in Fenton process was faster than Fenton-like reaction but the degree of degradation accomplished for two processes was similar after 100 min.

Equations 2.1 to 2.9 show the reactions and rate constants for Fenton and Fenton-like reactions and it is tabulated in Table 2.3 (Babuponnusami and

Muthukumar, 2014). Equation 2.1 is known as Fenton reaction and shows the oxidation of Fe^{2+} ions to Fe^{3+} ions in order to decompose H_2O_2 into $\cdot OH$. Equation 2.2 is known as Fenton-like reaction and shows that the generated Fe^{3+} ions can be reduced by reaction with excess H_2O_2 to form again Fe^{2+} ions and more radicals. Equations 2.2 to 2.5 are the rate limiting steps as H_2O_2 is consumed and Fe^{2+} ions are regenerated from Fe^{3+} ions through these reactions. Equations 2.6 to 2.9 are radical-radical reactions.

Table 2.3: Reactions and Rate Constants for Fenton and Fenton-like Reactions (Babuponnusami and Muthukumar, 2014)

Reactions	Rate Constants $(M^{-1}s^{-1})$	Equation No.
$Fe^{2+} + H_2O_2 \rightarrow Fe^{3+} + OH^- + \cdot OH$	$40 - 80$	(2.1)
$Fe^{3+} + H_2O_2 \rightarrow Fe^{2+} + HO_2 \cdot + H^+$	9.1×10^{-7}	(2.2)
$Fe^{2+} + \cdot OH \rightarrow Fe^{3+} + OH^-$	$2.5 - 5 \times 10^8$	(2.3)
$Fe^{2+} + HO_2 \cdot \rightarrow Fe^{3+} + HO_2^-$	$0.72 - 1.5 \times 10^6$	(2.4)
$Fe^{3+} + HO_2 \cdot \rightarrow Fe^{2+} + O_2 + H^+$	$0.33 - 2.1 \times 10^6$	(2.5)
$\cdot OH + \cdot OH \rightarrow H_2O_2$	$5 - 8 \times 10^9$	(2.6)
$\cdot OH + H_2O_2 \rightarrow H_2O + HO_2 \cdot$	$1.7 - 4.5 \times 10^7$	(2.7)
$HO_2 \cdot + HO_2 \cdot \rightarrow H_2O_2 + O_2$	$0.8 - 2.2 \times 10^6$	(2.8)
$\cdot OH + HO_2 \cdot \rightarrow H_2O + O_2$	1.4×10^{10}	(2.9)

In both Fenton and Fenton-like processes, iron ions work as catalyst which possess active site which decomposes H_2O_2 molecules into $\cdot OH$ (Soon and Hameed, 2011). Iron is considered to function as a catalyst as Fe^{2+} ion is oxidized to Fe^{3+} ion and then reduced back to Fe^{2+} ion during the process (Wang, Liu and Sun, 2012). Catalysis process can be classified according to the phase of catalyst used. Generally, it can be classified as homogeneous and heterogeneous processes.

2.3.1   Homogeneous Process

In homogeneous Fenton process, Fenton reagents such as H_2O_2 and Fe^{2+} ions are used and only one phase is involved. The source of $\cdot OH$ production is the externally added Fe^{2+} or Fe^{3+} ions (Nidheesh, 2015). For instance, it uses iron salts as the catalyst. Moreover, it involves chemical change only and no mass transfer limitation because of its homogeneous catalytic nature (Shaobin, 2008). In other words, chemical change wholly relies on the nature of the interaction between Fenton's reagents with target compounds (Soon and Hameed, 2011).

The range of pH for the catalytic activity of homogeneous Fenton and Fenton-like processes is very narrow which ranging from 2 to 4 thus strict control of pH is required (Bagal and Gogate, 2014). Its optimum pH is around pH 3 but the pH of wastewater in many cases is either neutral or alkali (Nidheesh, 2015). Gogate and Pandit (2004) state that at lower pH (pH< 2.5), $[Fe^{2+}(H_2O)]^{2+}$ are formed and it reacts more slowly with H_2O_2. Consequently, less amount of $\cdot OH$ is produced thus degradation efficiency also reduced. Moreover, H^+ ions will scavenge the $\cdot OH$ especially at very low pH and reaction between Fe^{3+} ions with H_2O_2 is prohibited. At higher pH (pH> 4), free iron species decrease in solution as the production of ferrous complexes with buffer restraining the production of free radicals and precipitation of ferric oxyhydroxide prohibits reformation of Fe^{2+} ions. Thus, decomposition rate decrease. In addition, increment in pH will decrease oxidation potential of $\cdot OH$. Thus, in order to have effective Fenton reaction, large amount of acid is required to add to reaction medium to achieve pH 3 of solution (Garrido-Ramirez, Theng and Mora, 2010).

In homogeneous process, extensive amount of ferric hydroxide sludge will be produced (Garrido-Ramirez, Theng and Mora, 2010). During the process, there is an increment of quantity of Fe^{3+} ions with reaction time but generation rate of Fe^{2+} ions is slow. Insoluble complexes are formed because of the increased concentration of Fe^{3+} ions. In addition, there is also an increment of concentration of hydroxyl ions (OH^-) with the reaction and lead to the further production of iron sludge as pH of solution is increased.

The generation of sludge lead to the disposal and other environmental problems (Garrido-Ramirez, Theng and Mora, 2010). Due to the large amount of sludge is produced, additional downstream treatment is required (Nidheesh, 2015). The downstream treatment is required to increase the pH, precipitate and settle ferric hydroxide. However, there is a difficulty to separate it due to the colloidal features of resulting dispersion (Araujo, et al., 2011). Last but not least, catalyst loss in homogeneous process is high as the amount of Fe^{2+} ions spent increases with the increment of reaction time.

Possible mechanism for the homogeneous Fenton and Fenton-like oxidation of organic compounds is shown in Figure 2.1. Babuponnusami and Muthukumar (2014) states that homogeneous Fenton and Fenton-like processes follow a complex mechanism. Desired $\cdot OH$ is produced through the chain initiation reaction (Equation 2.1). However, Fe^{2+} ions (Equation 2.3), H$_2$O$_2$ (Equation 2.7) and hydroperoxyl radicals $(HO_2 \cdot)$ (Equation 2.9) will scavenges $\cdot OH$. $\cdot OH$ may also be auto scavenged (Equation 2.6). Moreover, H_2O_2 may act both as radical generator (Equation 2.1) and as scavenger (Equation 2.7).

Figure 2.1: Possible Mechanism for the Homogeneous Fenton and Fenton-like Oxidation of Organic Compounds (Bouasla, Ismail and Samar, 2012)

2.3.2   Heterogeneous Process

Heterogeneous process involves solid and liquid phase where the reaction takes place at or near interface between phases (McNaught and Wilkinson, 1997). The application of heterogeneous catalyst can solve the limitations of homogeneous process. Catalyst consists of surface Fe^{2+} and Fe^{3+} ions which are the source of $\cdot OH$ generation that is different from homogeneous Fenton process (Nidheesh, 2015). The examples of heterogeneous catalysts are iron materials, goethite (α- FeOOH), Fe_3O_4, α- Fe_2O_3 and so on.

In heterogeneous process, besides chemical changes, it also depends on the physical steps arise on the catalyst's surface at the active sites where mass transfer limited adsorption of reactants happens. Products are desorbed from the active sites at the end of the reaction and new reactants can adsorb on the active sites. Therefore, kinetic rate, efficiency and stability of solid catalyst are strongly affected by their surface characteristics and pore structure (Soon and Hameed, 2011).

Garrido-Ramirez, Theng and Mora (2010) stated that heterogeneous solid catalysts were efficient in wide ranges of pH values as iron species was "immobilized" within the structure and in the interlayer of the space. Therefore, $\cdot OH$ can be generated from H_2O_2 continuously by catalyst and precipitation of iron hydroxide can be avoided.

Heterogeneous process is able to reduce the formation rate of sludge. Rate of sludge production is affected by catalyst's metal leaching properties. The production of sludge will increase when there is an increment in leaching rate. In general, there is slight leaching of metal ions from catalyst which lead to insignificant sludge production (Nidheesh, 2015).

No additional sludge treatment is needed for heterogeneous process as leaching of metal ions from catalyst is very limited (Araujo, et al., 2011). Furthermore, amount of iron species is less consumed as compared to homogeneous process. This is because of the very low leaching properties of catalyst. After the process, solid catalyst is easy to be recovered from liquid products.

For a chemical reaction mechanism, it comprises a series of elementary processes which illustrate how the overall reaction proceeds (Palanna, 2009). Possible mechanism for the heterogeneous Fenton and Fenton-like oxidation is shown in Figure 2.2. In analogy to Haber-Weiss mechanism, the activation of H_2O_2 through iron-surface species is accomplished by a few of steps (Kwan and Voelker, 2003). The surface Fe^{2+} react with H_2O_2 to form surface Fe^{3+}, $\cdot OH$ and OH^- (Equation 2.10). Meanwhile, surface Fe^{3+} react with H_2O_2 to form surface Fe^{2+}, $HO_2\cdot$ and H^+ (Equation 2.11) (Shi, et al., 2016). The generated $\cdot OH$ is able to degrade numerous organic substrates.

$$Fe^{2+}_{surface} + H_2O_2 \leftrightarrow Fe^{3+}_{surface} + \cdot OH + OH^- \qquad (2.10)$$

$$Fe^{3+}_{surface} + H_2O_2 \leftrightarrow Fe^{2+}_{surface} + HO_2\cdot + H^+ \qquad (2.11)$$
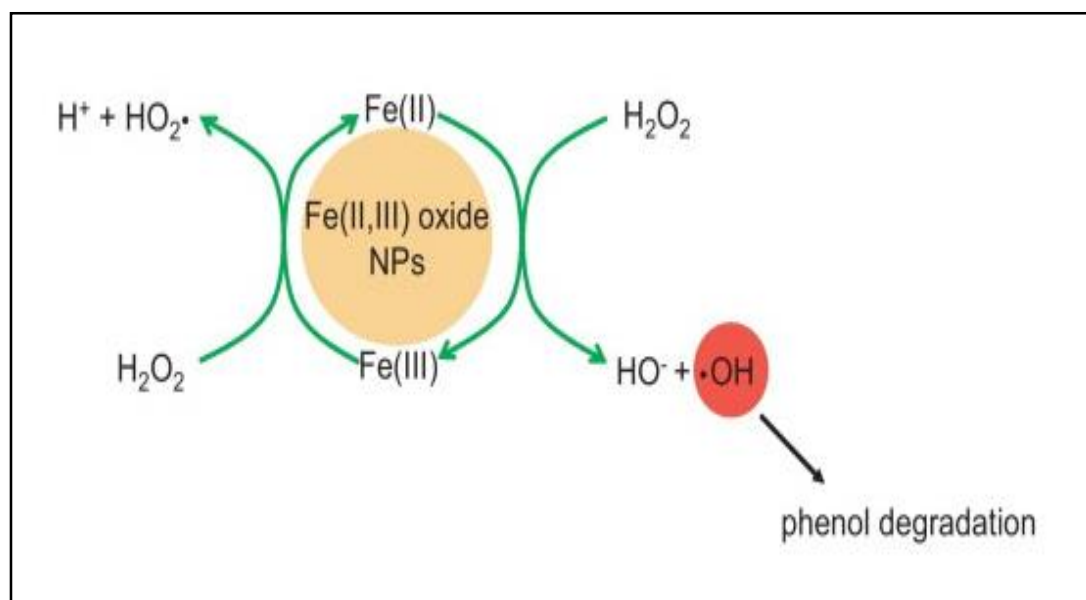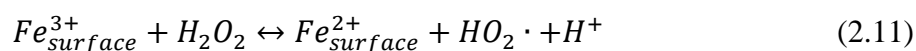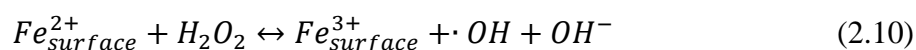
Figure 2.2: Possible Mechanism for the Heterogeneous Fenton and Fenton-like Oxidation of Phenol Degradation (Rusevova, Kopinke and Georgi, 2012)

The comparison of homogeneous and heterogeneous Fenton and Fenton-like processes under different phenomena is concluded in Table 2.4.

Table 2.4: Comparison of Homogeneous and Heterogeneous Fenton and Fenton-like Processes under Different Phenomena

Phenomena	Homogeneous Process	Heterogeneous Process
Phase	Single phase.	Involves solid and liquid phases.
Mechanism	Chemical reaction takes place solely.	Chemical reaction and dual processes of physical adsorption and desorption take place.
pH	Narrow acidic pH range, pH adjustment is required before and after.	Wide pH range.
Sludge Production	Large amount of solid sludge will be produced	Insignificant sludge production, depends on the metal leaching properties of catalyst
Downstream Treatment	Required.	Not required.
Catalyst Loss	High as the amount of Fe^{2+} ions spent increases with the increment of reaction time	Amount of iron species is less consumed as leaching of metal ions from catalyst is very limited

2.4   Iron Oxide

Iron oxides are present mainly in earth crust. It is applied in many fields extensively such as catalytic reactions, corrosion processes and electromagnetic devices. This is because it is inexpensive and relatively non-toxic as compared to other transition metals such as chromium and copper (Hou, et al., 2014). Fe_3O_4, α- $FeOOH$, γ- Fe_2O_3 and α- Fe_2O_3 are wisely employed in heterogeneous catalysis process (Pouran, Rahman and Daud, 2014). They are attractive options in treating the polluted soil, groundwater and wastewater. Especially, Fe_3O_4 has been reported as efficient catalyst

in heterogeneous Fenton (Liang, et al., 2014) and Fenton-like processes (Hou, et al., 2014).

In this study, Fe₃O₄ has been used as the heterogeneous catalyst. It is found in nature as mineral Fe₃O₄ and as a black powder in laboratory. It consists of both Fe^{2+} and Fe^{3+} ions and exhibit permanent magnetism. Fe₃O₄ in bulk is known as natural magnet because of its ferromagnetic behaviour (Morel, Martínez, and Mosquera, 2013). It also consists of the highest iron content among α- Fe₂O₃, limonite and siderite (Singh, Mukherjee and Dhillon, 2010).

It is also known as Fe₃O₄ with chemical formula of $(Fe^{3+})_{tet}[Fe^{2+}Fe^{3+}]_{oct}O_4$. Crystal structure of Fe₃O₄ is formed by the inverse spinel with a unit cell comprises thirty-two O atoms in a face-centred cubic structure and a unit cell edge length of 8.3963 Å. Fe^{2+} ions are located in octahedral sites only whereas Fe^{3+} ions are located in both octahedral sites and tetrahedral sites equally (Pouran, Rahman and Daud, 2014). Figure 2.3 and Figure 2.4 shows the crystal structure of Fe₃O₄ in a unit cell and arrangement of octahedral and tetrahedral respectively.
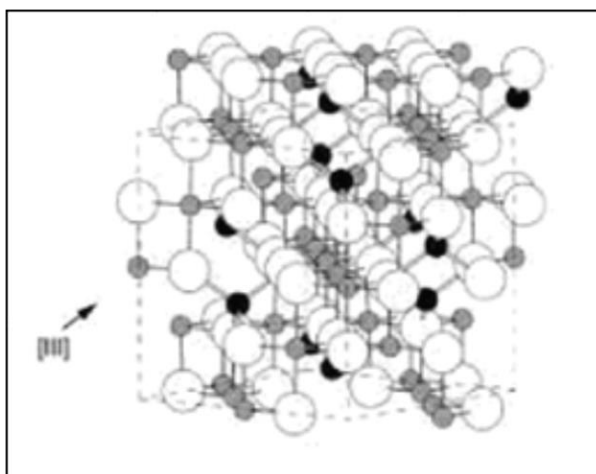
Figure 2.3: Crystal Structure of Fe₃O₄ in a Unit Cell (Cornell and Schwetmann, 2003)
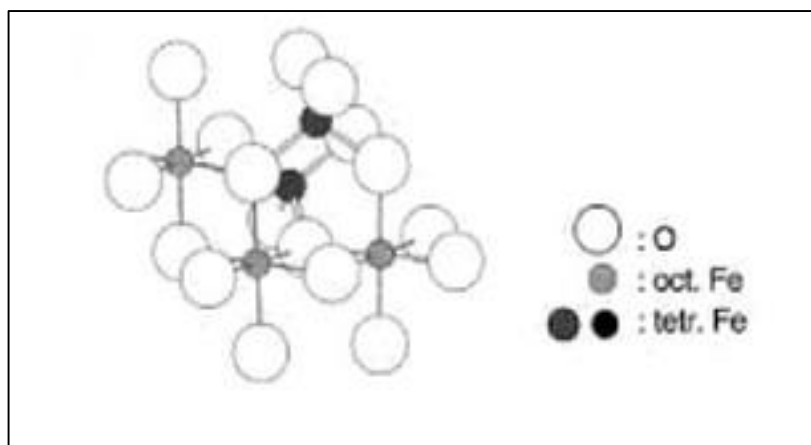
Figure 2.4: Crystal Structure of Fe₃O₄ of the Arrangement of Octahedral and Tetrahedral Position (Cornell and Schwetmann, 2003)

Application of Fe₃O₄ as heterogeneous Fenton catalyst is gaining considerable attention nowadays as it displays several features that are crucial for Fenton and Fenton-like processes. Firstly, it contains Fe^{2+} and Fe^{3+} ions which should have a positive effect on catalytic activity. According to Haber-Weiss mechanism, Fe^{2+} ions play significant role as an electron donor to initiate Fenton reaction (Nidheesh, 2015). Secondly, iron species allow reversible oxidation and reduction while structure is unchanged as the octahedral sites are occupied by both Fe^{2+} and Fe^{3+} ions (Liang, et al., 2013). Therefore, Fe₃O₄ could provide high catalytic activity in oxidation processes due to its special structural characters (Munoz, et al., 2015). Thirdly, Fe₃O₄ possesses peroxidase-like activity and can activate H₂O₂ (Hou, et al., 2014). In addition, strong magnetism of Fe₃O₄ is advantageous to the application in wastewater decontamination with facile recycle as separation of it from aqueous medium by means of magnetic separation (Liang, et al., 2013). It is also capable to function steadily without significant loss of mass (Nidheesh, 2015).

2.4.1   Heat-treated Fe₃O₄

Phase transition of Fe₃O₄ into γ- Fe₂O₃ and α- Fe₂O₃ can be achieved through heat treatment. γ- Fe₂O₃ is a metastable phase of iron oxide. It is the intermediate form of

Fe_3O_4 and α- Fe_2O_3. In addition, it can be considered as an entirely oxidised Fe_3O_4 (Khan, et al., 2015). Fe_3O_4 and γ- Fe_2O_3 have different structures although both of it present ferromagnetic behaviour. Fe_3O_4 consists of Fe^{2+} and Fe^{3+} ions whereas γ- Fe_2O_3 only consists of Fe^{3+} ions and vacancies in their sub-lattices (Can, Coskun and Firat, 2012). On the other hand, α- Fe_2O_3 is the most stable phase of iron oxide (Kazeminezhad and Mosivand, 2014) and exhibits the canted antiferromagnetism. It consists of only Fe^{3+} ions like γ- Fe_2O_3 but it has no periodic vacancies. Fe_3O_4 and γ- Fe_2O_3 have cubic cells while α- Fe_2O_3 has a rhombohedral crystal structure (Can, Coskun and Firat, 2012).

Khan, et al. (2015) reported that Fe_3O_4 nanoparticles (black in colour) heated in furnace at 300 to 400 °C for 20 min was transformed to γ- Fe_2O_3 (reddish brown in colour). Whereas Fe_3O_4 nanoparticles (black in colour) heated in furnace 600 and 800 °C for 60 min was transformed to α- Fe_2O_3 (dark red in colour). Different colour of the heated Fe_3O_4 nanoparticles showed different phases of iron oxide. From the results obtained, it can be concluded that Fe_3O_4 transformed to γ- Fe_2O_3 at lower temperature as compared to α- Fe_2O_3. This is due to Fe_3O_4 and γ- Fe_2O_3 have cubic closed packed (CCP) anion arrangement but the conversion of Fe_3O_4 to α- Fe_2O_3 requires change of CCP anion arrangement to hexagonal closed packed (HCP). Therefore, Fe_3O_4 can only transform to α- Fe_2O_3 at a higher temperature as substantial rearrangement of ions are required.

Kwan and Voelker (2003) reported that heterogeneous Fenton reaction happens at the surface of catalyst and the rate of production of $\cdot OH$ depends on the concentration of H_2O_2 and the surface area of iron oxide. Khan, et al. (2015) had founded that the size of Fe_3O_4 was the smallest followed by γ- Fe_2O_3 and α- Fe_2O_3 when it was synthesised through heat treatment. So, the rate of production of $\cdot OH$ of Fe_3O_4 may be higher than the γ- Fe_2O_3 and α- Fe_2O_3 since it has the highest surface area. Furthermore, Kwan and Voelker (2003) also concluded that ferric oxides are catalytically less active than their ferrous counterpart. Moreover, degradation of 2,4,6-trinitrotoluene by using ferric oxide such as γ- Fe_2O_3, α- Fe_2O_3 and α- FeOOH were less effective than those minerals embodying both Fe^{2+} ions and Fe^{3+} ions, such as

Fe$_3$O$_4$ (Matta, et al. 2007). As a conclusion, Fe$_3$O$_4$ is expected to have higher catalytic activity than γ- Fe$_2$O$_3$ and α- Fe$_2$O$_3$.

2.4.2   Characterization of Fe$_3$O$_4$

Characterization of a heterogeneous catalyst relates to the determination of its physical and chemical characteristics that are liable for its performance in a reaction. The principle purpose of catalyst characterization is to comprehend the relationship among physical, chemical and catalytic properties. Various types of characterization techniques are utilised to identify the physical and chemical properties of catalyst and relate these to its activity. Therefore, in this research, the developed catalysts will be characterized by XRD and SEM-EDX.

XRD is a powerful non-destructive technique which utilizes an X-ray beam to give details on structure, phases, preferred crystal orientations and other structural parameters, for instance grain size, crystallinity, strain and crystal defects (EAG, 2015). Basic principle of XRD is shown in Figure 2.5. The incident beam and diffracted beam are coplanar while the angle between the incident and scattered beam is 2θ. Bragg law is an easy way to describe the diffraction X-rays by a crystal (He, 2009). If the waves represented by 1' and 2' are in phase, a reflected beam of maximum intensity will obtain. According to Bragg law (Equation 2.12), the difference in path length between 1 to 1' and 2 to 2' must be an integral number of wavelengths.

$$n\lambda = 2d \sin\theta \qquad\qquad (2.12)$$

where n = integer

λ = wavelength of X-rays

d = d-spacing

θ = half scattering angle

A diffraction pattern which represents the periodic d-spacing present in sample is possible to be obtained by monitoring the reflected intensity versus 2θ. Several

diffraction peaks will be presented depending on the crystal structure of material in the case of polycrystalline material. On the other hand, the diffraction pattern will be formed by a single diffraction peak representing the mean d-spacing in the case of layered materials with a *d*-spacing (Martucci, 2014). Diffraction peaks for Fe_3O_4 are at 2θ = 18.2, 30.0, 35.4, 43.0, 53.4, 56.9, 62.5 and 74.0 °, marked by (111), (220), (311), (400), (422), (511), (440) and (533) (Wang, Wei and Qu, 2013).
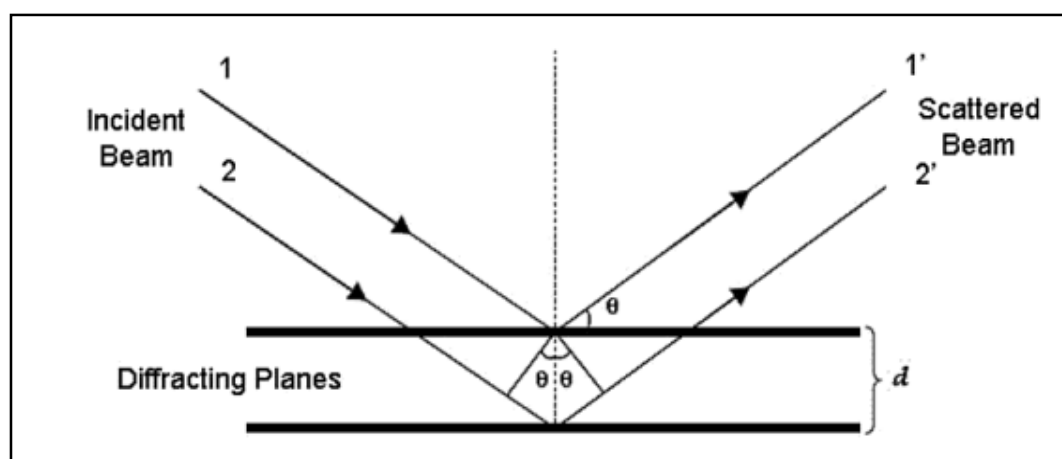
Figure 2.5: Representation of XRD Process. Angle θ is Made by Two Parallel Incident Rays 1 and 2 with the Diffracting Parallel Planes at a Distance *d* (Martucci, 2014)

The crystalline size of materials can be calculated from XRD pattern using the Scherrer equation (Abbas, et al., 2015).

$$D = \frac{K\lambda}{\beta cos\theta} \qquad (2.13)$$

where

K = shape factor, 0.9

λ = wavelength of X-ray, 1.540562 Å

β = full width at half maximum (FWHM), °

θ = Bragg angle for the studied peak, °

SEM is one of the most useful instruments for investigating the topography and morphology of samples. Generally, when there is an interaction between electrons and specimen with different mechanisms, signals such as backscattered electrons, secondary electrons, Auger electrons, characteristic X-rays, cathodoluminescince are produced. Any signal that is produced by electron beam can produce an image of the scanned surface region (Carlton, 2011). The samples for SEM must be electrically conductive to avoid a charge build up in sample that influences the incoming primary and emitted secondary electrons, causing in a poor and distorted image that is constantly altering in contrast and location. The sample which is non-electrically conductive must be coated with a thin conductive layer, for instance carbon or metal (ASM International and Lampman, 2003). EDX is complementary to SEM. EDX is utilized to identify the presence and relative abundance of elements that compose the sample surface. When an energetic electron beams reaches the surface of sample, X-ray photon are produced and detected. Energy of X-ray photon depends on which atom they came from (Olea-Mejia, et al., 2014).

2.5   Parameter Studies

2.5.1   Effect of Various organic dyes

Degradation rate was depending on the structure of organic dyes (Abo-Farha, 2010). Hence, different organic dyes will have different degradation rates by Fenton and Fenton-like processes as every organic dye has their own unique structures.

Based on the study of Su, et al. (2011), the degradation rates for reactive black 5, reactive orange 16 and reactive blue 2 were 96.3, 98.1 and 63.6 % respectively after 100 min. In addition, they found that rate of COD removal for reactive black 5, reactive orange 16 and reactive blue 2 were 31.2, 45.7 and 7.8 %, respectively. The degradation rate and COD removal rate for reactive orange 16 was higher than reactive black 5 and reactive blue 2 due to the simple structure and azo bond in reactive orange 16. Colour loss were resulted by the cleavage of the N=N bond of dyes. Reactive black 5 had two

N=N bonds whereas complex Reactive Blue 2 were only slightly cleaved. Thus, degradation rate of Reactive Blue 2 was the lowest.

From the study reported by Tantak and Chaudhari (2006), complete colour removal (>99 %) for 50 mg/L acid orange 7 can be accomplished by Fenton's reagent rapidly. Arslan-Alaton, Gursoy and Schmidt (2008) also reported that colour removal was practically complete within the first 2 min. Colour removal for azo dyes (acid red 183 and acid orange 51) and for reactive dye reactive blue 4 was 99 and 93 % respectively after 30 min. Generally, the fast colour removal of dyes is due to adequate $\cdot OH$ are generated by fast reaction between Fe^{2+} ions and H_2O_2 which cleave the dye chromophores promptly. The degradation of dye's chromophores at high percentage (90 %) can be achieved by the in situ formed oxidants that have enough oxidation capability.

On the other hand, Xu, et al. (2004) also reported the colour removals for acidic, reactive, direct and cationic dyes were range from 87 and 100 % and total organic carbon (TOC) removals were range from 56 to 79 %. Meanwhile, the colour and TOC removals for disperse and vat dyes were range from 30 to 56 % and 21 to 34 % respectively. According to the results, it can be concluded that molecules of disperse and vat dyes are harder to be destroyed by Fenton process. Moreover, the TOC removal of dyes is difficult as compared to colour removal. This indicates that the chromophoric groups are damaged and are partly mineralized to carbon dioxide and water during the degradation of dyes. Some colourless degradation intermediate compounds for instance adjacent aromatic ring structure are formed during reaction even though the chromophoric structures of dye molecules are damaged by $\cdot OH$.

2.5.2   Effect of Fe₃O₄ Dosage

The loading of Fe_3O_4 is a considerable parameter in determining the efficiency of Fenton and Fenton-like processes. Generation of $\cdot OH$ is depends on Fe_3O_4 dosage dependence and it can be seen from Equation 2.1 that discussed in Section 2.3.1. $\cdot OH$ are generated by the catalytic decomposition of H_2O_2 by Fe^{2+} ions.

The increase in the Fe_3O_4 dosage will increase the efficiency of degradation. Yaman and Gündüz (2015) have reported colour removal slightly increased from 97 to 100 % after 2 h of reaction by doubling the amount of catalyst. The increment of amount of catalyst also increased the COD reduction from 52 to 81 %. The increment in COD removal may be enhanced by the production of more $\cdot OH$. In addition, degradation is enhanced as more active catalytic site of Fe^{2+}/Fe^{3+} species is provided by the increase of amount of catalyst.

However, degradation rate will decease when there is an overdose of Fe_3O_4. This is because $\cdot OH$ will be scavenged by excessive Fe^{2+} which resulting in reduced degradation efficiency (Bagal and Gogate, 2014). It can be shown in Equations 2.3 and 2.4. Ali, Gad-Allah and Badawy (2013) had reported that the degradation rate was increased with the increment of catalyst concentration until reaching the highest value. After that, there was a slight decrease in the degradation rate due to the further increase of catalyst. Eventually, treatment cost will increase because amount of sludge increases due to the usage of excessive amount of iron salts (Bagal and Gogate, 2014).

2.5.3   Effect of H_2O_2 Dosage

H_2O_2 is a strong oxidizing agent and its dosage plays an important role in determining the overall degradation rate. When H_2O_2 dosage increases, degradation percentage of degradation of pollutants will increase (Babuponnusami and Muthukumar, 2014). However, excess amount of H_2O_2 should be avoided as unused portion of H_2O_2 during the process will contribute to COD. Excess H_2O_2 will affect the degradation efficiency as well as harmful to many organisms. According to Bagal and Gogate (2014), an optimum H_2O_2 dosage exists where maximum degradation of organic pollutants is obtained and excessive H_2O_2 dosage could decrease the degradation rate.

Yaman and Gündüz (2015) reported the initial rate of colour removal was positively affected when there was an increment of H_2O_2 concentration from 0.007 to 0.033 M. This is because the increase in the amount of H_2O_2 increases the formation

rate of $\cdot OH$. It can be shown in Equation 2.1. However, the initial degradation is slowed down when increasing the H₂O₂ concentration from 0.033 to 0.07 and to 0.267 M. This is due to H₂O₂ also acts as the scavenger to produce free radicals when there are large quantities of H₂O₂ and it can be seen in Equation 2.7 (Bagal and Gogate, 2014).

Furthermore, Yaman and Gündüz (2015) also reported that COD removal at all H₂O₂ dosage is significantly lower than colour removal. Precedence of the $\cdot OH$ attack on the N = N bonds and the slower devastation of the aromatic or olefinic carbons in dye is signified by the results. The increase in concentration of H₂O₂ will increase the treatment cost as the use of H₂O₂ (Bagal and Gogate, 2014). Therefore, it is crucial to optimise the H₂O₂ dosage in such a way that entire amount is used up.

2.5.4   Effect of Dye Concentration

Another significant parameter that will affect the degradation rate is the initial concentration of organic dye. On the basis of collision theory of chemical reactions, concentration of reactant is an important parameter in reactions. Hashemian (2013) reported the rate of degradation increased when there was an increment of initial dye concentration. This is because the frequency of collision between reactants increases when concentration of reactants increases. Moreover, the frequency of effective collision that causes a reaction to happen will also be high (Hassan and Hameed, 2011). Life time of $\cdot OH$ is very short such as only a few nanoseconds and can only react where they are formed. Thus, the increment of the quantity of dye molecules per volume unit enhances the probability of collision between dyes and $\cdot OH$. Eventually, degradation rate is increased.

On the other hand, Bouasla, Ismail and Samar (2012) observed that degradation of dye decreased from 97.5 to 67.26 % within 25 min when concentration of dyes increased from 0.03 to 0.15 mmol/L. In addition, according to the study that had been done by Ali, Gad-Allah and Badawy (2013), methyl orange took longer time to be degraded when its concentration was high. For example, for the 10, 20 and 40 mg/L

of methyl orange concentration, concentration of methyl orange was below the detectable level after 30 min whereas for 60 and 80 mg/L methyl orange concentration, 120 min was required for degradation rate of 99 and 97 % respectively. This is due to the increment of initial concentration cause an increase of the number of dye molecules but not the concentration of $\cdot OH$. Eventually, the number of $\cdot OH$ available for the complete destruction of organic compounds is insufficient (Bagal and Gogate, 2014). On top of that, excessive dye molecules are adsorbed onto the surface of catalyst at higher concentration of dyes. Consequently, the efficiency of catalyst to degrade dye molecules is limited (Abdullah and Pang, 2010).

2.5.5 Effect of Temperature

Temperature has a crucial role to increase the extent of degradation of dye with the production of $\cdot OH$ as it is a thermodynamic state function that increases the feasibility of a chemical process. As per Arrhenius law, the rate of $\cdot OH$ formation increases in a higher temperature. However, at higher temperature, the decomposition of H_2O_2 into oxygen and water will be accelerated (Velichkova, et al., 2013). This is because the decomposition of H_2O_2 to oxygen and water is affected by the evolution of heat. The rate of decomposition of H_2O_2 will be increased with temperature at about 2.3 times per 10 ℃ rise (Jones, 1999). A beneficial effect was shown in the study of Velichkova, et al. (2013) when there was an increment of temperature from 30 to 60 ℃.

Based on the study of Medien and Khalil (2010), an increment in the extent of dye degradation was observed during the reaction temperature raised from 298 to 328 K. The rate and extent of degradation of reaction were practically no difference in temperature between 323 and 328 K. The rates of degradation were decreased at higher reaction temperature more than 328 K. The decrease in rate of degradation might due to the thermal decomposition H_2O_2. Consequently, effective concentration of H_2O_2 for producing $\cdot OH$ was decreased. Thus, lower conversion of dye is happened at higher temperature.

Yaman and Gündüz (2015) reported when the temperature increased from 298 to 333 K, the degradation rate was increased clearly. Degradation and mineralization will increase with the increase of the reaction temperature on the basis of Arrhenius law (Queirós, 2015). This is because there is an increase in the collision frequency of the molecules at catalyst surface and the fraction of molecules that possess energy in surplus of the activation.

2.5.6   Effect of pH

In Fenton and Fenton-like processes, pH of wastewater is very crucial. It has been reported that the activity of catalyst, the activity of oxidant, the dominant iron species, and the stability of H_2O_2 will be controlled by pH of solution (Xu and Wang, 2011). In classic Fenton process, the optimum pH was found to be around 3 regardless of target substrate. However, in heterogeneous Fenton process, catalysts still can work efficiently in a wide pH range (Nidheesh, 2015). Garrido-Ramirez, Theng and Mora (2010) reported that iron oxide catalyst did not require strict control of pH that was similar to homogeneous Fenton process as Fe/H_2O_2 heterogeneous system can catalyse oxidation of pollutants through Fenton-like reaction at pH values between 3 and 7.

At acid conditions, degradation rate is higher as Fe^{2+} ions and H_2O_2 are more stable when pH ranges from pH 3 to 4. At very acidic pH values such as below 2, reaction between Fe^{2+} ions and H_2O_2 slows down as H_2O_2 can keep stable to form an oxonium ion ($H_3O_2^+$) by proton solvation as presented by Equation 2.14. $H_3O_2^+$ ions will reduce the reactivity of H_2O_2 with Fe^{2+} ions by making H_2O_2 to be electrophilic and enhancing its stability (Kwon, et al., 1999). Meanwhile, the existed complex species such as $[Fe(H_2O)_6]^{2+}$ and $[Fe(H_2O)_6]^{3+}$ also react with H_2O_2 more slowly. Moreover, scavenging effect of H^+ ions could consume $\cdot OH$ which will limit the degradation rate and it is presented by Equation 2.15 (Hassan and Hameed, 2011).

$$H_2O_2 + H^+ \rightarrow H_3O_2^+ \tag{2.14}$$

$$\cdot OH + H^+ + e^- \rightarrow H_2O \qquad (2.15)$$

In contrast, at higher pH values such as greater than 3, efficiency of oxidation decreases speedily as H_2O_2 becomes unstable. H_2O_2 begins to decompose rapidly into oxygen and substantial amounts of $\cdot OH$ do not formed. The formed oxygen is not able to oxidise the organics efficiently in mild operating conditions used (Hassan and Hameed, 2011). Lee, Oh and Park (2005) reported that modified iron oxide could degrade phenol efficiently up to neutral pH (pH = 7) as it was virtually insoluble and ferric hydroxide was not formed. However, it could not degrade phenol above pH 7 as $\cdot OH$ reacted with OH^- or H_2O_2 faster than organic compounds above pH 7. In addition, Zhuang, et al. (2015) reported that heterogeneous Fenton process with FeOx/SBAC catalyst could remove refractory pollutants efficiently over a wide range of pH as the catalyst possessed large specific surface area and high point of zero charge (7.6). These promoted the exposure of iron oxide to H_2O_2 at high pH and improved the $\cdot OH$ generation rate, further weakening the pH effect of solution.

2.6 Reusability Study

Reusability of catalyst is very important and it is necessary to be studied for economic and environmental reasons. The cost of wastewater treatment can be reduced by the reusability of catalyst. The advantage of heterogeneous process over homogeneous process is that catalyst can be reused. In homogeneous process, the iron content in solution decreases with longer reaction time due to sludge formation (Nidheesh, 2015). The remaining Fe^{2+} ions are hard to be separated from solution as it is homogeneously dissolved in water. However, in heterogeneous process, catalysts are solid thus it is not difficult to be separated from solution.

Zhang, et al. (2008) examined reusability of ferromagnetic nanoparticles by repeating phenol removal experiment for five times utilizing same ferromagnetic nanoparticles reproduced easily by sonication and rinsing by deionized water. The ferromagnetic nanoparticles' catalytic activity still remained almost 100 % after 5 rounds of catalytic cycle. In addition, magnetic recovery of ferromagnetic

nanoparticles can prevent secondary pollution such as generation of sludge. This was further reduced the cost per treatment. On the other hand, Nidheesh (2015) also reported Fe_3O_4 displayed higher stability even after five cycles. In addition, the reusability of Fe_3O_4 was studied by Zhuang, et al. (2008). It was found that catalytic activity of Fe_3O_4 was almost remains unchanged after three catalytic cycles.

Khataee (2015) evaluated the catalytic stability of plasma treated Fe_3O_4 in degradation of basic blue 3 dye by performing four continuous experiments at similar conditions. Catalyst was then separated from treated solution by an external magnetic field. After that, it was rinsed with distilled water and dried. Next, it was used for next test. The results showed that after four degradation cycles, the degradation efficiency of plasma treated Fe_3O_4 was still high. Thus, nanostructured Fe_3O_4 can be reused effectively without great activity loss.

2.7   Kinetic Study

Fundamental understanding of reaction kinetic is useful information for up-scale of catalytic chemical processes. Generally, chemical kinetics involves the experimental determination and analysis of quantity of a substance as a function of time. Rate of change in mass of chemicals per unit of time is described in terms of concentration rather than amount in kinetic process as the free concentration of a chemical is the driving force for its kinetics (Roberts, James and Williams, 2015). The "order" of the process is the power to which concentration is increased in the kinetic equation.

Kinetics of pollutant degradation by Fenton and Fenton-like oxidation processes follow the pseudo first or pseudo second reaction order. Liang, et al. (2014) reported that the degradation of acid orange II by Mn substituted magnetite was well fitted with pseudo first-order kinetic equation. Similar result was obtained by Sun and Lemley (2011) that the degradation rate of p-Nitrophenol followed the pseudo first-order degradation kinetics. On the other hand, He, et al. (2014) reported that the degradation of catechol and 4-chlorocatechol were best fitted with pseudo second-order kinetic equation.

CHAPTER 3

METHODOLOGY

3.1   Materials and Chemicals

Chemical reagents that will be used in this experiment and their specifications are listed in Table 3.1. pH of solution will be adjusted by hydrogen chloride (HCl) and sodium hydroxide (NaOH).

Table 3.1: Chemicals Used in Experiment and Their Specifications

Chemical Reagent	Purity (%)	Brand	Usage
Acid orange G	80	Sigma-Aldrich	Model pollutant
Congo red	40	R & M	Model pollutant
Fe_3O_4 nanopowder, 50-100 nm	97	Sigma-Aldrich	Catalyst
H_2O_2	30	Sigma-Aldrich	Source of $\cdot OH$
HCl	37	Sigma-Aldrich	pH adjustment
Iron (III) chloride hexahydrate	100	Friendemann Schmidt Chemicals	Standard solution for ICP-OES
Malachite green	99	Fisher Scientific	Model pollutant
Methyl orange	85	R & M	Model pollutant
Methylene blue	82	R & M	Model pollutant
NaOH powder	97	Sigma-Aldrich	pH adjustment
Rhodamine B	95	Sigma-Aldrich	Model pollutant

The model pollutants used in this study are acid orange G, congo red, malachite green, methylene blue, methyl orange and rhodamine B. Chemical structures and classifications of model pollutants are listed in Table 3.2.

Table 3.2: Chemical Structures and Classifications of Model Pollutants
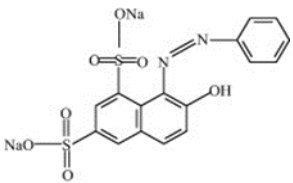
Dye	Chemical Structure	Classification	Molecular Weight (g/mol)	Maximum absorption wavelength, λ (nm)
Acid orange G		Anionic acid azo	452.37	479
Congo red		Anionic direct diazo	696.67	498
Malachite green		Cationic basic triarylmethane	364.911	619
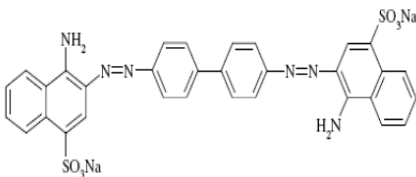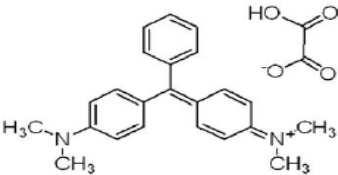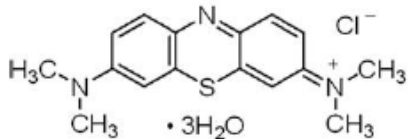
Dye	Chemical Structure	Classification	Molecular Weight (g/mol)	Maximum absorption wavelength, λ (nm)
Methylene blue		Cationic basic thiazine	373.88	665
Methyl orange		Anionic acid azo	327.33	464
Rhodamine B		Cationic basic xanthene	479.02	555
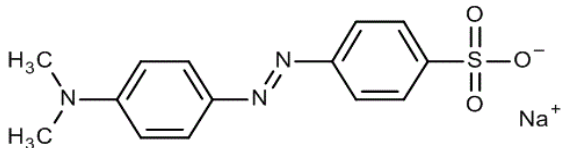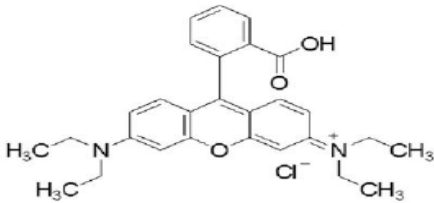
3.2   Equipments

The instruments needed for this study are presented in Table 3.3 together with their model. Furnace is used for heat treatment of Fe_3O_4. XRD and SEM-EDX are used for characterization of heat-treated Fe_3O_4. COD reactor was used to heat sample with COD digestion reagent vials. Analysis of liquid samples will be done by using ultraviolet-visible-infrared (UV-vis) spectrophotometer, spectrophotometer and inductively coupled plasma-optical emission spectroscopy (ICP-OES). pH meter is utilized to measure the pH of solution whereas incubator shaker is used to ensure uniform mixing of Fe_3O_4 and solution.

Table 3.3: Model of Apparatus

Apparatus	Model
Carbolite furnace	Carbolite RHF 1500
COD reactor	DRB200
ICP-OES	Optima 7000 DV
Incubator shaker	Labtech LSI-2016A
pH Meter	Eutech PC300
SEM-EDX	Hitachi SEM Model S-3400N
Spectrophotometer	DR3900
UV-vis spectrophotometer	Jenway 6320D
XRD	Shimadzu XRD-6000

3.3   Overall Experiment Flowchart

Figure 3.1 shows the flow chart for overall research activities. Fe_3O_4 catalysts are heat-treated in furnace at different temperature. The heat-treated Fe_3O_4 catalysts are then characterized through XRD and SEM-EDX. After that, the various parameters studies are done by varying type of organic dyes, Fe_3O_4 dosage, H_2O_2 dosage, concentration of organic dye, temperature and pH of solution. The liquid samples are then analysed through UV-vis spectrophotometer, COD analysis and ICP-OES. The reusability of Fe_3O_4 is studied. Lastly, the kinetic of organic dye degradation is also studied.
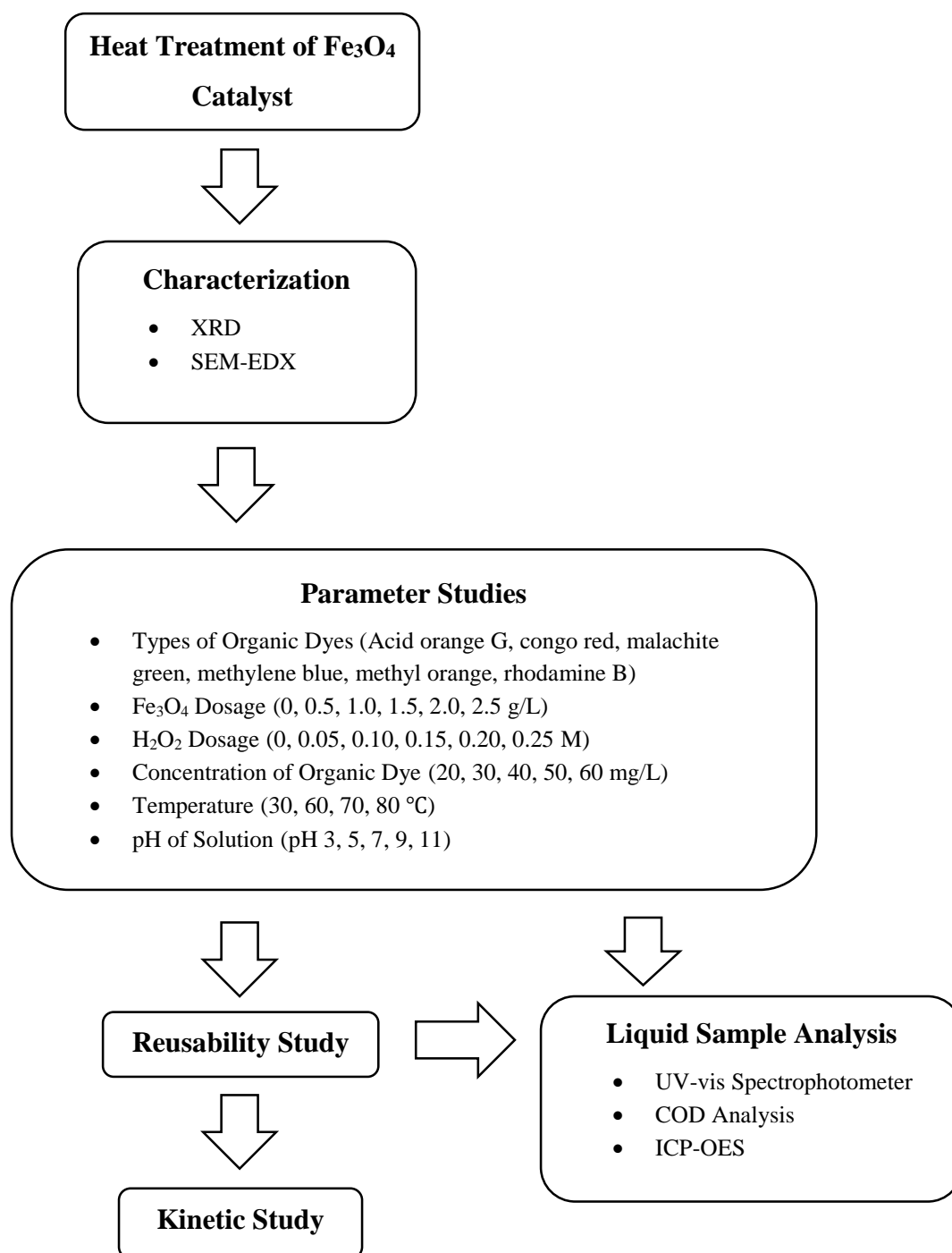
Figure 3.1: Flow Chart of Overall Research Activities

3.4   Experimental Setup

The experiment setup is shown in Figure 3.2. Incubator shaker was used to ensure uniform mixing of Fe_3O_4 in dye solution in the conical flask. Speed of agitation, time duration for mixing and temperature of the reaction can be controlled.
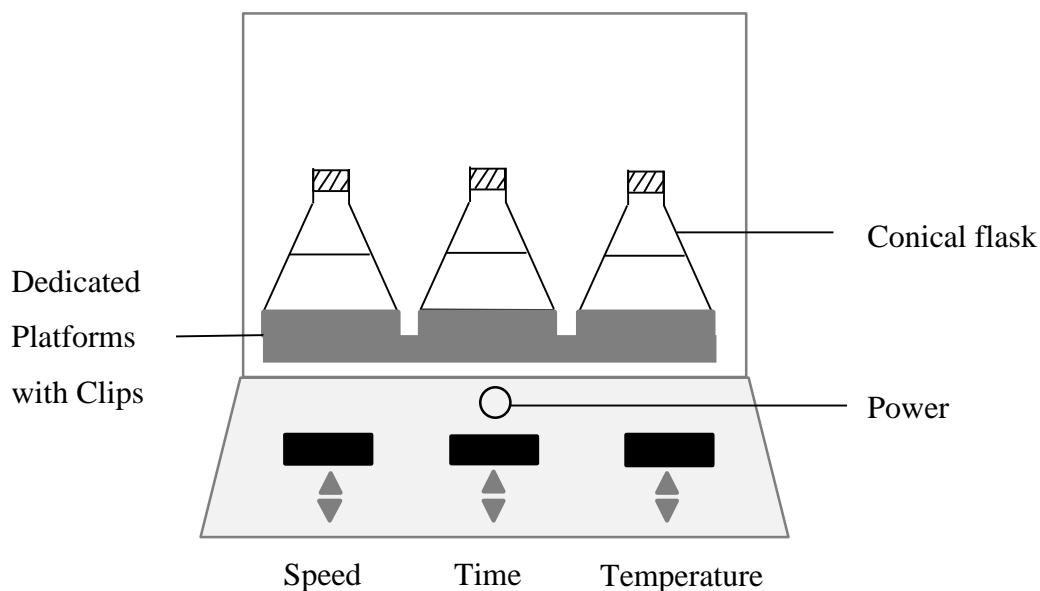
Figure 3.2: Schematic Diagram of Fenton and Fenton-like Processes using Incubator Shaker

3.5   Experiment Procedures

3.5.1   Preparation of Fe_3O_4

Fe_3O_4 was purchased from Chemolab Supplier. Five samples of original and heat-treated Fe_3O_4 were prepared. 1.5 g of Fe_3O_4 was weighted for each set. One set of Fe_3O_4 was not heat-treated and another four sets were heat-treated at temperatures of 200, 400, 600 and 800 °C in a furnace for 2 h to induce phase transformation. Original and heat-treated Fe_3O_4 at 200, 400, 600 and 800 °C were defined as Fe_3O_4-0, Fe_3O_4-200, Fe_3O_4-400, Fe_3O_4-600 and Fe_3O_4-800 respectively. Afterwards, the heat-treated Fe_3O_4 were characterized by using XRD and SEM-EDX.

3.5.2   Characterizations of Catalysts

3.5.2.1   XRD

The crystallization phase analysis was performed by XRD to study the crystalline structure of Fe_3O_4. The Cu-Kα (λ= 1.540562 Å) radiation source was manipulated at 40 kV/ 30 mA. Interference peak was removed by using K-beta filter. Divergence slit and scattering slit 1 ° together with 0.3 mm of receiving slit were applied. The sample was placed into a sample holder by smear uniformly onto a glass slide. The intensity of diffracted X-rays was recorded continuously by monitoring the diffraction pattern emerging in the 2θ ranging from 10 to 80 ° with a scan rate 2 °/min and a scan step 0.02 °. A peak in intensity happened when the mineral had lattice planes with d-spacing adequate to diffract X-rays at the value of θ.

3.5.2.2   SEM-EDX

SEM analysis was done with a scanning electron microscope in order to examine the morphological structure and measure particle size of heat-treated Fe_3O_4 catalysts. The catalysts were adhered on specimen holder by using the double-sided adhesive tape prior to observation under SEM. During sample preparation and transfer, gloves must be worn all the time to prevent contamination to SEM system. The scanning electron images were acquired by utilizing the acceleration voltage of 20 kV and magnification of 10, 20 and 40 kX. By using EDX coupled to SEM, the element composition of the catalysts was identified.

3.5.3 Parameter Studies

Varies operating parameters such as various organic dyes (Acid orange G, congo red, malachite green, methylene blue, methyl orange and rhodamine B), Fe_3O_4 dosage (0 to 2.5 g/L), H_2O_2 dosage (0 to 0.25 M), dye concentration (20 to 60 mg/L), pH (pH 3 to 11) and temperature (30 to 80 ℃) were studied for the purpose of investigating the efficiency of Fenton and Fenton-like processes.

3.5.3.1 Effect of Various Organic Dyes

Effect of various organic dyes on the rate of degradation was investigated. Six organic dyes used were acid orange G, congo red, malachite green, methylene blue, methyl orange and rhodamine B. 100 ml of organic dye solution with concentration of 20 mg/L was filled into conical flask. pH of solution was adjusted to pH 7 by utilizing 0.1 M HCl or 0.1 M NaOH. The dosages of Fe_3O_4 and H_2O_2 used were 1 g/L and 0.2 M respectively. Reaction temperature was maintained at 30 ℃ in incubator shaker with agitation at 130 rpm. The sample was withdrawn from the flask every 10 min in duration of 1 h for analysis. The experiments were carried out in six sets by using different types of organic dye solution. Malachite green was used for subsequent experiment due to its high degradation efficiency by Fe_3O_4.

3.5.3.2 Effect of Fe_3O_4 Dosage

The effect of Fe_3O_4 dosage on the rate of degradation was investigated by changing the dosage of Fe_3O_4 to 0, 0.5, 1.0, 1.5, 2.0 and 2.5 g/L. 100 ml of malachite green solution with concentration of 20 mg/L was filled into conical flask. pH of solution was adjusted to pH 7. After that, no Fe_3O_4 was added into the solution for 0 g/L. Reaction was initiated by adding H_2O_2 with dosage of 0.2 M. Then, the solution was placed into incubator shaker and agitated at 130 rpm. The experiment was conducted at room temperature of 30 ℃. The sample was withdrawn from the flask every 10 min

in duration of 1 h for analysis. The other five set was repeated by adding Fe_3O_4 and other parameters kept constant in the experiment. Fe_3O_4 with optimum dosage of 2.5 g/L was used for the subsequent experiment which varying the H_2O_2 dosage.

3.5.3.3   Effect of H_2O_2 Dosage

The dosage of H_2O_2 in 0, 0.05, 0.10, 0.15, 0.20 and 0.25 M was varied to investigate the effect of H_2O_2 dosage on the rate of degradation. Similarly, 100 ml of malachite green solution with concentration of 20 mg/L was filled into conical flask and adjusted to pH 7. After that, Fe_3O_4 with dosage of 2.5 g/L was added into the solution and no H_2O_2 was added. Next, the solution was placed into incubator shaker at 30 ℃ and agitation was provided at 130 rpm. The sample was withdrawn from the flask every 10 min in duration of 1 h for analysis. The other five set was repeated by adding H_2O_2 and other parameters kept constant in the experiment. H_2O_2 with optimum dosage of 0.20 M was used for the subsequent experiment which varying concentration of dye.

3.5.3.4   Effect of Dye Concentration

The effect of concentration of dyes was also studied by varying the concentration of malachite green solution to 20, 30, 40, 50 and 60 mg/L. 100 ml of malachite green solution with concentration of 20 mg/L was filled into conical flask. pH of solution was adjusted to pH 7. Fe_3O_4 with dosage of 2.5 g/L and H_2O_2 with dosage of 0.2 M was added into the solution. After that, the solution was placed into incubator shaker at 30 ℃ and agitated at 130 rpm. The sample was withdrawn from the flask every 10 min in duration of 1 h for analysis. The other four set of different concentration of malachite green solution were repeated by displacing the concentration 30 mg/L and other parameters kept constant in the experiment. Solution of malachite green of 20 mg/L was used for the subsequent experiment which varying the reaction temperature.

3.5.3.5   Effect of Temperature

The temperature of reaction was varied to 30, 60, 70 and 80 ℃ in the experiment thus the effect of temperature on the rate of degradation could be studied. In this experiment, 100 ml of malachite green solution with concentration of 20 mg/L was filled into conical flask and adjusted to pH 7. Fe_3O_4 with dosage of 2.5 g/L and H_2O_2 with dosage of 0.2 M was added into the solution. Then, the solution was placed into incubator shaker at 30 ℃ and agitated at 130 rpm. The sample was withdrawn from the flask every 10 min in duration of 1 h for analysis. The other three different temperatures were repeated by displacing the temperature of 30 ℃ and other parameters kept constant in the experiment. Reaction temperature of 30 ℃ was used for the subsequent experiment which varying the pH of solution.

3.5.3.6   Effect of pH

The effect of pH on the rate of degradation was also be studied by varying the pH to pH 3, 5, 7, 9 and 11. The pH of solution was adjusted by using 0.1 M HCl or 0.1 M NaOH. Similar to previous experiment, Fe_3O_4 with dosage of 2.5 g/L and H_2O_2 with dosage of 0.2 M was put into 100 ml of malachite green solution with concentration of 20 mg/L. In this case, initially pH 3 was set in this experiment. Then, the solution was placed into incubator shaker at 30 ℃ and agitated at 130 rpm. The sample was withdrawn from the flask every 10 min in duration of 1 h for analysis. The other four value of pH was repeated by replacing the pH 3 and other parameters remain unchanged in the experiment. Optimum solution pH was pH 9.

3.5.4   Reusability Study

The reusability of Fe_3O_4 catalyst was also studied. 2.5 g/L of Fe_3O_4 was placed in contact with 100 ml of malachite green solution with concentration of 20 mg/L at

pH 9. The dosage of H_2O_2 used was 0.2 M. Then, the solution was placed into incubator shaker with agitation at 130 rpm and temperature at 30 °C for 1 h. The sample was withdrawn from the flask every 10 min in duration of 1 h for analysis. The used Fe_3O_4 was then recovered by magnet. After that, it was rinsed with distilled water and dried. The Fe_3O_4 was subsequently used in another cycle keeping the same standard conditions and ratio of catalyst/dye.

3.5.5 Kinetic Study

Kinetic analysis was done in this experiment. Pseudo zero-order, first-order and second-order reaction kinetics were applied to investigate the degradation kinetics of dyes by Fenton and Fenton-like processes using Fe_3O_4 catalyst. The individual expression was shown as equations given below:

Apparent zero order reaction kinetics:

$$C_t = C_0 - k_0 t \tag{3.1}$$

Apparent first order reaction kinetics:

$$\ln C_t = \ln C_0 - k_1 t \tag{3.2}$$

Apparent second order reaction kinetics:

$$\frac{1}{C_t} = \frac{1}{C_0} + k_2 t \tag{3.3}$$

where

C_t = dye concentration at any time, $\frac{mg}{L}$

k_0 = apparent pseudo-zero order rate constant, $\frac{mg}{L \, min}$

k_1 = apparent pseudo-first order rate constant, $/min$

k_2 = apparent pseudo-second order rate constant, $\frac{L}{mg\ min}$

t = the reaction time, min

The regression analysis based on pseudo zero-order, pseudo first-order and pseudo second-order reaction kinetics for the colour of dye was conducted. A linear plot was obtained only if using correct order of reaction kinetics.

3.6 Liquid Sample Analysis

The residual concentration of organic dyes in the solution at different times of sampling was measured in order to study the course of degradation reactions. The absorbance of organic dyes was measured by using UV-vis spectrophotometer at the wavelength with highest absorbance, λ_{max}. The λ_{max} for different organic dyes is shown in Table 3.2. According to Lambert-Beer law, the organic dye concentration was quantified via a calibration curve. The degree of degradation of organic dye was computed by using Equation 3.4.

$$\text{Degradation efficiency (\%)} = \frac{C_0 - C_t}{C_0} \times 100\ \%$$ (3.4)

where
C_0 = dye concentration at time 0, mg/L
C_t = concentration of dye at time t, mg/L

COD is applied to identify the quantity of organic compounds. It is a useful measurement indicator of water quality. For COD test, its basis is almost all organic compounds can be completely oxidised by a strong oxidizing agent to carbon dioxide under acidic conditions. In order to study the extent of mineralization, COD of sample was determined by Colorimetric Determination Method 8000. In this study, sample was heated for 2 h with COD digestion reagent vials. After that, low range test was taken place.

ICP-OES is a powerful and popular analytical tool in determining trace elements in infinite sample types. This apparatus is based upon the spontaneous emission of photon from ions and atoms that have been stimulated in a radiofrequency discharge. Liquid samples may be injected directly into the instruments but solid samples need extraction or acid digestion so analytes will be existed in solution. The stability of Fe_3O_4 was studied by evaluating leaching of iron from Fe_3O_4. The concentration of leaded iron was determined by using an ICP-OES. Iron (III) chloride hexahydrate ($FeCl_3$) was used as the iron source to prepare the standard solution for the analysis. The concentration of standard solution was 10, 20, 30, 40 and 50 mg/L. The liquid samples without pH control and the liquid samples with pH control (pH 9) were tested. The other parameters used for the liquid samples was as followed: Fe_3O_4 dosage was 2.5 g/L, H_2O_2 dosage was 0.2 M, dye concentration was 20 mg/L, temperature was 30 ℃ and reaction time was 1 h.

CHAPTER 4

RESULTS AND DISCUSSION

4.1 Characterizations of Fe_3O_4

4.1.1 XRD Results

The crystal structures of original Fe_3O_4 and various heat-treated Fe_3O_4 at different temperatures were observed by using XRD measurement. The XRD patterns are shown in Figure 4.1. Fe_3O_4-0 had the same patterns with standard Fe_3O_4 where the characteristic peaks were at 2θ = 18.2, 30.0, 35.4, 43.0, 53.4, 56.9, 62.5 and 74.0 ° (Wang, Wei and Qu, 2013). Moreover, it was black in colour which black was the characteristic colour of Fe_3O_4 (Legodi and Waal, 2007). Therefore, it verified that it was Fe_3O_4 nanoparticles.

Based on the Figure 4.1, it could be observed that the XRD patterns for Fe_3O_4-0 and Fe_3O_4-200 had same characteristic peaks. It was reported that Fe_3O_4 and γ- Fe_2O_3 had same XRD characteristic peaks (Abbas, et al., 2015). The diffraction peaks of Fe_3O_4-200 were in consistent with the standard γ- Fe_2O_3 where 2θ = 18.3, 30.2, 35.6, 43.2, 53.7, 57.2 and 62.9 ° (Gatabi, Moghaddam and Ghorbani, 2016). In addition, Fe_3O_4-200 was in brown which was same as the characteristic colour for γ- Fe_2O_3 (Legodi and Waal, 2007) and it was considered as evidence for the formation of γ-Fe_2O_3 phase. Occurrence of phase transformation from Fe_3O_4 to γ- Fe_2O_3 was caused by the heat treatment of Fe_3O_4 at lower temperature and in the presence of air (oxygen). This was due to the unstable Fe_3O_4 sensitive to oxidation (Khan, et al., 2015).
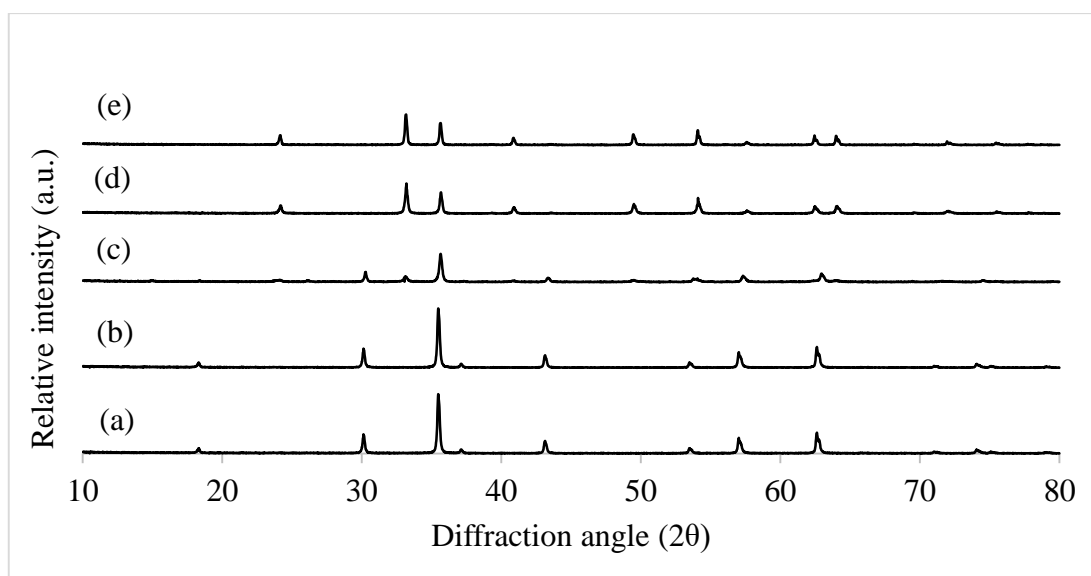
Figure 4.1: XRD Patterns for (a) Fe₃O₄-0, (b) Fe₃O₄-200, (c) Fe₃O₄-400, (d) Fe₃O₄-600 and (e) Fe₃O₄-800

The XRD pattern of Fe_3O_4-400 was slightly different from Fe_3O_4, γ- Fe_2O_3 and α- Fe_2O_3. Its XRD pattern showed the presence of both γ- Fe_2O_3 and α- Fe_2O_3 phases. At $\theta = 30.2$ °, it contained the peak which represented γ- Fe_2O_3 phase. Meanwhile, it also comprised the peak which represent α- Fe_2O_3 phase at $\theta = 33.1$ and 49.5 °. Thus, Fe_3O_4-400 might contain both γ- Fe_2O_3 and α- Fe_2O_3 phases. Besides, the colour of Fe_3O_4-400 was similar to brown of γ- Fe_2O_3 and red of α- Fe_2O_3 which could be considered as the evidence that it might consist both phases. At temperature of 400 °C , the incomplete phase changed from metastable γ- Fe_2O_3 to stable α- Fe_2O_3 might take place. Islam, et al. (2012) observed that γ- Fe_2O_3 could be obtained when oxidizing Fe_3O_4 at 250 °C for 8 h in the presence of oxygen and α- Fe_2O_3 could be obtained when sintering γ- Fe_2O_3 at 500 °C for 3 h in the presence of argon. In addition, Khan, et al. (2015) also reported that γ- Fe_2O_3 could be obtained when sintering iron oxide nanoparticles at 350 °C via dry oxidation for 30 min and α- Fe_2O_3 could be obtained at 600 °C via dry oxidation for 60 min. Therefore, 400 °C might be the phase transition temperature for γ- Fe_2O_3 transforming to α- Fe_2O_3.

Fe_3O_4-600 and Fe_3O_4-800 had the same patterns with standard α-Fe_2O_3 where the characteristic peaks were at $2\theta = 24.1, 33.2, 35.8, 40.7, 49.5, 54.2, 57.6$ and 62.5 ° (Ramasami, et al., 2016). Moreover, both samples were in red colour which red was

the characteristic colour of α- Fe_2O_3 (Legodi and Waal, 2007). Therefore, it was suggested that both samples mainly composed of α- Fe_2O_3 phase. As increasing the temperature from 400 until 600 and 800 ℃, the remaining of γ- Fe_2O_3 phase transformed completely to α- Fe_2O_3 (Bora, et al., 2012). Cudennec and Lecerf (2006) claimed that the formation of α- Fe_2O_3 is favoured at higher temperature. This was due to the substantial rearrangement of ions was required to transform from CCP anion arrangement of γ- Fe_2O_3 to HCP of α-Fe_2O_3 (Khan, et al., 2015).

The crystalline size of the samples was calculated from XRD pattern using the Scherrer equation (Equation 2.13) (Abbas, et al., 2015). The calculated values of crystalline size for original Fe_3O_4 and various heat-treated Fe_3O_4 are represented in Table 4.1. According to Table 4.1, crystalline size of sample decreased when temperature increased to 400℃. Similar result was obtained by Múzquiz-Ramos, et al. (2015). They found out that the crystalline size of γ- Fe_2O_3 obtained at different temperature was decreased when temperature increased from 200 to 300 ℃. This was due to the crystallization of γ- phase, whose particles were generally ultrafine (Cava, et al., 2007). However, crystalline size of sample increased when temperature increased from 400 to 800 ℃. The increase in crystalline size was due to the acquirement of a stable phase by minimizing surface energy (Bora, et al., 2012). In addition, crystallite growth or aggregation of Fe_3O_4 particles would be promoted by high temperatures (Abdullah and Pang, 2010).

Table 4.1: Crystalline Sizes for Original Fe_3O_4 and Various Heat-treated Fe_3O_4

Calcination Temperature (℃)	Crystalline size (nm)
0	47.39
200	44.53
400	39.51
600	40.37
800	50.51

4.1.2 SEM-EDX Results

The particle morphology of the original and various heat-treated Fe_3O_4 particles was studied using SEM as shown in Figure 4.2. The morphology of the majority particles was spherical in shape (Khan, et al., 2015). In addition, the size of particles in Fe_3O_4-0 was in the range of 150 to 180 nm whereas the size of particles in Fe_3O_4-800 was in the range of 220 to 250 nm. It could be seen that the increment of the sintering temperature up to 800 ℃ increased the mean particle size. There was an obvious particle agglomeration could be observed in Figure 4.2 (d) and (e) and it might be caused by the heating of Fe_3O_4 particles and magnetic dipole interaction of Fe_3O_4 magnetic particles (Kazeminezhad and Mosivand, 2014).
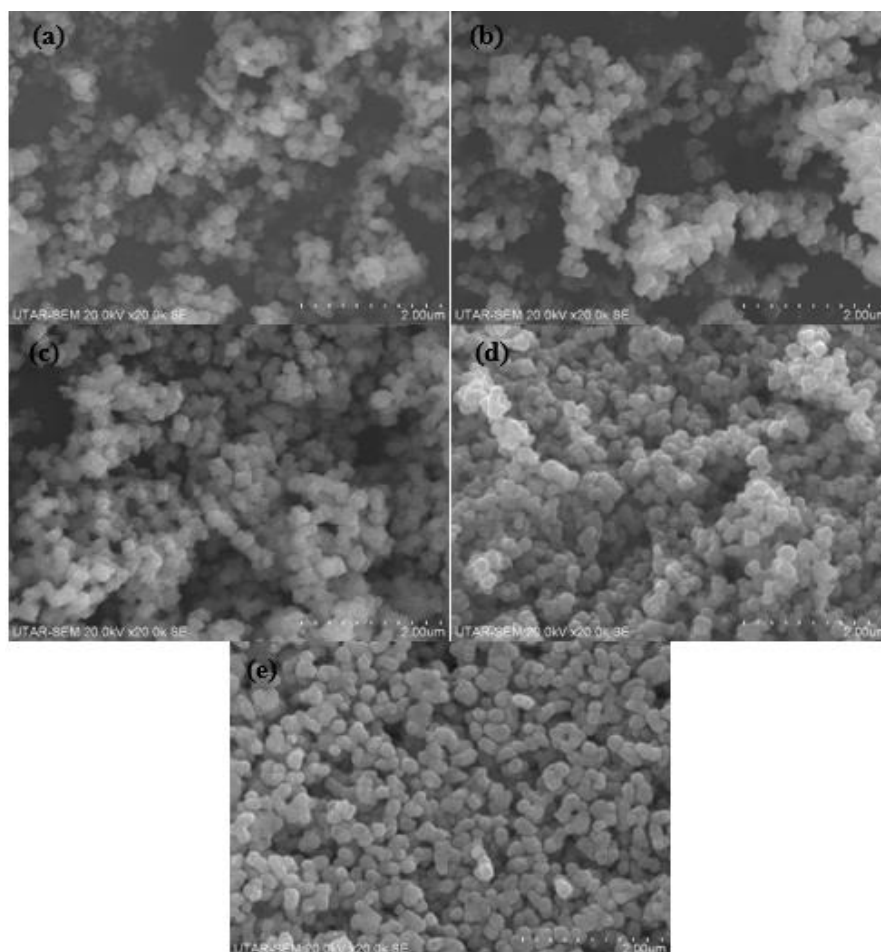
Figure 4.2: SEM Images of (a) Fe₃O₄-0, (b) Fe₃O₄-200, (c) Fe₃O₄-400, (d) Fe₃O₄-600 and (e) Fe₃O₄-800

Hu, et al. (2011) reported that agglomeration of Fe_3O_4 nanoparticles after heating at 650 and 700 ℃. Besides, Kazeminezhad and Mosivand (2014) observed that the size of electrooxidized Fe_3O_4 nanoparticles was in nano range and they agglomerated into clusters after heating at 650, 800 and 1000 ℃. Thus, the result in this research works was consistent with the reported results.

The EDX analysis of the samples is shown in Figure 4.3. It illustrated that all samples composed of Fe and O atoms only and no other elements presented. The theoretical atomic Fe/O ratio for Fe_3O_4 was 0.75 whereas for Fe_2O_3 was 0.667 (Wu and Wang, 2013). The atomic Fe/O ratio for the samples were calculated and summarized in Table 4.2. According to Table 4.2, the atomic ratio for Fe_3O_4-0 was closer to the theoretical atomic ratio of Fe_3O_4 as compared to Fe_2O_3. Thus, Fe_3O_4-0 was confirmed as Fe_3O_4. The rest of the samples possess the closer atomic ratio to theoretical value of Fe_2O_3 as compared to value of Fe_3O_4. Thus, it is anticipated that the samples had the molecular compound of Fe_2O_3. Even though the atomic ratio of Fe_3O_4-800 was quite closer to the value for both Fe_3O_4 and Fe_2O_3 the colour of the sample was red colour instead of black colour. Thus, there was a high possibility that Fe_3O_4-800 contains Fe_2O_3 instead of Fe_3O_4. γ- Fe_2O_3 and α- Fe_2O_3 possessed same atomic and weight ratio but it could be easily differentiated with the help of their colour (Legodi and Waal, 2007). By differentiating their colour, Fe_3O_4-200 was γ- Fe_2O_3 (brown) whereas Fe_3O_4-600 and Fe_3O_4-800 were α- Fe_2O_3 (red). In addition, sample Fe_3O_4-400 might contain both γ- Fe_2O_3 and α- Fe_2O_3 as its colour was similar to brown as well as red.

Table 4.2: Atomic Fe/O Ratio for Each Sample

Samples No.	Fe (%)	O (%)	Fe/O (Atomic %)
a	44.40	55.60	0.80
b	41.42	58.58	0.70
c	38.47	61.43	0.63
d	41.23	58.77	0.70
e	41.83	58.17	0.71
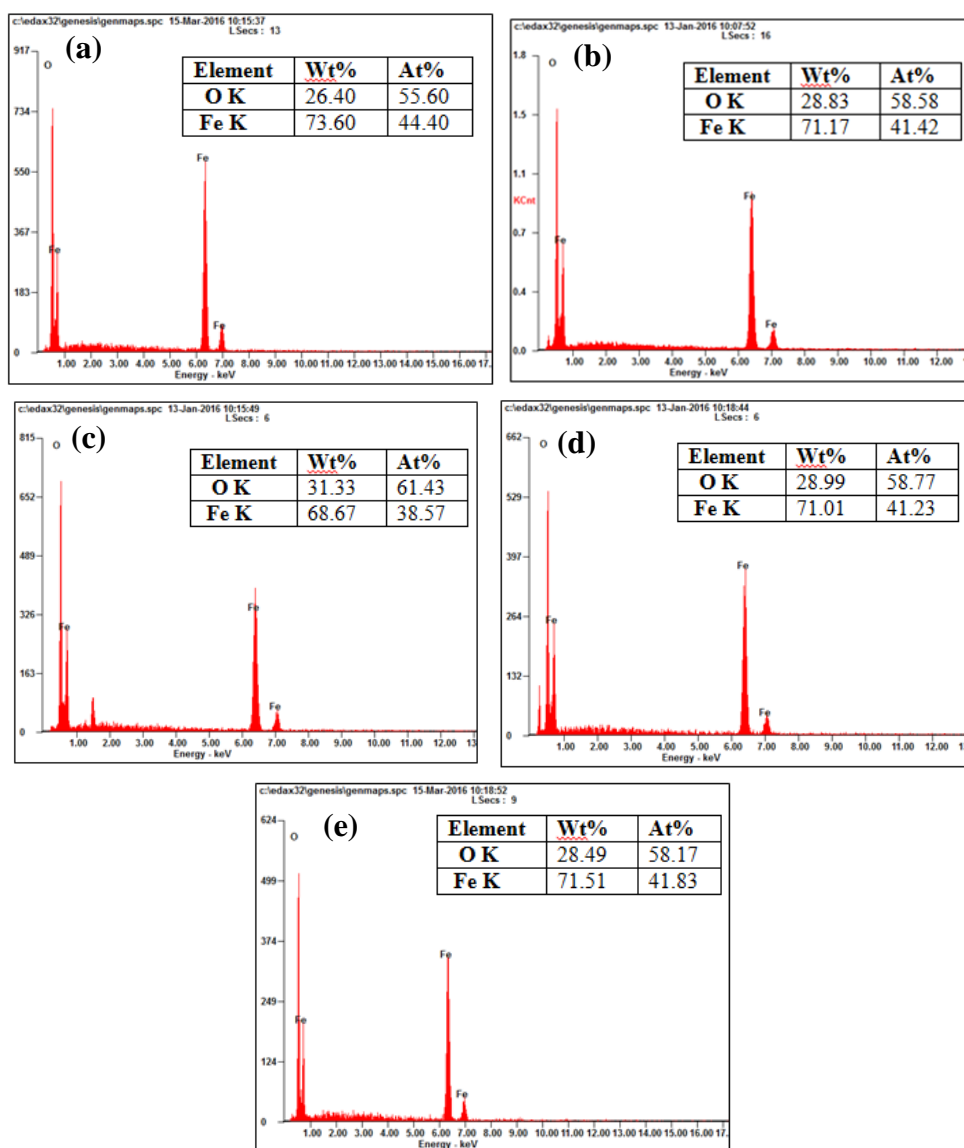
Figure 4.3: EDX Analysis of (a) Fe₃O₄-0, (b) Fe₃O₄-200 (c) Fe₃O₄-400, (d) Fe₃O₄-600 and (e) Fe₃O₄-800

4.2 Effect of Heat Treatment

The effect of various heat treatment of Fe_3O_4 (200, 400, 600 and 800 ℃) on the degradation of malachite green by Fenton and Fenton-like reactions was investigated. As noted in Figure 4.4, the highest degradation efficiency of malachite green was achieved by the original Fe_3O_4 without heat treatment. This observation demonstrated that Fe_3O_4 without any heat treatment already possessed the highest catalytic activity.
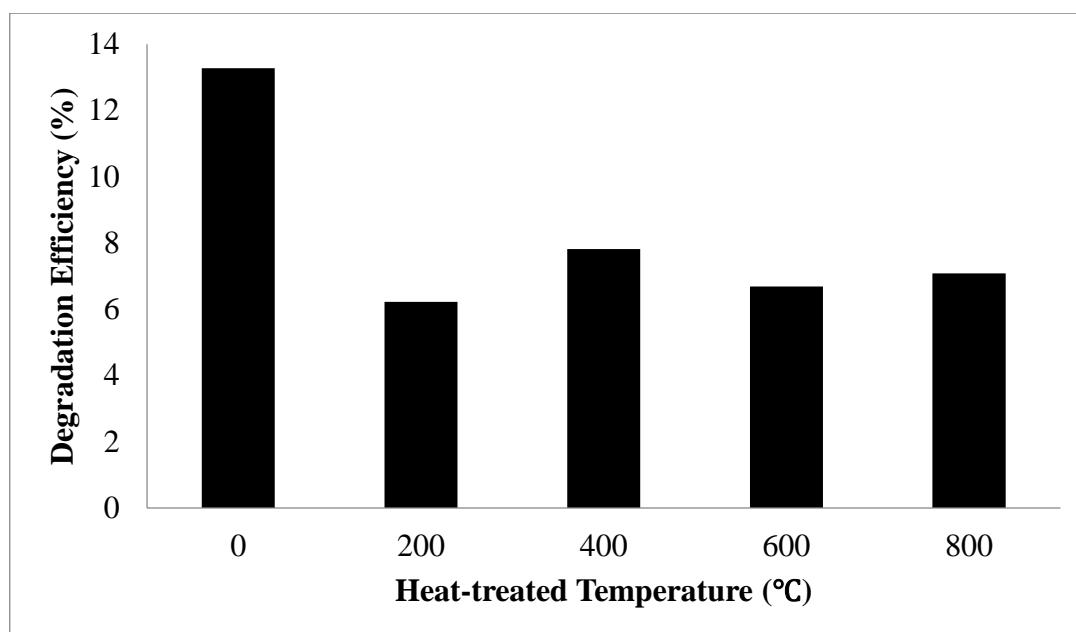
Figure 4.4: Degradation Efficiency of Malachite Green during Fenton and Fenton-like Processes by Different Heat-treated Fe₃O₄ Catalysts (Fe₃O₄ dosage = 1 g/L, initial dye concentration = 20 mg/L, H₂O₂ dosage = 0.2 M, reaction temperature = 30 ℃, pH = 7, reaction time)

Original Fe₃O₄ possessed the highest degradation efficiency in degradation of malachite green due to its unique characteristics. Fe₃O₄ without heat treatment had Fe^{2+} and Fe^{3+} ions in its structure whereas the heat-treated Fe₃O₄ contained predominantly Fe^{3+} ions only. Fe₃O₄ was the only most plentiful iron oxide with Fe^{2+} ions in its structure that enhanced the production of $\cdot OH$ (Pouran, Raman, and Daud, 2014). Xue, Hanna and Deng (2009) claimed that the structural Fe^{2+} content was influential in Fenton oxidation system as the rate constant of Equation 2.1 was much higher than Equation 2.2 ($40 - 80$ vs $9.1 \times 10^{-7}/M \cdot s$). Moreover, Matta, et al. (2008) reported that degradation efficiency was positively correlated with the Fe^{2+} content in the structure of mineral in Fenton oxidation of 2,4,6-trinitrotoluene. In addition, the octahedral structure of Fe₃O₄ could simply accommodate both Fe^{2+} and Fe^{3+} ions and allowed iron species to be reversibly oxidized and reduced while maintaining the same structure (Munoz, et al., 2015). Thus, Fe₃O₄ presented higher potential for degradation of dyes than γ-Fe₂O₃ and α-Fe₂O₃.

The particle size of catalyst was one of the significant parameter in the degradation of dye. From the SEM image, the mean particle size of Fe_3O_4 increased with the high temperature of heat treatment could be noted. Excessive heat treatment caused the agglomeration of particles. Particle agglomeration was a problem as it could reduce the surface area and active sites for adsorption or reaction (Wei and Viadero Jr, 2007). Consequently, the degradation efficiency of malachite green became lower. Therefore, Fe_3O_4 without heat treatment possessed higher degradation efficiency of malachite green than other heat-treated Fe_3O_4. In short, due to its high degradation efficiency, original Fe_3O_4 had been chosen to be used in the rest of experiment in order to study the organic dyes removal by heterogeneous Fenton and Fenton-like processes.

4.3   Parameter Studies

4.3.1   Effect of Various Organic Dyes

The effect of various organic dyes on the Fenton and Fenton-like degradation was investigated. Six organic dyes used were acid orange G, congo red, malachite green, methylene blue, methyl orange and rhodamine B. The results are shown in Figure 4.5. Based on the result, the degradation of malachite green was significantly increased as compared to other organic dyes. The organic dye degradation efficiency generally followed the order as below:

Malachite green > acid orange G > congo red > methylene blue > rhodamine B > methyl orange
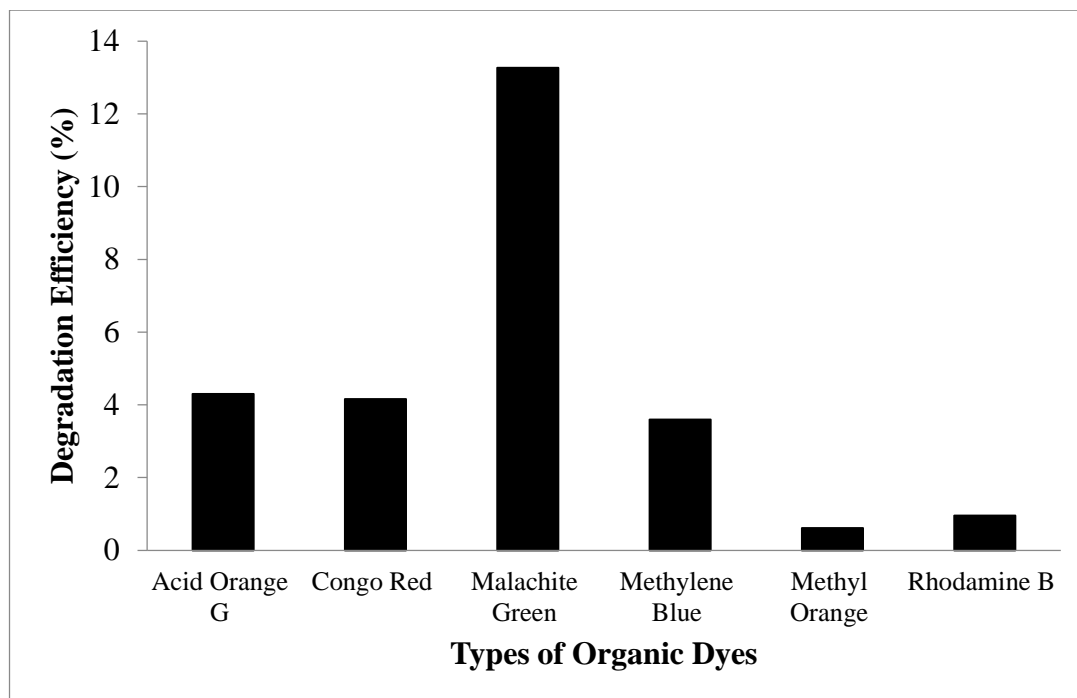
Figure 4.5: Degradation Efficiency of Various Organic Dyes during Fenton and Fenton-like Processes by Fe₃O₄ Catalyst (Fe₃O₄ dosage = 1 g/L, H₂O₂ dosage = 0.2 M, initial dye concentration = 20 mg/L, reaction temperature = 30 ℃, reaction time = 1 h, initial pH = 7)

The degradation process was mainly influenced by the molecular structures of organic molecules (Rao and Venkatarangaiah, 2014). Malachite green had the highest degradation efficiency compared to other organic dyes might due to the triphenyl methane structure of malachite green was the most vulnerable to electrochemical oxidation (Rao and Venkatarangaiah, 2014). Moreover, the structure of malachite green was considered simpler as compared to other organic dyes. Lavanya, et al. (2014) reported that organic dyes with simpler structure displayed higher rate of colour removal. The other five organic dyes could not be highly degraded might because of their complex chemical structures. For instances, the low degradation efficiency of acid orange G, congo red and methyl orange might due to the presence of azo (-N=N-) groups bound to aromatic ring. Methylene blue which was a thiazine dye had the heterocyclic aromatic structure which was resistant to degradation (Rao and Venkatarangaiah, 2014). Rhodamine B which was a xanthene dye had a comparatively high resistance to oxidation degradation (Xue, Hanna and Deng, 2009). In addition, the high degradation efficiency of malachite green might also partially due to the

decolourization by OH^-. This is because the basic hydrolysis of malachite green causes the formation of triphenylcarbinol structure and leads to the loss of conjugation in its structure (Rao and Venkatarangaiah, 2014). This further lead to the mineralization of dye. Process of hydrolysis is shown in Figure 4.6. Therefore, due to the high degradation efficiency of malachite green by Fe$_3$O$_4$ as compared to other organic dyes, it had been chosen to be used in the rest of experiment.
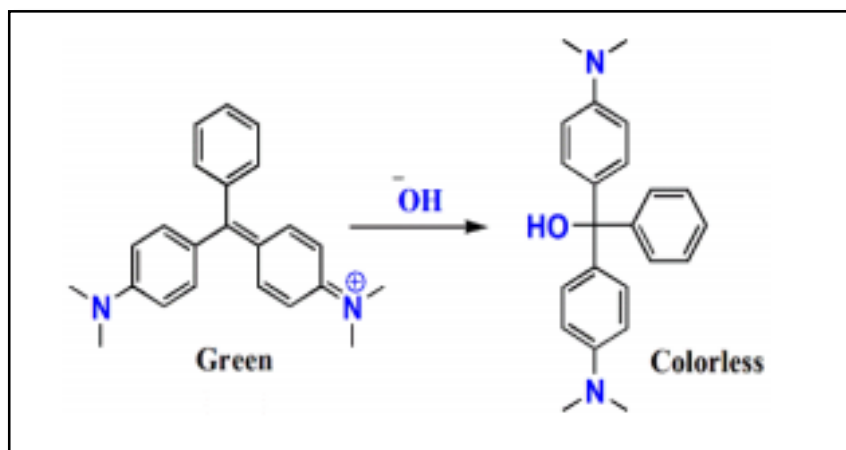
Figure 4.6: Basic Hydrolysis of Malachite Green (Rao and Venkatarangaiah, 2014)

4.3.2   Effect of Fe₃O₄ Dosage

The effect of Fe$_3$O$_4$ dosages (0, 0.5, 1.0, 1.5, 2.0 and 2.5 g/L) was investigated on the Fenton and Fenton-like degradation of malachite green. The result is shown in Figure 4.7. The result indicated that the degradation of dye solution was positively influenced by the Fe$_3$O$_4$ dosage. In other words, the increase of Fe$_3$O$_4$ dosage increased the degradation rate of dye solution. The degradation efficiency for catalyst dosage of 0, 0.5, 1.0, 1.5, 2.0 and 2.5 g/L was 2.46, 5.47, 13.27, 18.94, 29.25 and 40.09 % respectively. The degradation efficiency for catalyst dosage of 2.5 g/L was the highest among the other catalyst dosages.

The increment of Fe$_3$O$_4$ dosage increased the surface area available for the reaction. This indicated more active catalytic sites for Fe^{2+}/Fe^{3+} species to

accelerate the decomposition of H_2O_2 to highly reactive $\cdot OH$. This was in agreement with the result observed by Kwan and Voelker (2003) where the decomposition rate of H_2O_2 was favoured by increasing the Fe_3O_4 dosage in a heterogeneous Fenton-like reaction. Moreover, Kong, et al. (1998) reported that for Fenton reaction, the decomposition of the compounds was promoted by the increase of the concentration of the mineral suspension as the increment of available area or amount of available iron promoted the generation of $\cdot OH$. A similar trend where α- Fe_2O_3 dosage influenced the reactive dye degradation was also reported by Yaman and Gündüz (2015).
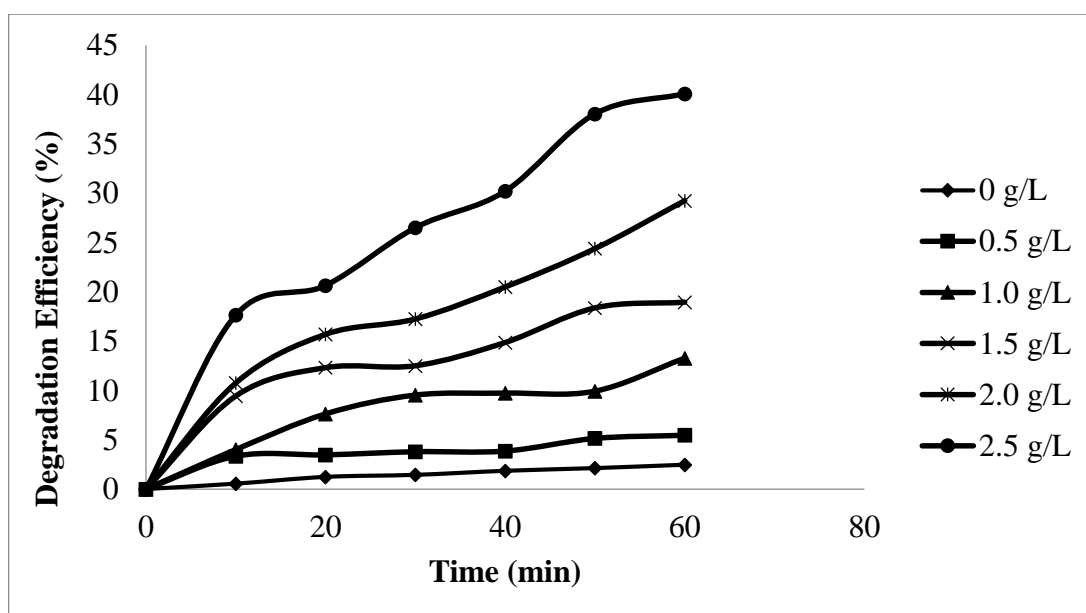
Figure 4.7: Effect of Fe₃O₄ Dosages on the Fenton and Fenton-like Degradation of Malachite Green (H₂O₂ dosage = 0.2 M, initial dye concentration = 20 mg/L, reaction temperature = 30 ℃, pH = 7, reaction time = 1 h)

In short, the higher the Fe_3O_4 dosage, the higher the degradation rate of dye solution as decomposition of H_2O_2 to $\cdot OH$ was accelerated. The optimal dosage of Fe_3O_4 catalyst was 2.5 g/L as it had the highest degradation efficiency.

4.3.3   Effect of H₂O₂ Dosage

The effect of H₂O₂ dosages (0, 0.05, 0.10, 0.15, 0.20 and 0.25 M) was investigated on the Fenton and Fenton-like degradation of malachite green. The result is represented in Figure 4.8. As noted in Figure 4.8, no significant degradation of malachite green was observed without H₂O₂ as only 5.10 % of degradation efficiency was achieved in 60 min. By adding the H₂O₂ dosage from 0.05 to 0.20 M, the degradation efficiency of malachite green was increased from 10.47 to 40.09 % in 60 min. However, when the H₂O₂ dosage was further increased to 0.25 M, it was observed that the degradation efficiency of malachite green decreased to 27.54 %.
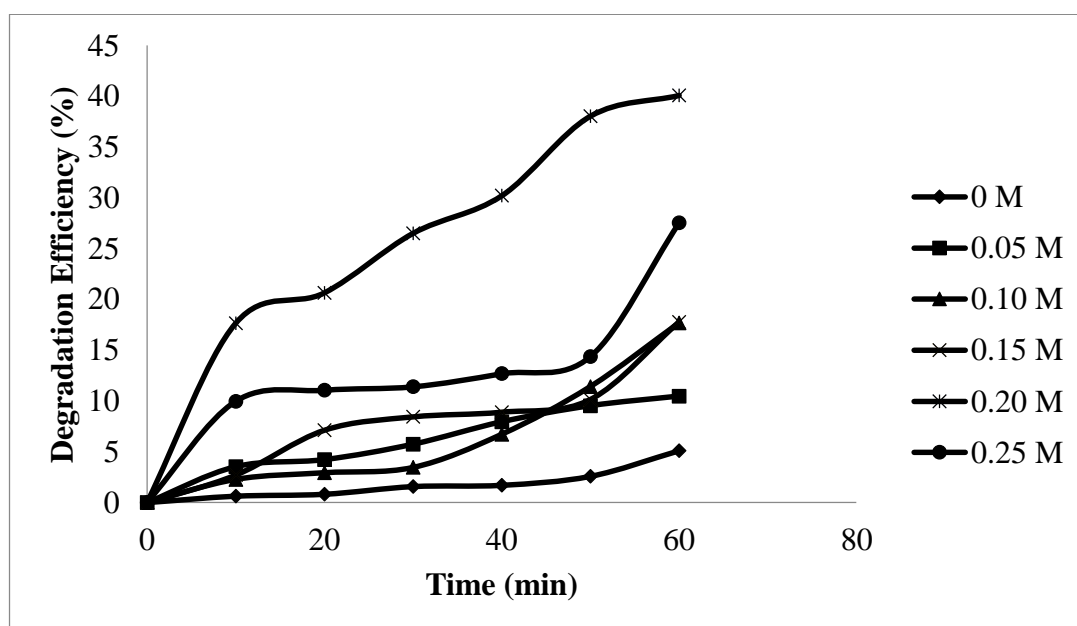
Figure 4.8: Effect of H₂O₂ Dosages on the Fenton and Fenton-like Degradation of Malachite Green (Fe₃O₄ dosage = 2.5 g/L, initial dye concentration = 20 mg/L, reaction temperature = 30 ℃, pH = 7, reaction time = 1 h)

Without adding H₂O₂, the degradation efficiency of malachite green was very low as the adsorption of dye on the catalyst did not contribute to significant removal. However, it did not imply that dye molecules did not adsorb on the surface of catalyst. A positive contribution of H₂O₂ addition on the degradation of malachite green was expected. It could be explained by the fact that the oxidation power of Fenton and Fenton-like process was enhanced. At low H₂O₂ concentration, insufficient $\cdot OH$ in

solution was produced to degrade the dye molecules as H_2O_2 could be easily consumed. Therefore, when increasing the H_2O_2 dosage, quantity of $\cdot OH$ was increased from the decomposition of increasing H_2O_2 and the degradation efficiency could be enhanced (Hassan and Hameed, 2011; Wu, et al., 2015).

Beyond critical concentrations, the degradation efficiency of malachite green was decreased with increasing H_2O_2 dosage. This might be caused by two factors. Firstly, the concentration of dyes on the surface of catalyst was limited by the competition of the excessive H_2O_2 for adsorption on the surface of catalyst (Zhuang, et al., 2015). Secondly, it might be caused by the scavenging effect of H_2O_2 and the recombination of $\cdot OH$ (Bouasla, Ismail and Samar, 2012). $\cdot OH$ that had been produced were scavenged by H_2O_2 itself to form $\cdot HO_2$ with a lower oxidizing power (Equation 2.7). Meanwhile, produced $\cdot HO_2$ could also scavenge $\cdot OH$ to form H_2O and O_2 (Equation 2.9). $\cdot OH$ itself could also recombined to form H_2O_2 back (Equation 2.6). Moreover, H_2O_2 might auto decomposed to water and oxygen instead of being selectively converted to $\cdot OH$. These reactions lowered the likelihood of attack of dye molecules by $\cdot OH$ and resulted a decrease in the degradation rate.

Similar results have been reported by Sun, et al. (2007) and Sun, et al. (2009), in the Fenton oxidation of amido black 10B and orange G, respectively. Excessive H_2O_2 dosage would detrimental to the degradation of dye and increase the cost of the wastewater treatment, thus it is crucial to control the dosage. Therefore, a concentration 0.2 M appeared as an optimal H_2O_2 dosage.

4.3.4   Effect of Dye Concentration

The effect of malachite green concentration (20, 30, 40, 50 and 60 mg/L) was investigated on the Fenton and Fenton-like degradation. The result is depicted in Figure 4.9. It was observed that the degradation efficiency was decreased from 40.09 to 5.19 % when increasing the concentration of malachite green from 20 to 60 mg/L. It could be said that an increase of concentration of organic dye led to a decreasing degradation efficiency (Daneshvar, et al., 2008).
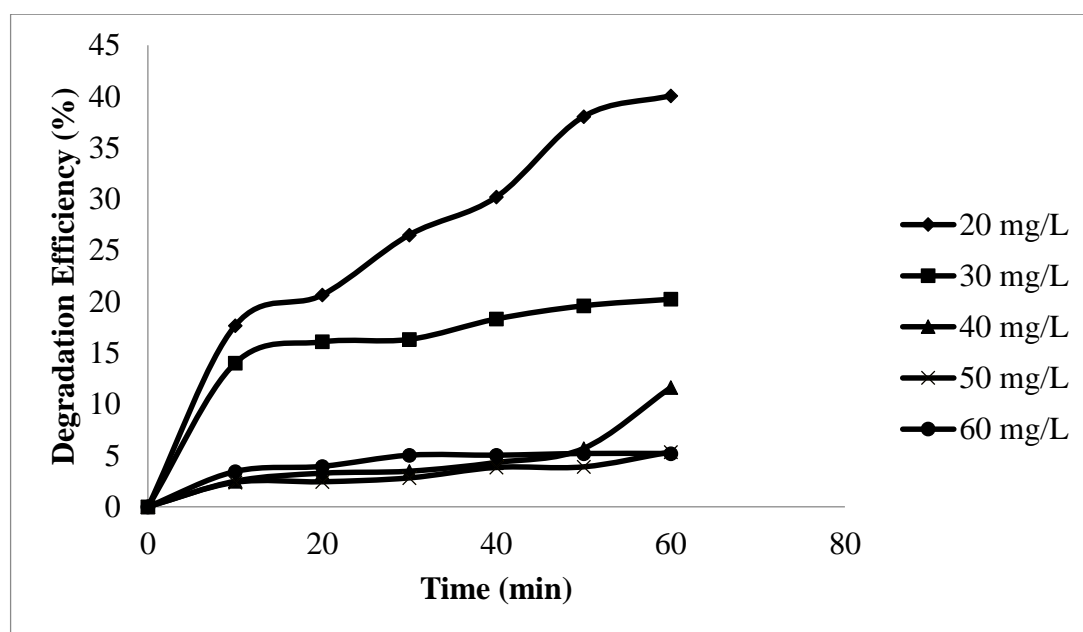
Figure 4.9: Effect of Malachite Green Concentration on the Fenton and Fenton-like Degradation of Malachite Green (Fe$_3$O$_4$ dosage = 2.5 g/L, H$_2$O$_2$ dosage = 0.2 M, reaction temperature = 30 ℃, pH = 7, reaction time = 1 h)

The lower degradation efficiency at high concentration could be explained by the fact that the increase of the concentration of organic dye led to an increment of the number of dye molecules. This indicated that more dye molecules were adsorbed and reacted on the surface of catalyst when increasing the concentration of organic dye. Thus, the generation of $\cdot OH$ was reduced as active sites were occupied by dye ions (Ali, Gad-Allah and Badawy, 2013). This result was in agreement with those found in the literature (Bouasla, Ismail and Samar, 2012; Zhang, Fu and Zhang, 2009).

For the concentration of 60 mg/L, dye was degraded more in 40 min as compared to the concentration of 50 mg/L might due to the fact that the interaction between dye and $\cdot OH$ was enhanced by the increase of the dye concentration. It could be explained by the collision theory of chemical reaction. The increase of dye concentration increased the frequency of collision between dye and $\cdot OH$. Thus, the frequency of effective collisions that caused the reaction to occur would also be high. Eventually, the degradation efficiency was increased (Hassan and Hameed, 2011). The degradation efficiency for 60 mg/L was slightly lower than 50 mg/L as it might due to the reason that with constant H$_2$O$_2$ dosage and Fe$_3$O$_4$ dosage, more H$_2$O$_2$ was

consumed in first 40 min. After 40 min, amount of H_2O_2 was lesser and so the degradation of dye slowed down (Sun, et al., 2007).

In short, the higher the concentrations of malachite green, the lower the degradation efficiency of dye solution. The optimal concentration of malachite green was 20 mg/L as it had the highest degradation efficiency.

4.3.5   Effect of Temperature

The effect of temperature (30, 60, 70 and 80 °C) was investigated on the Fenton and Fenton-like degradation of malachite green. The result is represented in Figure 4.10. As noted in Figure 4.10, raising the temperature had a positive impact on the degradation of malachite green. The degradation efficiency of malachite green was increased from 40.09 to 98.99 % within 60 min as temperature of solution increased from 30 to 80 °C. Nevertheless, the degradation efficiency after 60 min was very similar at 60, 70 and 80 °C. Moreover, the period of time required for the degradation of malachite green was also much shorter at higher temperature. In 10 min, the degradation efficiency of malachite green for 80 °C already reached 53.89 % as compared to the degradation efficiency for 30 °C which only reached 17.65 %.

A positive contribution of the increasing temperature on the degradation of malachite green was expected. It could be explained according to the Arrhenius kinetics. Fenton's reaction could be accelerated by increasing temperature as higher temperature could supply more energy to conquer the activation energy of reaction and then quicken the reaction rate between H_2O_2 and iron species on the surface of catalyst (Wang, et al., 2016). This enhanced the production rate of $\cdot OH$ and hence degradation of malachite green was raised (Sun, et al., 2009). In literature, similar enhancement results had been reported in Fenton-like oxidation of orange II solutions using heterogeneous catalysts of saponite clay (Ramirez, et al., 2007) and iron-based nanoparticles (Wu, et al., 2015).
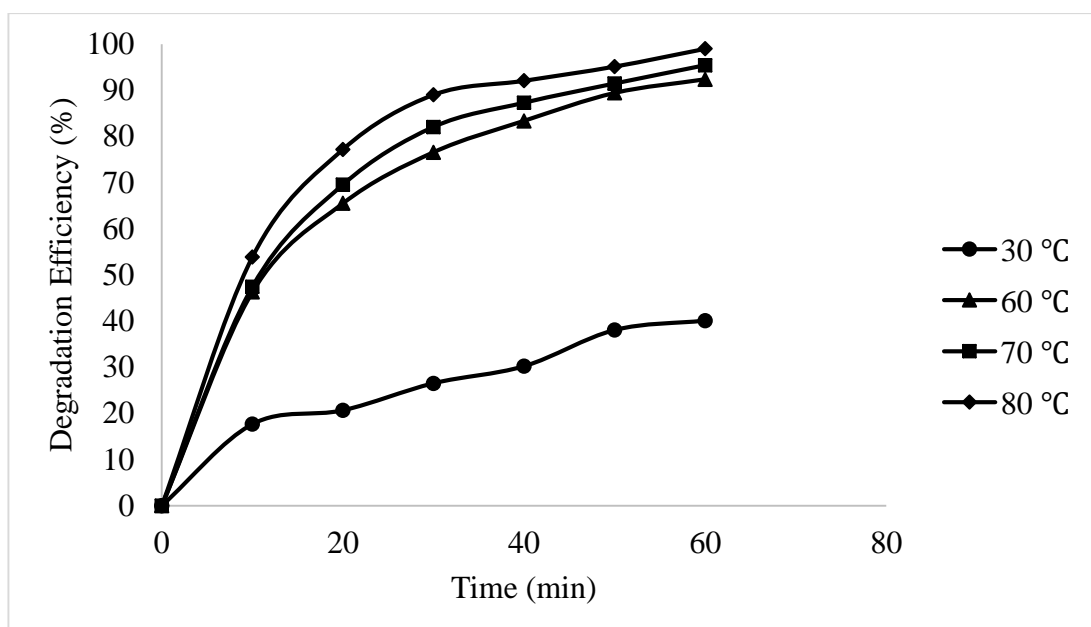
Figure 4.10: Effect of Temperature on the Fenton and Fenton-like Degradation of Malachite Green (Fe_3O_4 dosage = 2.5 g/L, H_2O_2 dosage = 0.2 M, initial dye concentration = 20 mg/L, pH = 7, reaction time = 1 h)

In conclusion, the degradation efficiency of malachite green was increased with the increasing of the reaction temperature. Although the degradation efficiency for temperature at 30 ℃ is lower than those obtained at higher temperature (60, 70 and 80 ℃), 30 ℃ was chosen as an ideal temperature to conduct the following experiment as its degradation of dye might be considered satisfactory and lower temperature might lower the process cost.

4.3.6   Effect of solution pH

The effect of solution pH (pH 3, 5, 7, 9 and 11) was observed on the Fenton and Fenton-like degradation of malachite green. The pH was adjusted from pH 3 to 11 by using 0.1 M HCl and 0.1 M NaOH. The result is represented in Figure 4.11. Figure 4.11 illustrated that the increment of pH from pH 3 to 11 positively affected the degradation efficiency of malachite green. It clearly showed that the heterogeneous

Fenton and Fenton-like process with Fe_3O_4 can efficiently remove malachite green in pH range from 7 to 11.
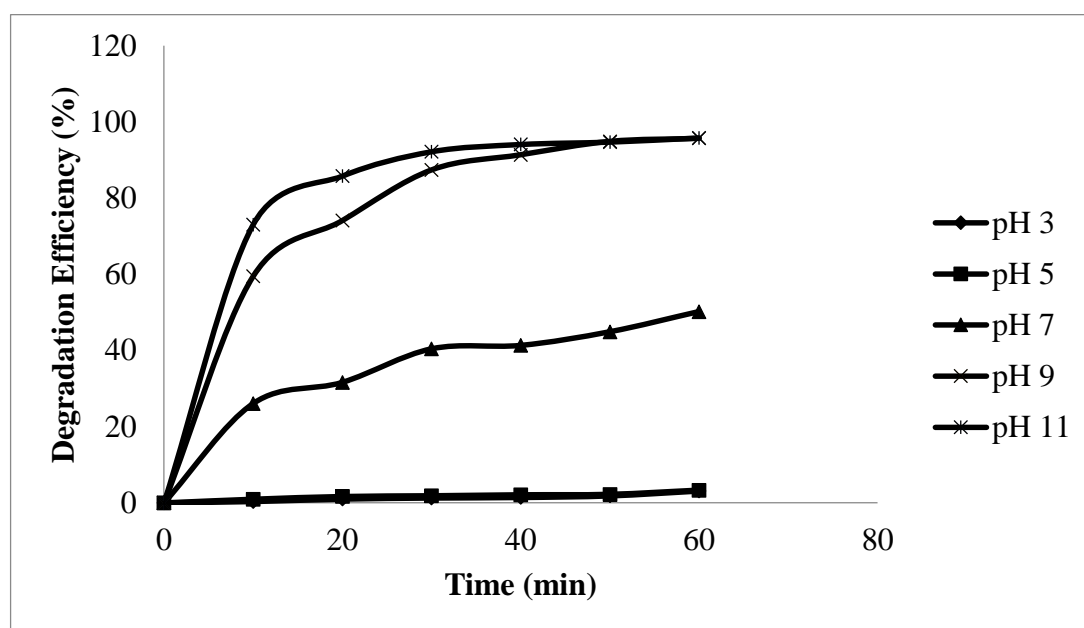
Figure 4.11: Effect of pH on the Fenton and Fenton-like Degradation of Malachite Green (Fe_3O_4 dosage = 2.5 g/L, H_2O_2 dosage = 0.2 M, initial dye concentration = 20 mg/L, reaction temperature = 30 ℃, reaction time = 1 h)

It was well known that the homogeneous Fenton and Fenton-like processes were efficient in the acidic range from pH 3 to 4 (Bagal and Gogate, 2014). However, in this research works, it was observed that there was an increase in malachite green degradation through heterogeneous Fenton and Fenton-like processes at alkaline pH range. The degradation of malachite green by Fe_3O_4 was partially accomplished when surface of catalyst was negative charge. In alkaline solution (> pH 7), the surface of Fe_3O_4 contained abundant hydroxyl groups ($-OH$) that supplied a negatively charge to the catalyst surface as the pH was greater than the point of zero charge of Fe_3O_4 surface (pH_{pzc} = 6.9) (Iram, et al., 2010). On the other hand, malachite green could present in two ionic forms: cationic form of the dye and colourless carbinol form in aqueous solution (Mitrowska, Posyniak and Zmudzki, 2008). The negative charge on the surface of Fe_3O_4 would cause electrostatic attraction between Fe_3O_4 and cationic malachite green molecules. Consequently, malachite green was adsorbed and degraded (Dahri, Kooh and Lim, 2014).

In acidic solution, the degradation efficiency of malachite green was low and it might due to the $\cdot OH$ was consumed by the scavenging effect of H^+ ions and H_2O_2 was solvated to form stable oxonium ion when H^+ and $[H_3O_2]^+$ ions were highly concentrated (Wu, et al., 2015). Moreover, it might be also caused by the electrostatic repulsion and poor interaction between Fe_3O_4 and cationic malachite green molecules as Fe_3O_4 surface became positively charge (Iram, et al., 2010).

In conclusion, the degradation efficiency of malachite green by Fe_3O_4 increased with increment of pH. The optimum pH of this experiment was pH 9 instead of pH 11 as the degradation efficiencies of pH 9 and 11 were similar and it saved money from the economic point of view.

4.4 Reusability Study

The degradation efficiency of malachite green by used Fe_3O_4 catalyst was studied. The used catalyst was regenerated through washing by distilled water. According to Figure 4.12, the degradation efficiency for fresh Fe_3O_4 and reused Fe_3O_4 were 95.70 and 96.43 % respectively. It was noted that reused Fe_3O_4 still maintained high catalytic activity and this indicated that Fe_3O_4 was reusable under this experimental conditions.

Similar results were reported by other researchers. Chen, et al. (2016) reported that Fe_3O_4 magnetic nanoparticles remained the high catalytic activity after continuously running for 12 h in total as degradation efficiency of rhodamine B in 2 h was more than 98 % in each run. In addition, Zhang, et al. (2008) claimed that the catalytic activity of ferromagnetic nanoparticles still maintained almost 100 % for the degradation of phenol after 5 rounds of recycle. Baldrian, et al. (2006) also reported that Fe_3O_4 had remarkable stability of performance and no decrease in degradation efficiency was observed during five 72 h cycles of degradation of chicago sky blue 6B using 25 mg/L of catalyst. Therefore, it could be concluded Fe_3O_4 was reusable and represented a promising alternative to other conventional catalyst because of their reusability as well as easy recovery by using magnet.
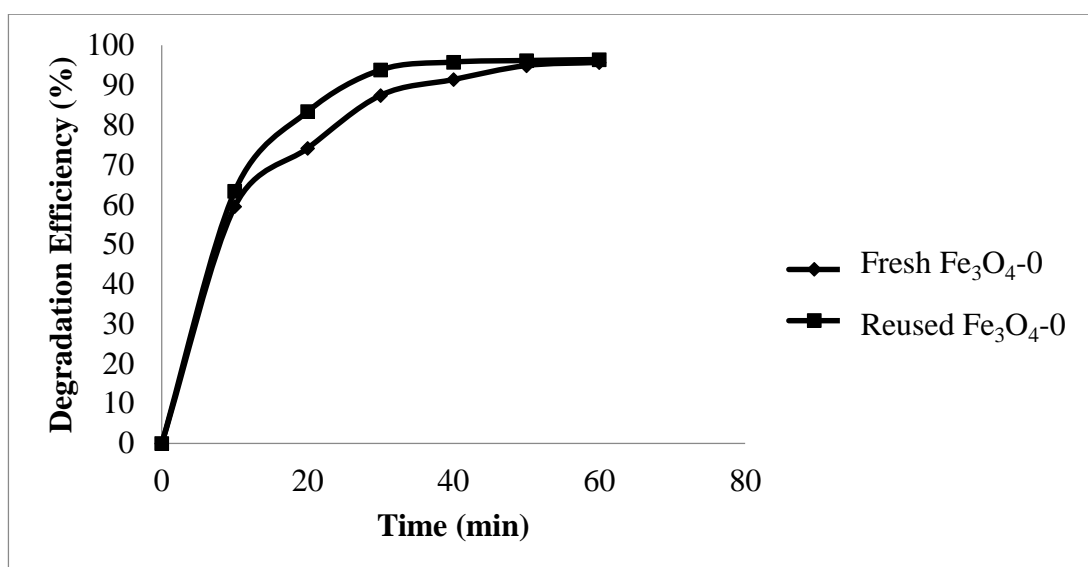
Figure 4.12: Degradation of Malachite Green by Fresh and Reused Fe₃O₄ Catalyst (Fe₃O₄ dosage = 2.5 g/L, H₂O₂ dosage = 0.2 M, initial malachite green concentration = 20 mg/L, pH = 9, temperature = 30 ℃, reaction time = 1 h)

4.5 Kinetic Study

Kinetic studies were performed on the basis of the rate of disappearance of malachite green in order to determine the order of the reaction for Fenton and Fenton-like degradation of the dye. Zero, first and second orders graph were studied for the experimental data acquired using malachite green at an initial concentration of 20 mg/L with different temperature.

Since $\cdot OH$ is the main oxidants responsible to attack organic matter in Fenton and Fenton-like reactions, the kinetics of the reaction on the degradation of malachite green can be presented as follows:

$$-\frac{dC_{MG}}{dt} = kC_{MG}^m C_{\cdot OH}^n \tag{4.1}$$

where C_{MG} is concentration of malachite green (mg/L) at time t, $C_{\cdot OH}$ is the concentration of $\cdot OH$ at time t, m is the reaction order with respect to malachite green,

n is the reaction order with respect to $\cdot OH$, t is the reaction time (min) and k is the reaction rate constant. It is difficult to measure and consider $\cdot OH$ as constant at specific time as its life time is relatively short (Momani, 2008). Therefore, Equation 4.1 can be simplified in the form:

$$-\frac{dC_{MG}}{dt} = k_{app}C_{MG}^m \tag{4.2}$$

where k_{app} is an apparent reaction rate constant. In this experiment, pseudo first-order was satisfactory fitted all the data. It was consistent with the result of Elhami, Karimi and Aghbolaghy (2015) in the study of decolourization of malachite green. In addition, Shi, et al. (2016) reported that the degradation of methylene blue by Fe_2SiS_4 Fenton system was fitted to the pseudo-first order rate law. Since the reaction is well-fitted to pseudo first-order, m is equal to 1. By integrating Equation 4.2, the equation relating the concentration of malachite green to the reaction time can be acquired and it is shown in Equation 4.3.

$$ln\frac{C_0}{C_t} = k_{app}t \tag{4.3}$$

where C_0 and C_t are the concentration of malachite green (mg/L) at time 0 and t respectively. Plot of $ln\frac{C_0}{C_t}$ versus time (t) for the four cases of different temperatures considered can be approximately as straight lines. Figure 4.13 suggested that the degradation of malachite green satisfactory fitted the pseudo first-order kinetics because of high determination of coefficient ($r^2 > 0.91$). Therefore, the slope of the straight lines should be equal to the apparent first-order rate constant (k_{app}). The values of k_{app} and r^2 are shown in Table 4.3. It was noted that the rate constant significantly increased from 0.0093 to 0.0694 /min as the temperature increased from 30 to 80 ℃. It could be explained that more energy was supplied at higher temperature to conquer energy of reaction (Wang, et al., 2016). Kuang et al. (2013) claimed that the increment of rate constant was due to faster catalysis of H_2O_2 at a higher temperature. The number of $\cdot OH$ was increased and eventually the oxidation of malachite green was accelerated. Similar trend was obtained by Aygun, et al. (2012).
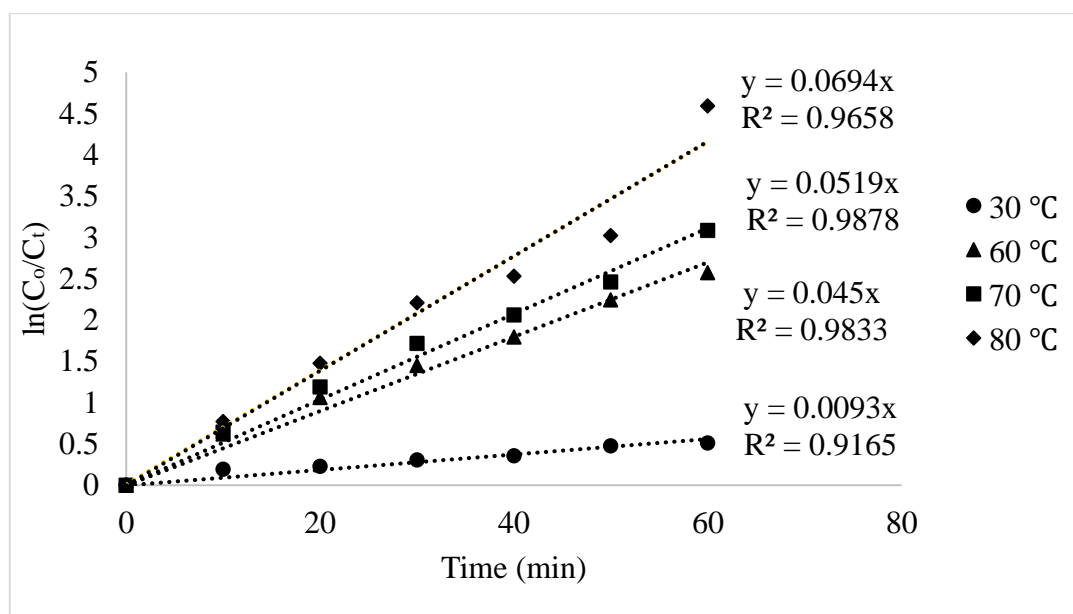
Figure 4.13: Pseudo First-order Reaction Kinetics Plot for Fenton and Fenton-like Degradation of Malachite Green

Table 4.3: Rate Coefficients for Degradation of Malachite Green by Fe₃O₄ under Different Temperature

Temperature (°C)	Pseudo zero-order model		Pseudo first-order model		Pseudo second-order model	
	r^2	k_{app} $(\frac{mg}{L\ min})$	r^2	k_{app} $(/min)$	r^2	k_{app} $(\frac{L}{mg\ min})$
30	0.9243	−0.1191	0.9165	0.0093	0.9723	0.0005
60	0.8122	−0.2693	0.9833	0.0450	0.9219	0.0099
70	0.7933	−0.2595	0.9878	0.0519	0.8427	0.0167
80	0.7410	−0.2596	0.9658	0.0694	0.5608	0.0655

k_{app} values obtained can be correlated by an Arrhenius-type expression for the experiment conducted at different temperatures. The graphical representation of ln k_{app} on the basis of $1/T$ permits the calculation of the parameters of Arrhenius equation:

$$\ln k_{app} = lnA_0 - \frac{E_a}{RT} \tag{4.4}$$

where E_a is the activation energy (kJ/mol) and A_0 is the pre-exponential factor (/min), R is ideal gas constant (8.314 J/mol·K) and T is absolute temperature (K). Based on Figure 4.14, good linear relationships exist between the plots of ln k and $1/T$ as r^2 was higher than 0.97. The Arrhenius relationship can be shown in Equation 4.5.

$$\ln k_{app} = -4377.7\left(\frac{1}{T}\right) + 9.8323 \qquad r^2 = 0.9756 \tag{4.5}$$

E_a and A in Arrhenius form were determined according to the slope $(-E_a/R)$ and intercepts (ln A). E_a and A for degradation of malachite green under different temperature were 36.40 kJ/mol and 1.86×10^3 /min respectively. The E_a value was very close to the E_a (35.90 kJ/mol) obtained in the study for heterogeneous Fenton-like oxidation of reactive red 141 (Yaman, Gündüz and Dükkancı, 2013). Moreover, it was lower than the E_a (43.00 kJ/mol) gained in the study for heterogeneous Fenton-like oxidation of monochlorobenzene (Kuang, et al., 2013). The degradation of malachite green by Fe_3O_4 was a process of surface-controlled reaction as E_a value for surface was more than 29 kJ/mol while for diffusion-controlled reaction ranged from 8 to 21 kJ/mol (Shi, et al., 2011).
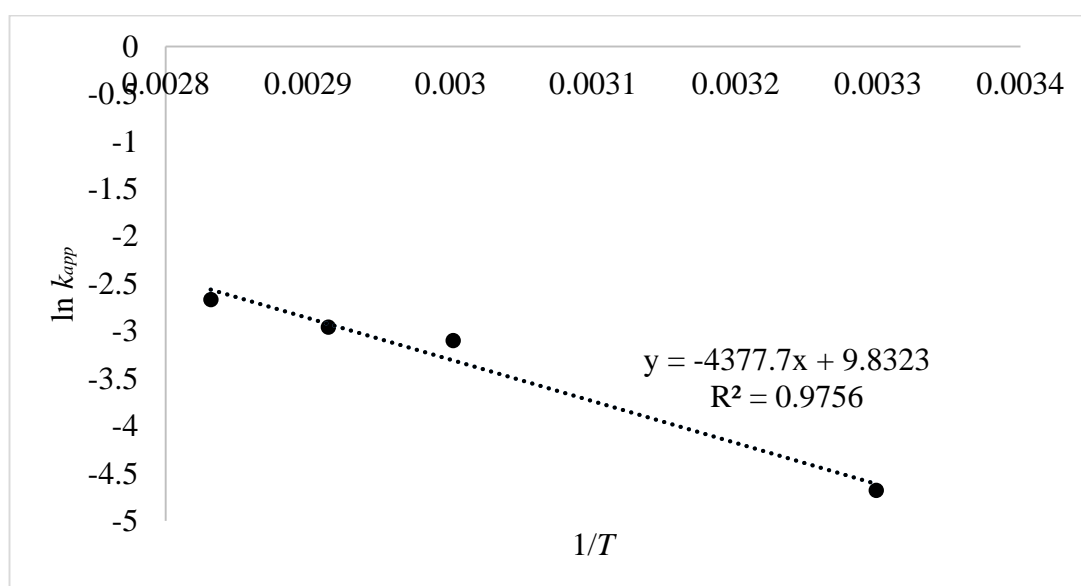
Figure 4.14: Arrhenius Plot of ln k_{app} against $1/T$

4.6   Liquid Sample Analysis

4.6.1   COD Results

The COD removal by the heterogeneous Fenton and Fenton-like reactions was investigated. COD of the solution with the optimum condition (Fe_3O_4 dosage = 2.5 g/L, H_2O_2 dosage = 0.2 M, initial malachite green concentration = 20 mg/L, pH 9, 30 ℃, time = 1 h) for the case before reaction and after reaction had been determined by Colorimetric Determination Method 80000. 32 % of the COD had been removed by the reaction after 1 h. At the end of reaction, only partial COD removal was attained as reaction decelerated due to the cleavage of dye chromophores and this led to partially degradation of highly complex-structured dye molecules into comparatively small organic fragments (Arslan-Alaton, Gursoy and Schmidt, 2008). It should be noted that the intermediate products of malachite green are hard to be oxidized by AOP and the complete oxidation might continue in a longer time.

Similar observation had been reported by other researchers. Alaton and Teksoy (2007) observed that the overall COD removal efficiency of synthetic acid effluent by Fenton oxidation after 30 min was only 23 % although the colour removal efficiency can be achieved to 92 %. Arslan-Alaton, Gursoy and Schmidt, 2008 also reported that only partial COD had been removed during Fenton treatment of acid red 183, acid orange 51 and reactive blue 4. Therefore, a complete oxidation of malachite green would require more than 1 h oxidation process.

4.6.2   ICP-OES Results

Stability of catalyst is one of the important properties for its practical applications. From the environmental point of view, the leaching of transition metals such as iron should be limited in order to avoid their toxic effects on living organisms (Pouran, et al., 2015). The amount of iron loss from Fe_3O_4 catalyst was determined with ICP-OES

by determining iron concentration in the solution after 1 h reaction. Two liquid samples had been tested, which were the liquid samples without pH control and the liquid samples with pH control (pH 9).

According to the ICP results, the concentration of leached iron concentration for liquid samples without pH control and the liquid samples with pH control (pH 9) were 0.793 and 0.673 mg/L respectively. The concentration of leached iron for both samples could be considered as quite low as the value was within the acceptance condition for discharge of iron (below 1 mg/L) according to Environmental Quality (Industrial Effluent) Regulations 2009 (DOE, 2009). However, more iron ions leached from Fe_3O_4 for liquid sample without pH control. It might due to the solution was originally in acidic condition. Matei, et al. (2011) reported that iron dissolution tended to be higher for acidic conditions as compared with neutral and basic media. Baba, et al. (2007) also reported that the rate of iron ore dissolution is directly proportional to the concentration of H^+.

CHAPTER 5

CONCLUSION AND RECOMMENDATIONS

5.1   Conclusion

In this study, the characteristics of heat-treated Fe_3O_4 catalyst were investigated. Heat-treated Fe_3O_4 was prepared by heating in a furnace at temperatures of 200, 400, 600 and 800 ℃ for 2 h. The heat-treated Fe_3O_4 were then characterized by XRD and SEM-EDX. XRD patterns indicated that the transformation of Fe_3O_4 into γ-Fe_2O_3 occurred at temperature of 200 ℃ and further transformed into α-Fe_2O_3 completely at temperature 800 ℃. SEM showed that majority Fe_3O_4 particles were spherical shape and the mean particle sizes of Fe_3O_4 increased when increasing temperature up to 800 ℃. EDX illustrated all the original and heat-treated Fe_3O_4 samples composed of Fe and O atoms only. Original Fe_3O_4 showed better catalytic activity than other heat-treated Fe_3O_4. This was due to the available Fe^{2+} and Fe^{3+} ions where Fe^{2+} ions had the higher oxidation rate constant to produce $\cdot OH$.

The effect of various parameters such as various organic dyes, Fe_3O_4 dosage, H_2O_2 dosage, malachite green dye concentration, pH of solution and temperature for Fenton and Fenton-like processes were identified in order to determine the optimum conditions. The degradation of organic dyes (acid orange G, congo red, malachite green, methylene blue, methyl orange and rhodamine B) depended on the chemical structures of organic dyes. Triphenyl methane structure of malachite green was the most vulnerable to chemical oxidation compared to other structures such as azo, thiazine and xanthene structures. Malachite green could be degraded the most among other organic dyes by Fe_3O_4 catalyst during Fenton and Fenton-like processes. The

optimum conditions for degradation efficiency of malachite green were obtained at an initial dye concentration of 20 mg/L, Fe_3O_4 dosage of 2.5 g/L, H_2O_2 dosage of 0.2 M, reaction temperature at 30 ℃ and pH 9 in 1 h to achieve to 96 %. However, only partial COD removal (32 %) was achieved. This was due to the intermediate products were more difficult to be oxidized.

On the other hand, the reusability of Fe_3O_4 catalyst on the degradation of dye was studied. The reused Fe_3O_4 which regenerated through washing by distilled water still maintained high catalytic activity. ICP-OES results illustrated that Fe_3O_4 had high stability as the concentration of leached iron in water samples could be considered as quite low. The reaction kinetics of Fenton and Fenton-like reaction on degradation of organic dyes was also studied. The degradation process of malachite green at different temperatures (30, 60, 70 and 80 ℃) were followed pseudo first-order kinetics. The E_a and A for degradation of malachite green were 36.40 kJ/mol and 1.86×10^3 /min respectively.

5.2   Recommendation for Future Work

Original and heat-treated Fe_3O_4 should be characterized by using Brunauer-Emmett-Teller (BET) surface analysis in order to study the effect of heat treatment on the specific surface area and porosity of Fe_3O_4. Specific surface area was a significant property for Fe_3O_4 as it determines the catalytic reaction of Fenton and Fenton-like processes. Catalytic activity of Fe_3O_4 could be higher if possessing larger specific surface area. This was due to high surface area of catalyst potentially provided more active sites for the generation of $\cdot OH$. Therefore, it was important to study specific surface area and porosity of heat-treated Fe_3O_4.

FTIR analysis can be carried out for malachite green, fresh and used Fe_3O_4 for the degradation of malachite green. FTIR was powerful in identifying the types of chemical bonds in a molecule by generating an infrared absorption spectrum. By using FTIR, the functional groups and chemical bonds of malachite green and Fe_3O_4 catalyst could be identified. Adsorption of malachite green and its degraded products on the

surface of Fe_3O_4 might also be observed by comparing the FTIR spectrum of Fe_3O_4 before and after the degradation of malachite green.

REFERENCES

Abbas, M., Islam, M.N., Rao, B.P. and Abdel-Hamed, M.O., 2015. Facile one-pot chemical approach for synthesis of monodisperse chain-like superparamagnetic maghemite (γ-Fe$_2$O$_3$) nanoparticles. *Journal of Industrial and Engineering Chemistry*, 31, pp. 43–46.

Abdullah, A.Z. and Pang, Y.L., 2010. Heat treatment effects on the characteristics and sonocatalytic performance of TiO$_2$ in the degradation of organic dyes in aqueous solution. *Journal of Hazardous Materials*, 173(1-3), pp.159-167.

Abo-Farha, S.A., 2010. Comparative study of oxidation of some azo dyes by different advanced oxidation processes: Fenton, Fenton-Like, Photo-Fenton and Photo-Fenton-Like. *Journal of American Science*, 6(10), pp. 128-142.

Afroz, R., Masud, M.M., Akhtar, R. and Duasa, J.D., 2014. Water pollution: challenges and future direction for water resource management policies in Malaysia. *Environment and urbanization ASIA*, 5(1), [Online] pp. 63-81. Available at: <http://www.researchgate.net/publication/269371159_Water_Pollution_Challenges_and_Future_Direction_for_Water_Resource_Management_Policies_in_Malaysia> [Accessed 24 June 2015].

Ahmad, A. L., Harris, W. A., Syafiie and Ooi, B. S., 2002. Removal of dye from wastewater of textile industry using membrane technology. *Journal Technology*, 36(F), pp. 31-44.

Alaton, I. A. and Teksoy, S., 2007. Acid dyebath effluent pretreatment using Fenton's reagent: Process optimization, reaction kinetics and effects on acute toxicity. *Dyes and Pigments*, 73(1), pp. 31-39.

Ali, M.E.M., Gad-Allah, T.A. and Badawy, M.I., 2013. Heterogeneous Fenton process using steel industry wastes for methyl orange degradation. *Applied Water Science,* 3(1), pp. 263-270.

Araujo, F.V.F., Yokoyama, L., Teixeira, L.A.C. and Campos, J.C., 2011. Heterogeneous Fenton process using the mineral hematite for the discolouration of a reactive dye solution. *Brazilian Journal of Chemical Engineering*, 28(4), pp. 605-616.

Arora, S., 2014. Textile Dyes: It's Impact on Environment and its Treatment. *Journal of Bioremediation & Biodegradation*, 5(3), pp. 1000e146.

Arslan-Alaton, I., Gursoy, B.H. and Schmidt, J.E., 2008. Advanced oxidation of acid and reactive dyes: Effect of Fenton treatment on aerobic, anoxic and anaerobic processes. *Dyes and Pigments*, 78(2), pp. 117-130.

ASM International and Lampman, S., 2003. Surface analysis. In: *Characterization and failure analysis of plastics*. United States: ASM International. pp. 383-403.

Aygun, A., Yilmaz, T., Nas, B. and Berktay, A., 2012. Effect of temperature on Fenton oxidation of young landfill leachate: Kinetic assessment and sludge properties. *Journal of Global NEST*, 4(4), pp. 487-495.

Baba, A.A., Adekola, F.A. and Lawal, A.J., 2007. Investigation of Chemical and Microbial Leaching of Iron ore in Sulphuric acid. *Journal of Applied Sciences and Environmental Management*, 11(1), pp. 39 – 44.

Baban, A., Yediler, A., Avaz, G. and Hostede, S.S., 2010. Biological and oxidative treatment of cotton textile dye-bath effluents by fixed and fluidized bed reactors. *Bioresource Technology*, 101(4), pp. 1147-1152.

Babuponnusami, A. and Muthukumar, K., 2014. A review on Fenton and improvements to the Fenton process for wastewater treatment. *Journal of Environmental Chemical Engineering*, 2(1), pp. 557-572.

Bagal, M.V. and Gogate P.R., 2014. Wastewater treatment using hybrid treatment schemes based on cavitation and Fenton chemistry: A review. *Ultrasonics Sonochemistry*, 21(1), pp.1-14.

Baldrian, P., Merhautová, V., Gabriel, J., Nerud, N., Stopka, P., Hrubý, M. and Beneš, M.J., 2006. Decolorization of synthetic dyes by hydrogen peroxide with heterogeneous catalysis by mixed iron oxides. *Applied Catalysis B: Environmental*, 66(3–4), pp. 258–264.

Beyene, H.D., 2014. The potential of dyes removal from textile wastewater by using different treatment technology, a review. *International Journal of Environmental Monitoring and Analysis,* 2(6), pp. 347-353.

Bhongsuwan, D., Chomchoey, N., Bhongsuwan, T. and Boripan, M., 2013. *Adsorption of methylene blue by natural aluminosilicates*. [Online] Available at:<http://mining.eng.cmu.ac.th/wp-content/uploads/2013/11/Posterpresentation_2_PaperID-92.pdf> [Accessed 28 June 2015].

Bora, D.K., Braun, A., Erat, S., Safonova, O., Graule, T. and Constable, E.C., 2012. Evolution of structural properties of iron oxide nano particles during temperature treatment from 250 ℃ - 900 ℃: X-ray diffraction and Fe K-shell pre-edge X-ray absorption study. *Current Applied Physics*, 12(3), pp.817-825.

Bouasla, C., Ismail, F. and Samar, M.E., 2012. Effects of operator parameters, anions and cations on the degradation of AY99 in an aqueous solution using Fenton's reagent. Optimization and kinetics study. *International Journal of Industrial Chemistry*, 3(15), pp. 1-11.

Can, M.M., Coskun, M. and Firat, T., 2012. A comparative study of nanosized iron oxide particles; magnetite (Fe_3O_4), maghemite (γ- Fe_2O_3) and hematite (α- Fe_2O_3), using ferromagnetic resonance. *Journal of Alloys and Compounds*, 542, pp.241-247.

Carlton, R.A., 2011. Scanning electron microscopy and energy-dispersive X-ray spectrometry. In: *Pharmaceutical microscopy*. New York: Springer Science+Business Media, pp. 85-130.

Carmen, Z. and Daniela, S., 2012. Textile organic dyes – characteristics, polluting effects and separation/elimination procedures from industrial effluents – A critical overview. In: Puzyn, T. and Mostrag-Szlichtyng, A., eds. *Organic pollutants ten years after the stockholm convention - environmental and analytical update*. Croatia: InTech. pp. 55-86.

Cava, S., Tebcherani, S.M., Souza, I.A., Pianaro, S.A., Paskocimas, C.A., Longo, E. and Varela, J.A., 2007. Structural characterization of phase transition of Al_2O_3 nanopowders obtained by polymeric precursor method. *Materials Chemistry and Physics*, 103(2–3), pp. 394-399.

Cecen, F. and Aktas, O., 2012. Fundamentals of adsorption onto activated carbon in water and wastewater treatment. In: *Activated carbon for water and wastewater treatment: Integration of adsorption and biological treatment*. Weinheim: Wiley-VCH & Co. KGaA. pp. 13-41.

Chen, F., Xie, S., Huang, X. and Qiu, X., 2016. Ionothermal synthesis of Fe_3O_4 magnetic nanoparticles as efficient heterogeneous Fenton-like catalysts for degradation of organic pollutants with H_2O_2. *Journal of Hazardous Materials*. Article in press.

Chequer, F.M.D., Oliveira, G.A.R.D., Ferraz, E.R.A., Cardoso, J.C., Zanoni, M.V.B. and Oliveira, D.P.D., 2013. *Textile Dyes: Dyeing Process and Environmental Impact*. [Online] Available from: <http://www.intechopen.com/bo oks/eco-friendly-textile-dyeing-and-finishing/textile-dyes-dyeing-process-and-environmen tal-impact> [Accessed 25 June 2015].

Choudhury, A.K.R., 2006. Water requirements and treatments. In: *Textile preparation and dyeing*. United State: Science Publishers. pp. 40-87.

Christie, R. M., 2015. Colour and the Environment. In: *Colour chemistry*. 2nd ed. UK: The Royal Society of Chemistry.

Cornell, R.M. and Schwetmann, U. eds., 2003. Crystal structure. In: *The iron oxides: Structure, properties, reactions, occurrences and uses*. Weinheim: WILEY-VCH Verlag GmbH & Co. KGaA. pp. 9-37.

Cudennec, Y. and Lecerf, A., 2006. The transformation of ferrihydrite into goethite or hematite, revisited. *Journal of Solid State Chemistry*, 179(3), pp. 716–722.

Dahri, M.K., Kooh, M.R.R. amd Lim, L.B.L., 2014. Water remediation using low cost adsorbent walnut shell for removal of malachite green: Equilibrium, kinetics, thermodynamic and regeneration studies. *Journal of Environmental Chemical Engineering*, 2(3), pp. 1434-1444.

Daneshvar, N., Aber, S., Vatanpour, V., Rasoulifard, R.M., 2008. Electro-Fenton treatment of dye solution containing Orange II: Influence of operational parameters. *Journal of Electroanalytical Chemistry*, 615(2), pp.165-174.

Department of Environmental, 2009. *Environmental quality (industrial effluent) regulation 2009*. [Online] Available at: <http://www.doe.gov.my/portalv1/wp-content/uploads/2015/01/Environmental_Quality_Industrial_Effluent_Regulations_2009_-_P.U.A_434-2009.pdf> [Accessed 3 April 2016].

Department of Environmental, 2012. *Malaysia environmental quality report 2012*. [Online] Available at: < https://enviro.doe.gov.my/lib/digital/1391999272-1391998509-Malaysia%20Environment%20Report%202012(NEW).pdf> [Accessed 24 June 2015].

EAG, 2015. *X-ray diffraction (XRD) analysis*. [Online] Available at: < http://www.eag.com/mc/x-ray-diffraction.html> [Accessed on 25 July 2015].

Elhami, V., Karimi, A. and Aghbolaghy, M., 2015. Preparation of heterogeneous bio-Fenton catalyst for decolorization of malachite green. *Journal of the Taiwan Institute of Chemical Engineers*, 56, pp. 154-159.

Evans, G.M. and Furlong, J.C., 2003. Treatment technologies of dyes. In: *Environmental biotechnology: Theory and application*. New Delhi: I.K. International Pvt. Ltd. pp. 429-431.

Garrido-Ramirez, E.G., Theng, B.K.G. and Mora, M.L., 2010. Clays and oxide minerals as catalysts and nanocatalysts in Fenton-like reactions – A review. *Applied Clay Science*, 47(3-4), pp. 182-192.

Gatabi, M.P., Moghaddam, H.M. and Ghorbani,M., 2016. Point of zero charge of maghemite decorated multiwalled carbon nanotubes fabricated by chemical precipitation method. *Journal of Molecular Liquids*, 216, pp. 117–125.

Gogate, P.R. and Pandit, A.B., 2004. A review of imperative technologies for wastewater treatment I: oxidation technologies at ambient conditions. *Advances in Environment Research, 8(3-4)*, pp. 501-551.

Gonawala, K.H. and Mehta, M.J., 2014. Removal of colour from different dye wastewater by using ferric oxide as an adsorbent. *Journal of Engineering Research and Applications*, 4(5), pp. 102-109.

Hariani, P.L., Faizal, M., Ridwan, Marsi, and Setiabudidaya, D., 2013. Synthesis and properties of Fe_3O_4 nanoparticles by co-precipitation method to removal procion dye. *International Journal of Environmental Science and Development*, 4(3), pp. 336-340.

Hashemian, S., 2013. Fenton-like oxidation of malachite green solutions: Kinetic and thermodynamic study. *Journal of Chemistry*, 2013, pp. 1-7.

Hassan, H. and Hameed, B.H., 2011. Decolorization of acid red 1 by heterogeneous Fenton-like reaction using Fe-ball clay catalyst. *International Conference on Environment Science and Engineering*, 8, pp. 232-236.

He, B.B., 2009. Introduction: Principles of X-ray diffraction. In: *Two-dimensional X-ray diffraction*. New Jersey: John Wiley & Sons, Inc. pp. 1-27.

He, J., Yang, X.F., Men, B., Bi, Z., Pu, Y.B. and Wang, D.S., 2014. Heterogeneous Fenton oxidation of catechol and 4-chlorocatechol catalysed by nano-Fe_3O_4: Role of the interface. *Chemical Engineering Journal*, 258, pp.433-441.

Hou, L.W., Zhang, Q.H., Jérôme, F., Duprez, D., Zhang, H. and Royer, S., 2014. Shape-controlled nanostructured magnetite-type materials as highly efficient Fenton catalysts. *Applied Catalysis B: Environmental*, 144, pp. 739-749.

Hu, P., Zhang, S., Wang, H., Pan, D., Tian, J., Tang, Z. and Volinsky, A.A., 2011. Heat treatment effects on Fe_3O_4 nanoparticles structure and magnetic properties prepared by carbothermal reduction. *Journal of Alloys and Compounds*, 509 (5), pp. 2316–2319.

IHS, 2014. *Dyes*. [Online] Available at: <https://www.ihs.com/products/dyes-chemical-economics-handbook.html> [Accessed 4 July 2015].

Inoue, M., Okada, F., Sakurai, A. and Sakakibara, M., 2006. A new development of dyestuffs degradation system using ultrasound. *Ultrasonics Sonochemistry*, 13(4), pp. 313-320.

Iram, M., Guo, C., Guan, Y., Ishfaq, A. and Liu, H., 2010. Adsorption and magnetic removal of neutral red dye from aqueous solution using Fe_3O_4 hollow nanospheres. *Journal of Hazardous Materials*, 181, pp. 1039-1050.

Islam, M.S., Kurawaki, J., Kusumoto, Y., Abdulla-Al-Mamun, M. and Bin Mukhlish, M.Z., 2012. Hydrothermal novel synthesis of neck-structured hyperthermia-suitable magnetic (Fe_3O_4, γ-Fe_2O_3 and α-Fe_2O_3) nanoparticles. *Journal of Scientific research*, 4(1), pp. 99-107.

Jiang, C.C., Gao, Z., Qua, H.L., Li, J.W., Wang, X.X., Li, P. and Liu, H., 2013. A new insight into Fenton and Fenton-like processes for water treatment: Part II. Influence of organic compounds on Fe(III)/Fe(II) interconversion and the course of reactions. *Journal of Hazardous Materials*, 250–251, pp. 76–81.

Jones, C.W., 1999. Introduction to the preparation and properties of hydrogen peroxide. In: *Applications of Hydrogen Peroxide and Derivatives*. UK: The Royal Society of Chemistry. pp. 1-34.

Joshi, M., Bansal, R. and Purwar R., 2004. Colour removal from textile effluents. *Indian Journal of Fibre & Textile Research*, 29, pp. 239-259.

Kalska-Szostko, B., Wykowska, U., Satula, D. and Nordblad,P., 2015. Thermal treatment of magnetite nanoparticles. *Beilstein Journal of Nanotechnology*, 6, pp. 1385-1396.

Kant, R., 2012. Textile dyeing industry an environmental hazard. *Journal of Natural Science*, 4(1), pp. 22-26.

Kazeminezhad, I. and Mosivand, S., 2014. Phase transition of electrooxidized Fe_3O_4 to γ and α-Fe_2O_3 nanoparticles using sintering treatment. *Acta Physica Polonica A*, 125(5), pp. 1210-1214.

Khan, U.S., Amanullah, Manan, A., Khan, N., Mahmood, A. and Rahim, A., 2015. Transformation mechanism of magnetite nanoparticles. *Materials Science-Poland*, 33(2), pp. 278-285.

Kharea, U.K. and Boseb P., 2015. Integrated ozonation and aerobic biodegradation of acid red 14 and congo red azo dyes. *International Journal of Innovative and Emerging Research in Engineering*, 2(1), pp. 66-71.

Khataee, A., Taseidifar, M., Khorram, S. and Sheydaei, M., 2015. Preparation of nanostructured magnetite with plasma for degradation of a cationic textile dye by the heterogeneous Fenton process. *Journal of the Taiwan Institute of Chemical Engineers*, 53, pp. 132-139.

Kong, S.H., Watts, R.J. and Choi, J.H., 1998. Treatment of petroleum-contaminated soils using iron mineral catalyzed hydrogen peroxide. *Chemosphere*, 37 (8), pp. 1473-1482.

Kuang, K., Wang, Q., Chen, Z., Megharaj, M. and Naidu, R., 2013. Heterogeneous Fenton-like oxidation of monochlorobenzene using green synthesis of iron nanoparticles. *Journal of Colloid and Interface Science*, 410, pp. 67–73.

Kwan, W.P., and Voelker, B.M., 2003. Rates of hydroxyl radical generation and organic compound oxidation in mineral-catalyzed Fenton-like systems. *Environmental Science & Technology* 37(6), pp. 1150-1158.

Kwon, B.G., Lee, D.S., Kang, N. and Yoon, J., 1999. Characteristic of p-chlorophenol oxidation by Fenton's reagent. *Water Resources*, 33, pp. 2210-2218.

Lavanya, C., Dhankar, R., Chhikara, S. and Sheoran, S., 2014. Degradation of toxic dyes: A review. *International Journal of Current Microbiology and Applied Sciences*, 3(6), pp. 189-199.

Lee. S.H., Oh, J.Y., Park, Y.C., 2006. Degradation of phenol with Fenton-like treatment by using heterogeneous catalyst (modified iron oxide) and hydrogen peroxide. *Bulletin of the Korean Chemical Society*, 27(4), pp.489-494.

Legodi, M.A. and Waal, D.d., 2007. The preparation of magnetite, goethite, hematite and maghemite of pigment quality from mill scale iron waste. *Dyes and Pigments*, 74(1), pp. 161-168.

Liang, X.L., He, Z.S., Wei, G.L., Liu, P., Zhong, Y.H., Tan, W., Du, P.X., Zhu, J.X., He, H.P. and Zhang, J., 2014. The distinct effects of Mn substitution on the reactivity of magnetite in heterogeneous Fenton reaction and Pb(II) adsorption. *Journal of Colloid and Interface Science*, 426, pp.181-189.

Liang, X.L., He, Z.S., Zhong, Y.H., Tan, W., He, H.P., Yuan, P., Zhu, J.X. and Zhang, J., 2013. The effect of transition metal substitution on the catalytic activity of magnetite in heterogeneous Fenton reaction: In interfacial view. *Colloids and Surfaces A: Physicochemical and Engineering Aspects*, 435, pp. 28-35.

Ling, K.B., 2010. *Water quality study and its relationship with high tide and low tide at Kuantan river*. Degree student. Universiti Malaysia Pahang. Available at: <http://umpir.ump.edu.my/2449/1/JACKY_LING_KUO_BAO.PDF> [Accessed 25 June 2015].

Lopez, A., Di laconi, C., Mascolo, G. and Pollice, A., 2012. Integrated process. In: *Innovative and integrated technologies for the treatment of industrial wastewater (INNOWATECH)*. London: IWA Publishing. pp. 91-177.

Man, H.C.B., Akinbile, C.O. and Chin, X.J., 2015. Coconut husk adsorbent for the removal of methylene blue dye from wastewater. *BioResource*, 10(2), pp. 2859-2872.

Martucci, A., 2014. Characterization methods. In: Guglielmi, M., Kickelbick, G. and Martucci, A., eds. *Sol-Gel Nanocomposites*. New York: Springer Science+Business Media. pp. 83-108.

Matei, E., Predescu, C., Berbecaru, A., Predescu, A. and Trusca, R., 2011. Leaching tests for synthesized magnetite nanoparticles used as adsorbent for metal ions from liquid solutions. *Digest Journal of Nanomaterials and Biostructures*, 6(4), pp. 1701-1708.

Matta, R., Hanna, K. and Chiron, S., 2007 Fenton-like oxidation of 2, 4, 6-trinitrotoluene using different iron minerals. *Journal of Science of the Total Environment*, 385(1-3), pp. 242-251.

Matta, R., Hanna, K., Kone, T. and Chiron, S., 2008. Oxidation of 2,4,6-trinitrotoluene in the presence of different iron-bearing minerals at neutral pH. *Journal of Chemical Engineering*, 144(3), pp. 453–458.

Mattioli, D., Malpei, F. and Bortone, G., 2002. Water minimisation and reuse in the textile industry. In: Lens, P. and Pol, L.H., Wilderer, P. and Asano, T., eds. *Water recycling and resource recovery in industry: Analysis, technologies and implementation*. Surrey, UK: IWA Publishing. pp. 545-581.

McNaught, A.D. and Wilkinson, A., 1997. Catalyst. In: *IUPAC Compendium of Chemical Terminology*. 2nd ed. UK: John Wiley & Sons, Inc. pp. 220.

Medien, H.A.A. and Khalil, S.M.E., 2010. Kinetics of the oxidative decolourization of some organic dyes utilizing Fenton-like reaction in water. *Journal of King Saud University*, 22(3), pp. 147-153.

Mitrowska, K., Posyniak, A. and Zmudzki, J., 2008. Determination of malachite green and leucomalachite green residues in water using liquid chromatography with visible and fluorescence detection and confirmation by tandem mass spectrometry. *Journal of Chromatography A*, 1207, pp. 94-100.

Momani, F. A., Shawaqfah M., Shawaqfeh A. and Al-Shannag M., 2008. Impact of Fenton and ozone on oxidation of wastewater containing nitroaromatic compounds. *Journal of Environmental Sciences*, 20(6), pp. 675-682.

Morel, M., Martínez, F. and Mosquera, E, 2013. Synthesis and characterization of magnetite nanoparticles from mineral magnetite. *Journal of Magnetism and Magnetic Materials*, 343, pp. 76-81.

Munoz, M., de Pedro, Z.M., Casas, J.A. and Rodriguez, J.J., 2015. Preparation of magnetite-based catalysts and their application in heterogeneous Fenton oxidation – A review. *Applied Catalysis B: Environmental*, 176–177, pp. 249-265.

Múzquiz-Ramos, E.M., Guerrero-Chávez, V., Macías-Martínez, B.I., López-Badilloa, C.M. and García-Cerdab, L.A., 2015. Synthesis and characterization of maghemite nanoparticles for hyperthermia applications. *Ceramics International*, 41(1), pp. 397–402.

Nidheesh, P.V., 2015. Heterogeneous Fenton catalysts for the abatement of organic pollutants from aqueous solution: a review. *RSC Advances*, 5(51), pp. 40552-40577.

Nisar, N., Ali, S. and Hussian, T., 2007. Dyeing properties of natural dyes extracted from Eucalyptus. *Journal of The Chemical Society of Pakistan*, 29(1), pp. 12-16.

Olea-Mejia, O., Contreras-Bulnes, R., Zamudio-Ortega, C.M., Morales-Luckie, R.A., Olea-Cardoso, O. and López-Castañares, R., 2014. Scanning electron microscopy and energy dispersive spectroscopy microanalysis applied to human dental specimens under laser irradiation for caries prevention. In: Méndez-Vilas, A., ed. *Microscopy: advances in scientific research and education*. Spain: Formatex Research Center. pp. 70-77.

Palanna, 2009. Dynamics of chemical processes. In: *Engineering Chemistry*. New Delhi: Tata McGraw Hill Education Pvt. Ltd.. pp. 546-577.

Pang, Y.L. and Abdullah A.Z., 2013. Current status of textile industry wastewater management and research progress in Malayia: A review. *Clean−Soil, Air, Water*, pp. 1-14.

Pang, Y.L., Abdullah, A.Z. and Bhatia, S., 2010. Comparison of sonocatalytic activities on the degradation of Rhodamine B in the presence of TiO_2 powder and nanotubes. *Journal of Applied Sciences*, 10(12), pp. 1068-1075.

Pati, S.S., Gopinath, S., Panneerselvam, G., Antony, M.P. and Philip, J., 2012. High temperature phase transformation studies in magnetite nanoparticles doped with Co^{2+} ion. *Journal of Applied Physics*, 112, pp. 0054320.

Pouran, S.R., Aziz, A.R.A., Daud, W.M.A.W. and Embong, Z., 2015. Niobium substituted magnetite as a strong heterogeneous Fenton catalyst for wastewater treatment. *Applied Surface Science*, 351, pp. 175–187.

Pouran, S.R., Rahman, A.A.A. and Daud, W.M.A.W., 2014. Review on the application of modified iron oxides as heterogeneous catalysts in Fenton reactions. *Journal of Cleaner Production*, 64, pp. 24-35.

Queirós, S., Morais, V., Rodrigues, C.S.D., Maldonado-Hódar, F.J. and Madeira, L.M., 2015. Heterogeneous Fenton's oxidation using Fe/ZSM-5 as catalyst in a continuous stirred tank reactor. *Separation and Purification Technology*, 141, pp. 235-245.

Ramasami, A.K., Ravishankar, T.N., Sureshkumar, K., Reddy, M.V., Chowdari, B.V.R., Ramakrishnappa, T. and Balakrishna, G.R., 2016. Synthesis, exploration of energy storage and electrochemical sensing properties of hematite nanoparticles. *Journal of Alloys and Compounds*, 671, pp. 552–559.

Ramirez, J.H., Costa, C.A., Madeira, L.M., Mata, G., Vicente, M.A., Rojas-Cervantes, M.L., Lo´pez-Peinado, A.J. and Martı´n-Aranda, R.M., 2007. Fenton-like oxidation of Orange II solutions using heterogeneous catalysts based on saponite clay. *Applied Catalysis B: Environmental*, 71(1-2), pp. 44–56.

Rangabhashiyam, S., Anu, N. and Selvaraju, N., 2013. Sequestration of dye from textile industry wastewater using agricultural waste products as adsorbents. *Journal of Environmental Chemical Engineering*, 1(4), pg. 629-641.

Rao, A.N.S. and Venkatarangaiah, V.T.,2014. The effect of cathode materials on indirect electrochemical oxidation of methyl orange, malachite green and methylene blue. *Portugaliae Electrochimica Acta*, 32(3), pp. 213-231.

Roberts, S.M., James, R.C. and Williams, P.L., 2015. Toxicokinetics. In: *Principles of toxicology: Environmental and industrial applications*. New Jersey: John Wiley & Sons, Inc.. pp.59-88.

Rusevova, K., Kopinke, F. and Georgi, A., 2012. Nano-sized magnetic iron oxides as catalysts for heterogeneous Fenton-like reactions—Influence of Fe(II)/Fe(III) ratio on catalytic Performance. *Journal of Hazardous Materials,* 241-242, pp. 433-440.

Saranraj, P., 2013. Bacterial biodegradation and decolourization of toxic textile azo dyes. *African Journal of Microbiology Research*, 7(30), pp. 3885-3890.

Shahwana, T., Abu Sirriaha, S., Nairat, M., Boyacı, E., Eroglu, A.E., Scott, T.B. and Hallam, K.R., 2011. Green synthesis of iron nanoparticles and their application as a Fenton-like catalyst for the degradation of aqueous cationic and anionic dyes. *Chemical Engineering Journal*, 172(1), pp. 258–266.

Shaobin, W., 2008. A comparative study of Fenton and Fenton-like reaction kinetics in decolourisation of wastewater. *Dyes and Pigments*, 76(3), pp.714-720.

Shi, L., Lin, Y., Zhang, X. and Chen, Z., 2011. Synthesis, characterization and kinetics of bentonite supported nZVI for the removal of Cr(VI) from aqueous solution. *Chemical Engineering Journal*, 171(2), pp. 612–617.

Shi, X., Tian, A., You, J., Yu, Z., Yang, H. and Xue, X., 2016. Fe2SiS4 nanoparticle— A new heterogeneous Fenton reagent. *Materials Letters*, 169, pp. 153-156.

Singh, V., Mukherjee, A. and Dhillon, J., 2010. Geography: Mineral and power resources. In: *Longman Vistas 8: Social Science*. India: Dorling Kindersley Pvt. Ltd.. pp. 137-145.

Soon, A.N. and Hameed, B.H., 2011. Heterogeneous catalysis treatment of synthetic dyes in aqueous media using Fenton and photo-assisted Fenton process. *Journal of Desalination*, 269(1-3), pp. 1-16.

Soudani, A., Chiban, M., Zerbet, M. and Sinan, F., 2011. Use of Mediterranean plant as potential adsorbent for municipal and industrial wastewater treatment. *Journal of Environmental Chemistry and Ecotoxicology*, 3(8), pp. 199-205.

Su, C., Pukdee-Asa, M., Ratanatamskul, C. and Lu, M., 2011. Effect of operating parameters on decolorization and COD removal of three reactive dyes by Fenton's reagent using fluidized-bed reactor. *Journal of Desalination*, 278(1-3), pp. 211-218.

Sun, J.H., Sun, S.P., Wang, G.L. and Qiao, L.P., 2007. Degradation of azo dye Amido black 10B in aqueous solution by Fenton oxidation process. *Dyes and Pigments*, 74(3), pp. 647-652.

Sun, S.P. and Lemley, A.T., 2011. p-Nitrophenol degradation by a heterogeneous Fenton-like reaction on nano-magentite: Process optimization, kinetics, and degradation pathways. *Journal of Molecular Catalysis A: Chemical*, 349(1-2), pp. 71-79.

Sun, S.P., Li, C.J., Sun, J.H., Shi, S.H., Fan, M.H. and Zhou, Q., 2009. Decolorization of an azo dye Orange G in aqueous solution by Fenton oxidation process: Effect of system parameters and kinetic study. *Journal of Hazardous Materials*, 161(2-3), pp. 1052-1057.

Swaminathan, M., Muruganandham, M. and Sillanpaa M., 2012. Advanced oxidation processes for wastewater treatment. *International Journal of Photoenergy*, 2013(2013), pp. 1-3.

Tantak, N.P. and Chaudhari, S., 2006. Degradation of azo dyes by sequential Fenton's oxidation and aerobic biological treatment. *Journal of Hazardous Materials*, 136(3), pp. 698-705.

Tchobanoglous, G., Burton, F.L. and Stensel, D.H., 2003. *Wastewater engineering: treatment and reuse*. [e-book] New York: McGraw-Hill. Available at: < http://www.sswm.info/sites/default/files/reference_attachments/TCHOBANOGL OUS%20et%20al.%202003%20Wastewater%20Engineering.pdf> [Accessed 24 June 2015].

Textile Technologist, 2012. *Dyes/ Classification of dyes.* [Online] Available at: <http://textilefashionstudy.com/dyes-classification-of-dyes/> [Accessed on 14 July 2015].

Velichkova, F., Julcour-Lebigue, C., Koumanova, B. and Delmas, D., 2013. Heterogeneous Fenton oxidation of paracetamol using iron oxide (nano)particles. *Journal of Environmental Chemical Engineering*, 1(4), pp. 1214-1222.

Verma, A.K., Dash, R.D. and Bhunia P., 2012. A review on chemical coagulation/ flocculation technologies for removal of colour from textile wastewaters. *Journal of Environmental Management*, 93, pp. 154-168.

Wang, B.Y., Wei, Q.F., and Qu, S.L., 2013. Synthesis and characterization of uniform and crystalline magnetite nanoparticles via oxidation-precipitation and modified co-precipitation methods. *International Journal of Electrochemical Science*, 8, pp.3786-3793.

Wang, C., Liu, H. and Sun, Z., 2012. Heterogeneous photo-Fenton reaction catalysed by nanosized iron oxides for water treatment. *International Journal of Photoenergy*, 2012, pp. 1-10.

Wang, J., Pan, Z.J., Zhang, Z.H., Jiang, Y.F., Ma, T., Wen, F., Li, Y. and Zhang, P., 2007. The investigation on ultrasonic degradation of acid fuchsine in the presence of ordinary and nanometer rutile TiO_2 and the comparison of their sonocatalytic activities. *Dyes and Pigments*, 74(3), pp. 525-530.

Wang, N., Zheng, T., Zhang, G. and Wang, P., 2016. A review on Fenton-like processes for organic wastewater treatment. *Journal of Environmental Chemical Engineering*, 4(1), pp. 762-787.

Wei, X. and Viadero Jr, R.C., 2007. Synthesis of magnetite nanoparticles with ferric iron recovered from acid mine drainage: Implications for environmental engineering. *Colloids and Surfaces A: Physicochemical and Engineering Aspects*, 294 (1-3), pp. 280–286.

Williams, M., 2014. *What percent of earth is water?* [Online] Available at: <http://www.universetoday.com/65588/what-percent-of-earth-is-water/> [Accessed 24 June 2015].

Wu, T.Y., Guo, N., Teh, C.Y. and Hay, X.W., 2012. *3.5* Ultrasound treatment of dye wastewater. In: *Advances in Ultrasound Technology for Environmental Remediation:* New York: Springer Dordrecht Heidelberg. pp.41-42.

Wu, Y., Zeng, S., Wang, F., Megharaj, M., Naidu, R. and Chen, Z., 2015. Heterogeneous Fenton-like oxidation of malachite green by iron-based nanoparticles synthesized by tea extract as a catalyst. *Separation and Purification Technology*. 154, pp. 161-167.

Wu, Y., Zhoua, S., Qin, F., Zheng, K. and Ye, X., 2010. Modeling the oxidation kinetics of Fenton's process on the degradation of humic acid. *Journal of Hazardous Materials*, 179(1-3), pp. 533–539.

Wu, Z. and Wang, Y., 2013. One-pot synthesis of magnetic γ-Fe_2O_3 nanoparticles in ethanol-water mixed solvent. *Materials Science-Poland*, 31(4), pp. 577-580.

Xu L. and Wang J., 2011. A heterogeneous Fenton-like system with nanoparticulate zero-valent iron for removal of 4-chloro-3-methyl phenol. *Journal of Hazard Material*, 186, pp. 256–264.

Xu, X.R., Li, H.B., Wang, W.H. and Gu, J.D., 2004. Degradation of dyes in aqueous solutions by the Fenton process. *Chemosphere*,57(7), pp. 595-600.

Xue, X., Hanna, K. and Deng, N., 2009. Fenton-like oxidation of Rhodamine B in the presence of two types of iron (II, III) oxide. *Journal of Hazardous Materials*, 166(1), pp. 407-414.

Xu Z., Li, H., Cao, G., Cao, Z., Zhang, Q., Li, K., Hou, X., Li, W. and Cao, W., 2010. Synthesis of hybrid graphene carbon-coated nanocatalysts. *Journal of Materials Chemistry*, 20, pp. 8230-8232.

Yagub, M.T., Sen, T.K., Afroze, S. and Ang, H.M., 2014. Dye and its removal from aqueous solution by adsorption: A review. *Advances in Colloids and Interface Science*, 209, pp. 172-184.

Yaman, C. and Gündüz, G., 2015. A parametric study on the decolourization and mineralization of C.I. Reactive Red 141 in water by heterogeneous Fenton-like oxidation over FeZSM-5 zeolite. *Journal of Environmental Health Science & Engineering*, 13(7), pp. 1-12.

Yaman, Y.C., Gündüz, G. and Dükkancı, M., 2013. Degradation of CI reactive red 141 by heterogeneous Fenton-like process over iron-containing ZSM-5 zeolites. *Coloration Technology*, 129(1), pp. 69–75.

You, S.J. and Teng, J.Y., 2009. Anaerobic decolourization bacteria for the treatment of azo dye in a sequential anaerobic and aerobic membrane bioreactor. *Journal of Taiwan Institute Chemical Engineers*, 40(5), pp. 500-504.

Zhang, H., Fu, H. and Zhang, D.B., 2009. Degradation of C.I. Acid Orange 7 by ultrasound enhanced heterogeneous Fenton-like process. *Journal of Hazardous Materials*, 172(2-3), pp. 654-660.

Zhang, J.B., Zhuang, J., Gao, L.Z., Zhang, Y., Gu, N., Feng, J., Yang, D.L., Zhu, J.D. and Yan, X.Y., 2008. Decomposing phenol by the hidden talent of ferromagnetic nanoparticles. *Chemosphere*, 73(9), pp. 1524–1528.

Zhuang, H.F., Han, H.J., Ma, W.C., Hou, B.L., Jia, S.Y. and Zhao, Q., 2015. Advanced treatment of biologically pretreated coal gasification wastewater by a novel heterogeneous Fenton oxidation process. *Journal of Environmental Sciences*, 33, pp.12-20.

Zhuang, J., Zhang J.B., Gao, L.Z., Zhang, Y., Gu, N., Feng, J., Yang, D.L. and Yan, X.Y., 2008. A novel application of iron oxide nanoparticles for detection of hydrogen peroxide in acid rain. *Materials Letters*, 62(24), pp. 3972–3974.

APPENDICES

APPENDIX A: Preparation of Various Concentrations of Organic Dyes

In order to obtain the concentration of organic dye that required for experiment from a stock solution, dilution is needed. By knowing the concentration of stock solution, desired concentration and volume of organic dye, the volume from stock solution that is required can be computed by using

$$C_1 V_1 = C_2 V_2$$

where

C_1 = Stock solution's concentration, g/L

V_1 = Stock solution's volume, L

C_2 = Diluted solution's final concentration, g/L

V_2 = Diluted solution's final volume, L

After the value of V_1 is computed, V_1 of stock solution is pipetted and then it is diluted by adding distilled water until the volume reach V_2 value.

To prepare the stock solution of 80 % Acid Orange G with concentration of 500 mg/L in 1 L, the mass of Acid Orange G required is calculated as below:

$$mass\ of\ Acid\ Orange\ G = \frac{1}{0.80} \times 500 \frac{mg}{L} \times 1\ L$$
$$= 625\ mg$$
$$= 0.625\ g$$

Therefore, 0.625 g of Acid Orange G is dissolved in 1 L distilled water to get the stock solution with concentration of 500 mg/L in l L.

Volume of 80 % Acid orange G stock solution with 500 mg/L required to prepare different concentration of organic dyes in 100 ml solution is shown in Table A.1. The volume of 80 % Acid Orange G stock solution with concentration 500 mg/L required to prepare 100 ml of diluted Acid Orange G solution with concentration 50 mg/L is calculated as below:

$$(500 \ mg/L)(V_1) = (50 \ mg/L)(100 \ ml)$$
$$V_1 = 10 \ ml$$

Hence, 10 ml of Acid Orange G stock solution is pipetted and then it is diluted by adding distilled water until the volume reach 100 ml.

Table A.1: Volume of 80 % Acid orange G Stock Solution with 500 mg/L Required to Prepare Different Concentration of Organic Dyes in 100 ml Solution

Concentration of Acid Orange G (mg/L)	Volume of 80 % Acid orange G Stock Solution with 500 mg/L Required (ml)
50	10
100	20
150	30
200	40
250	50

APPENDIX B: Preparation 0.1 M HCl from a 37 % HCl

Molarity of 37 % HCl is determined first.

HCl – 37 % v/v = 37 ml/ 100 ml

Specific gravity of 37 % HCl = 1.19 g/ml

Molecular weight of HCl = 36.46 g/mol

Concentration of HCl in g/L $= \frac{37\ ml}{100\ ml} \times \frac{1.19\ g}{ml}$

$$= \frac{0.4403\ g}{ml} \times \frac{1000\ ml}{1\ L}$$

$$= 440.3\ g/L$$

Molarity of HCl $= \frac{440.3\ g}{L} \times \frac{mol}{36.46 g}$

$$= 12.07\ mol/L$$

Volume of 0.37 % HCl required can be computed in order to get 0.1 M by using equation

$$M_1 V_1 = M_2 V_2$$

Where

M_1 = Concentration of 37 % HCl solution, mol/L

V_1 = Volume from 37 % HCl solution, L

M_2 = Final concentration of diluted HCl solution, mol/L

V_2 = Final volume of diluted HCl solution, L

M_1 = 12.07 M, M_2 = 0.1 M, V_2 = 500 ml

$$V_1 = \frac{M_2 V_2}{M_1}$$

$$= \frac{0.1\ M \times 500\ ml}{12.07\ M}$$

$$= 4.14\ ml$$

Therefore, 4.14 ml of 37 % HCl is pipetted and then it is diluted by adding distilled water until the volume reach 500 ml.

APPENDIX C: Preparation of 0.1 M NaOH from a 97 % NaOH

To prepare 0.1 M of NaOH in 500 ml, the mass of NaOH powder required is computed.

$$Number\ of\ moles\ of\ NaOH = Molarity \left(\frac{mol}{L}\right) \times Volume(L) \times purity$$
$$= \frac{0.1\ mol}{L} \times 500\ ml \times \frac{1\ L}{1000\ ml} \times \frac{100}{97}$$
$$= 0.052\ moles$$

NaOH's Molecular weight = 40 g/mol,

$$Mass\ of\ NaOH$$
$$= No.of\ moles\ of\ NaOH\ (moles) \times NaOH's\ Molecular\ weight \left(\frac{g}{mol}\right)$$
$$= 0.052\ moles \times 40 \frac{g}{mol}$$
$$= 2.08\ g$$

Therefore, 0.1 M of NaOH can be obtained by adding 2.08 g of NaOH to 500 ml of distilled water.

APPENDIX D: Preparation of H_2O_2 from 30 % H_2O_2

Concentration of H_2O_2 used in this experiment is 30 % H_2O_2 (w/w) in H_2O which indicates that 30 g of H_2O_2 is present in 100 g of solution. Density of 30 % H_2O_2 is 1.11 g/ml. Volume of 100 g of 30 % H_2O_2 solution is calculated by using

$$\rho = \frac{m}{V}$$

Where

ρ = Density, g/ml

m = Mass, g

V = Volume, ml

$V = \frac{m}{\rho}$

$\quad = \frac{100\ g}{1.11\ g/ml}$

$\quad = 90.09\ ml$

Next, the percentage concentration (w/v) of H_2O_2 solution is computed by

$$Percent\ Concentration\left(\frac{w}{v}\right) = 100 \times \frac{Amount\ of\ solute\ (g)}{Amount\ of\ solution\ (ml)}$$

$$= 100 \times \frac{30\ g}{90.09\ ml}$$

$$= 33.30\ g/ml$$

Mole of H_2O_2 present in 33.30 g of H_2O_2 is calculated.

$$Moles = \frac{Mass\ of\ substance\ (g)}{Atomic\ Weight\ (\frac{g}{mol})}$$

$$= \frac{33.30\ g}{34.01\ g/mol}$$

$$= 0.98\ moles\ of\ H_2O_2$$

It means that 0.98 moles of H_2O_2 is present in 100 ml solution.

Now, the molarity of H_2O_2 solution is calculated by

$$Molarity = \frac{Number\ of\ moles\ of\ solute\ (moles)}{Volume\ of\ solution\ (L)}$$

$$= \frac{0.98\ moles}{0.1\ L}$$

$$= 9.80\ M$$

Volume of 0.30 % H_2O_2 required can be computed in order to get the desired concentration of H_2O_2 by using equation

$$M_1V_1 = M_2V_2$$

where

M_1 = Concentration of 30 % H_2O_2 solution, mol/L

V_1 = Volume of 30 % H_2O_2 solution, L

M_2 = Final concentration of diluted H_2O_2 solution, mol/L

V_2 = Final volume of diluted H_2O_2 solution, L

After value of V_1 is computed, V_1 of stock solution is pipetted and then it is diluted by adding distilled water until the volume reach V_2 value.

Volume of 30 % H_2O_2 required to prepare different dosage in 100 ml solution is shown in Table D.1. The volume of H_2O_2 required is calculated as below:

$$(9.80\ M)(V_1) = (0.1\ M)(100\ ml)$$

$$V_1 = 1.0204\ ml$$

Table D.1: Volume of H_2O_2 Required to Prepare Different Dosage in 100 ml Solution

H_2O_2 Dosage (M)	Volume of 30 % H_2O_2 solution Required (ml)
0.1	1.0204
0.2	2.0408
0.3	3.0612
0.4	4.0816
0.5	5.1020

APPENDIX E: Preparation of Standard Solution for ICP-OES Analysis

In order to obtain the concentration of FeCl₃ that required from a stock solution, dilution is needed. By knowing the concentration of stock solution, desired concentration and volume of FeCl₃, the volume from stock solution that is required can be computed by using

$$C_1V_1 = C_2V_2$$

where

C_1= Stock solution's concentration, g/L

V_1= Stock solution's volume, L

C_2= Diluted solution's final concentration, g/L

V_2= Diluted solution's final volume, L

After the value of V_1 is computed, V_1 of stock solution is pipetted and then it is diluted by adding distilled water until the volume reach V_2 value.

To prepare the stock solution of FeCl₃ with concentration of 1000 ppm (1000 mg/L) in 100 ml, the mass of FeCl₃ required is calculated as below:

$$mass\ of\ FeCl_3 = 1000\ \frac{mg}{L} \times \frac{1\ L}{1000\ ml} \times 100\ ml$$

$$= 100\ mg$$

Therefore, 100 mg of FeCl₃ is dissolved in 100 ml distilled water to get the stock solution with concentration of 1000 ppm in 100 ml.

Volume of $FeCl_3$ stock solution with 1000 ppm required to prepare different concentration of $FeCl_3$ in 100 ml solution is shown in Table E.1. The volume of $FeCl_3$ stock solution with concentration 1000 ppm required to prepare 100 ml of $FeCl_3$ solution with concentration 10 ppm is calculated as below:

$$(1000\ ppm)(V_1) = (10\ ppm)(100\ ml)$$
$$V_1 = 1\ ml$$

Hence, 1 ml of $FeCl_3$ stock solution is pipetted and then it is diluted by adding distilled water until the volume reach 100 ml.

Table E.1: Volume of $FeCl_3$ Stock Solution with 1000 pm Required to Prepare Different Concentration of $FeCl_3$ in 100 ml Solution

Concentration of $FeCl_3$ (ppm)	Volume of $FeCl_3$ Stock Solution with 1000 ppm Required (ml)
10	1
20	2
30	3
40	4
50	5

APPENDIX F: Calibration Curve of Organic Dyes

Calibration curves for each organic dye are shown in Figure below.
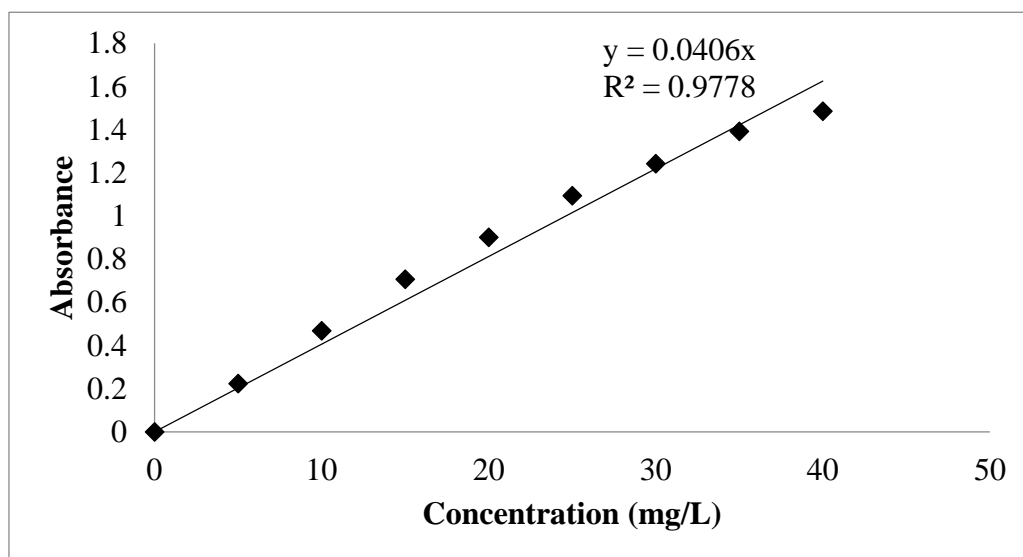
Figure F.1: Calibration Curve of Acid Orange G
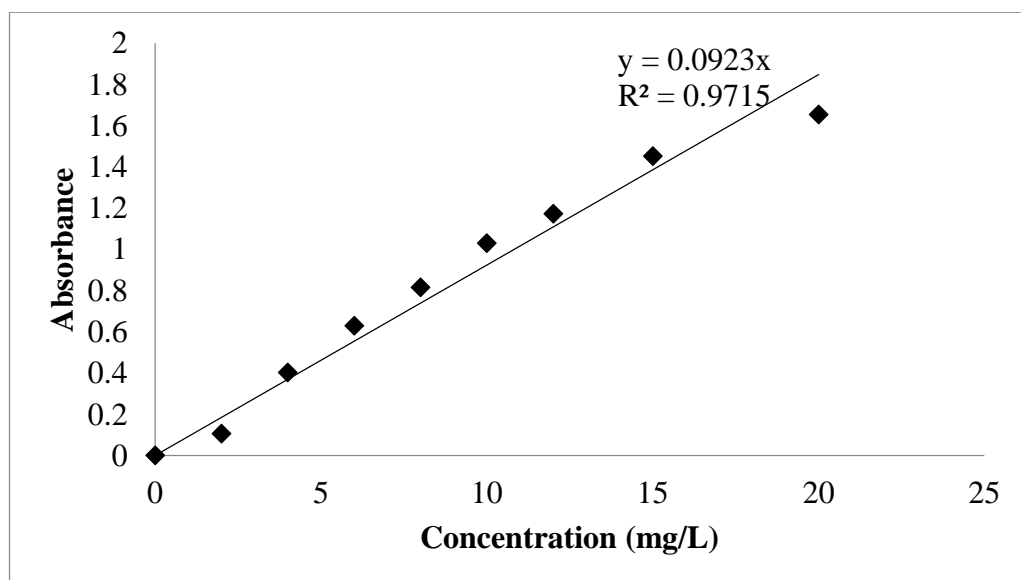
Figure F.2: Calibration Curve of Congo Red
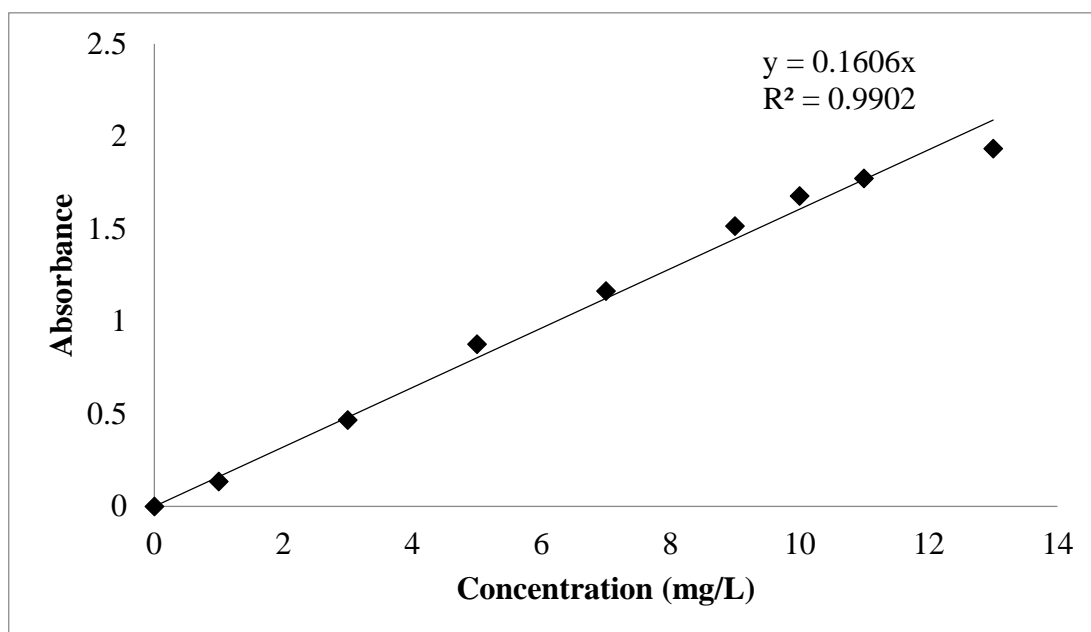
Figure F.3: Calibration Curve of Malachite Green
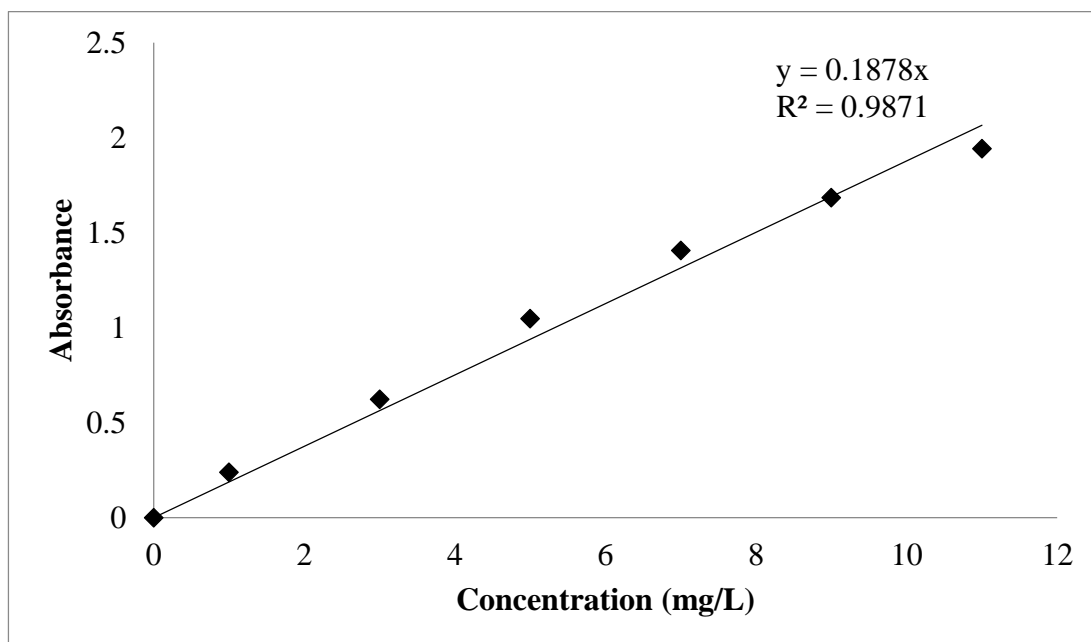
Figure F.4: Calibration Curve of Methylene Blue
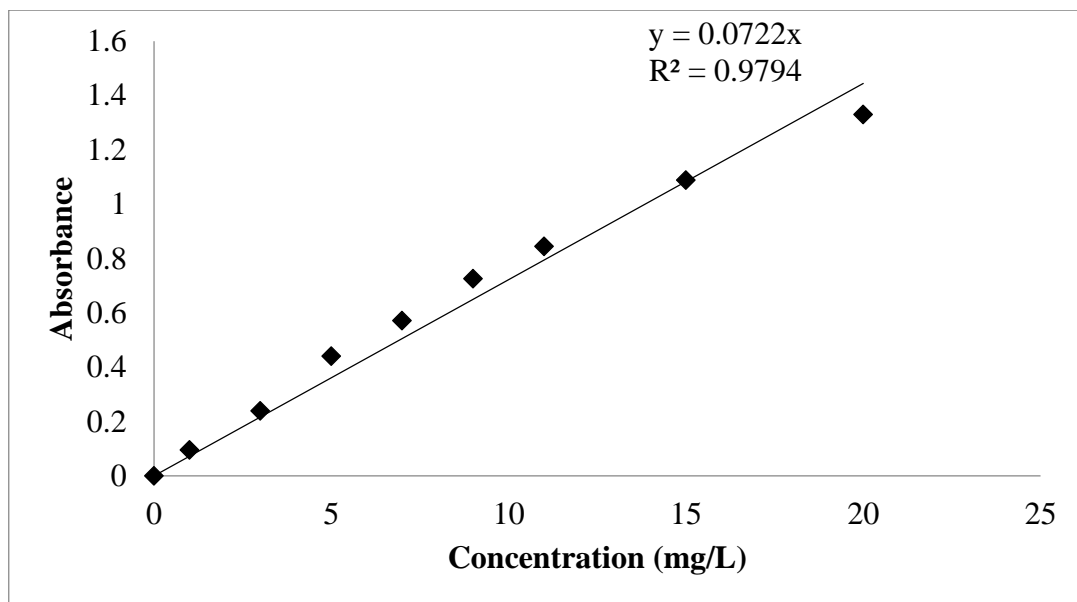
Figure F.5: Calibration Curve of Methyl Orange
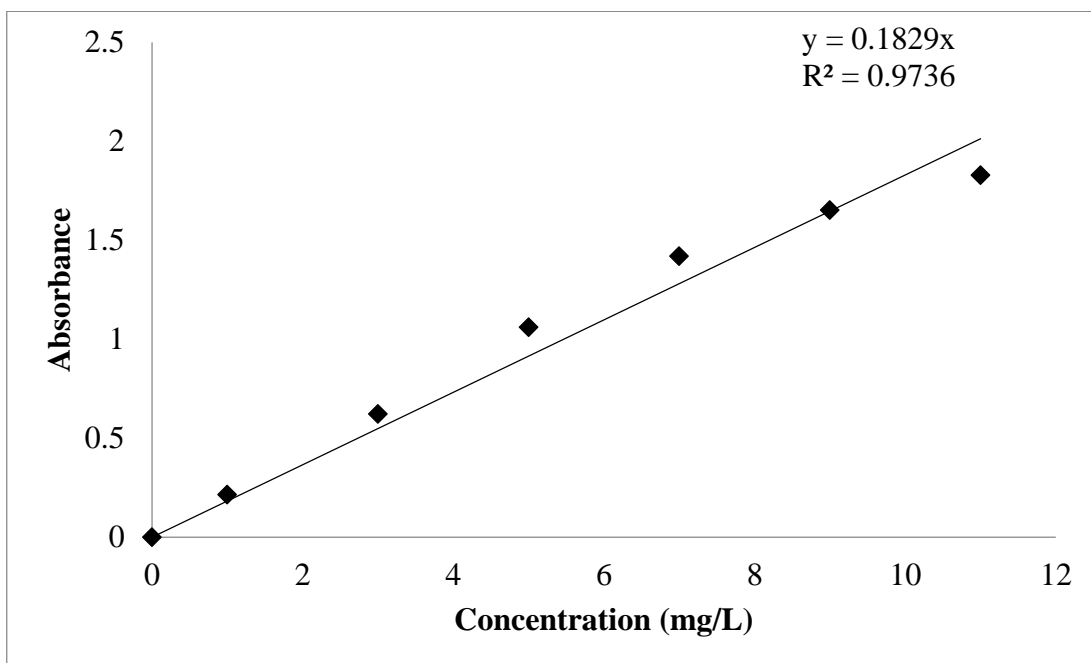
Figure F.6: Calibration Curve of Rhodamine B

APPENDIX G: Calibration Curve of Standard Solution for ICP-OES Analysis
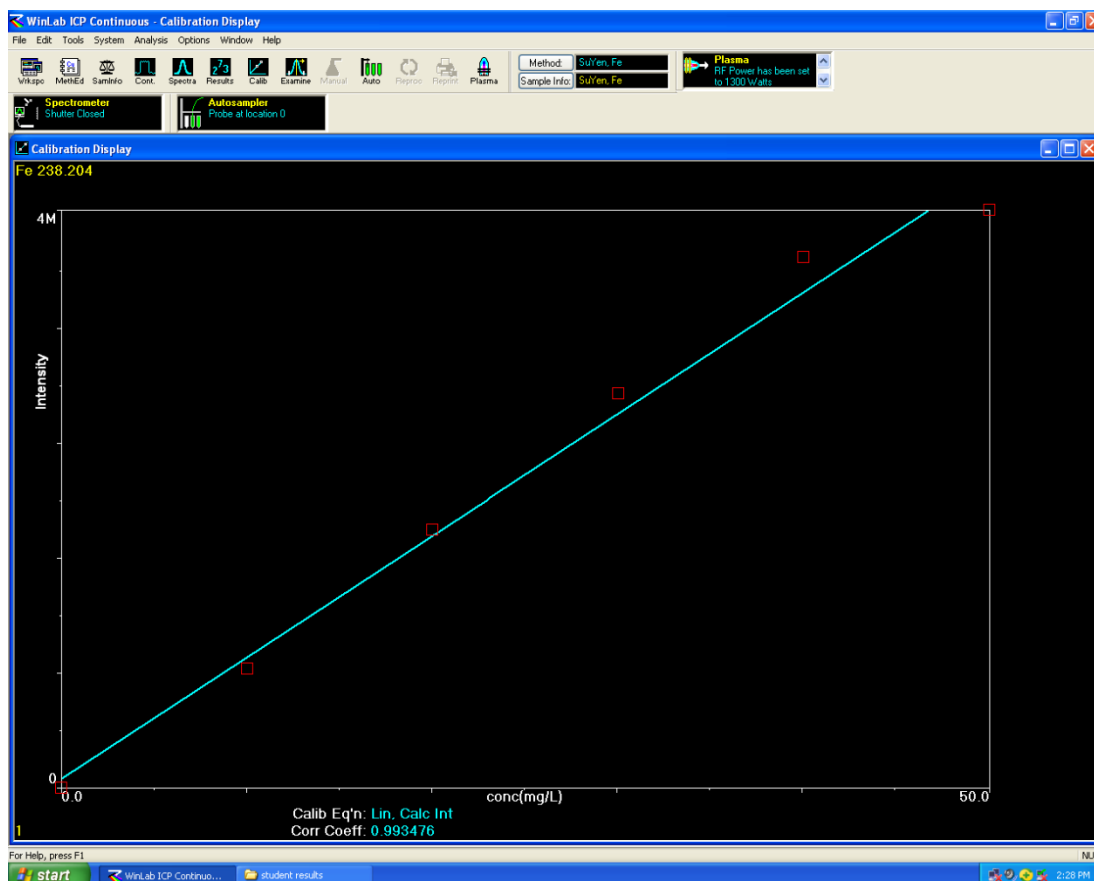
Figure G.1: Calibration Curve of Standard Solution for ICP-OES Analysis

APPENDIX H: Calculation of Crystalline Size

The crystalline size of materials can be calculated from XRD pattern using the Scherrer equation (Abbas, et al., 2015)

$$D = \frac{K\lambda}{\beta cos\theta}$$

where

K = shape factor, 0.9

λ = wavelength of X-ray, 1.540562 Å

β = width at half maximum (FWHM), °

θ = Bragg angle for the studied peak, °

Peak data for Fe_3O_4-0:

β = 0.17600 °

θ = 35.4723 °

Crystalline size of Fe_3O_4-0 is calculated as below:

$$D = \frac{K\lambda}{\beta cos\theta}$$

$$= \frac{0.90 \times 1.540562}{(0.17600 \times \frac{\pi}{180})cos(\frac{35.4723}{2})}$$

$$= 473.9 \text{ Å}$$

$$= 47.39 \, nm$$

APPENDIX I: Reaction Kinetics Plot

The kinetics of the Fenton and Fenton-like reaction on the degradation of malachite green can be described as:

$$-\frac{dC_{MG}}{dt} = k_{app}C_{MG}^m$$

where

C_{MG} = concentration of malachite green at time t, mg/L

m = reaction order with respect to malachite green

t = reaction time, min

k_{app} = reaction rate constant

For pseudo zero-order reaction, the above equation after integration becomes:

$$C_t = C_0 - k_0t$$

A plot of C_t against t is shown in Figure I.1.

For pseudo second-order reaction, the integrated equation becomes:

$$\frac{1}{C_t} = \frac{1}{C_0} + k_2t$$

A plot of $\frac{1}{C_t}$ against t is shown in Figure I.2.
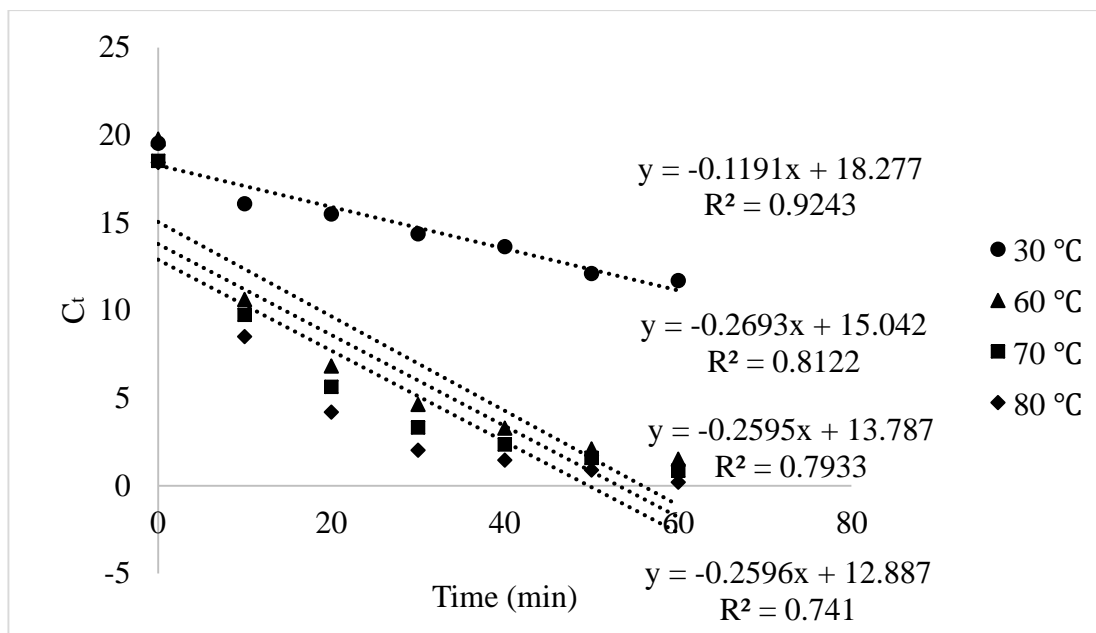
Figure I.1: Pseudo Zero-order Reaction Kinetics Plot for Fenton and Fenton-like Degradation of Malachite Green
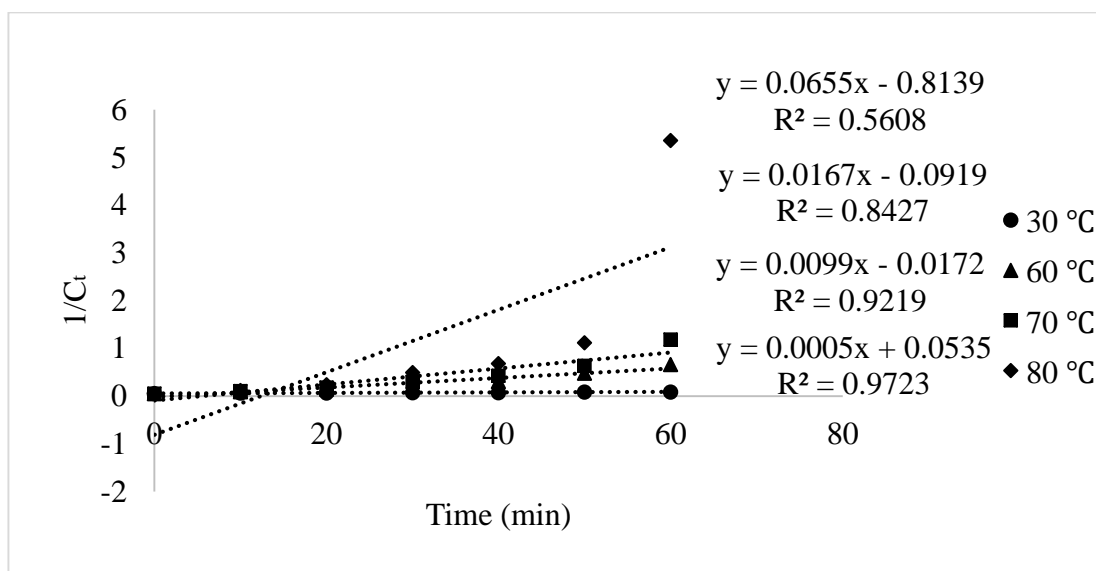
Figure I.2: Pseudo Second-order Reaction Kinetics Plot for Fenton and Fenton-like Degradation of Malachite Green

APPENDIX J: MSDS